UNIVERSITY OF CALIFORNIA
RIVERSIDE

Enzymatic Intermediates of Tryptophan Synthase at Atomic Resolution Using Solid-State NMR

A Dissertation submitted in partial satisfaction
of the requirements for the degree of

Doctor of Philosophy

in

Chemistry

by

Bethany Gayle Caulkins

June 2017

Dissertation Committee:
- Dr. Leonard J. Mueller, Chairperson
- Dr. Eric L. Chronister
- Dr. Ludwig Bartels

The Dissertation of Bethany Gayle Caulkins is approved:

Committee Chairperson

University of California, Riverside

Acknowledgments

Graduate school was the best of times, and only sometimes the worst. There are countless people to whom I owe this success, and I only hope to scratch the surface with this list.

Thank you to the NIH for funding our research. Thank you to everyone at the National High Magnetic Field Laboratory for their excellent facility and the countless hours of running experiments for us. Particularly, thank you to Peter Gor'kov, Ivan Hung, and Zhehong Gan. To Joanna Long and Adam Smith, we would not have any DNP data without all your work. Thank you for all your time and help.

Thank you to my committee, Eric Chronister, Ludwig Bartels, and Len Mueller, for all your feedback and genuine interest over the years. You have made me a better scientist, and I know I would not be as successful without your guidance. Thank you to all the staff who have made my time here pleasant and fun. There are so many faculty members who have been instrumental to my success, particularly Len Mueller, Greg Beran, Richard Hooley, Mike Dunn, Cindy Larive, Jack Eichler, and Chia-en Chang. Your ideas and feedback have been greatly appreciated over the years, and you have been great examples of what a researcher and teacher should be.

I met some remarkable people during my time in graduate school, and their friendship has proven invaluable. To Preston Williams, my time here was made better and richer because of you. I am so happy for you and Nicole and Baby Williams! I wish you three the best of luck. To Geoff Piland, I will never be able to thank you enough for all your

help our first year or for the fun we had after that. To Magi Mettry, you are awesome! I cannot wait to see what you end up doing because I know it will be great! Mike Sterling and Zack Palchak, thank you for making this last year so much more fun! To Klaus and Christina Schnackerz, thank you for being great people who welcomed me into the PLP community. To Kevin Millis, you are so much fun! Thank you for all the good times and all the great deals from CIL.

To all of my lab mates over the years, thank you so much for your support, help, laughter, and love. Chen Yang, Tommy Neubauer, Ryan Kudla, and Robert Young – You four made my time here unforgettable! I will always remember our camping trips, concerts, conferences, lunch outings, tensor videos, and fun. Mary Hatcher-Skeers, I do not know what I would have done without you this last year! I am so happy to know you, and I appreciate all your help! Dan Borchardt, I will miss our morning coffee more than you will ever know. Roberto, you are truly one of the greatest people I have ever known! I cannot begin to tell you how proud I am of you or how happy I am to know you! I leave UCR worried only that the best times of my life may be behind me because I cannot imagine ever loving a group of people more than all of you!

To Jessica Harper, thank you for being such a wonderful and inspirational friend!

To my parents and siblings, thank you for always believing in me and loving me! You are all insane, but I love you all the more for it! Thank you for your love and support. And especially thank you to Mom and Dad, who kept me company on my drive home almost every day! I treasure that time with you.

To Mike Dunn, thank you for all your knowledge and guidance and friendship. You are the giant upon whose shoulders I stand. This whole project would not be possible without you. I love you and Linda like my own family, and I hope we get to travel more together in the future.

Richard Hooley… All I can say is thank you for keeping me sane! I appreciate all your time and all your encouragement and for being my home away from home. You have an uncanny ability to calm me down when I am stressed out, and I love you!

To my husband Richard Caulkins, I would not be here without you. You have been tirelessly patient and endlessly encouraging since I met you. Our life is great because of you, and I only hope I can do for you all the things you have done for me. Thank you for giving me everything I could ever dream of. You are truly a remarkable man, and I love you!

To my boss Len Mueller, will I ever be able to repay everything you have done for me? I doubt it. You have been my boss, my ally, my mentor, and one of my best friends ever! I feel so lucky that you found me in the hall, and it is impossible to imagine a better experience in graduate school. You have always been there when I need you for anything. I will miss everything! My life will have a huge hole in it without our daily interaction. I truly hope you know how much you have impacted my life, and I love you from the bottom of my heart forever! I wish nothing more than to make you proud and to live up to the example you have set. Thank you so much!

The work in this thesis comes entirely or in part from the following publications:

Caulkins, B. G.; Bastin, B.; Yang, C.; Neubauer, T. J.; Young, R. P.; Hilario, E.; Huang, Y. M.; Chang, C. A.; Fan, L.; Dunn, M. F.; Marsella, M. J.; Mueller, L. J. Protonation States of the Tryptophan Synthase Internal Aldimine Active Site from Solid-State NMR Spectroscopy: Direct Observation of the Protonated Schiff Base Linkage to Pyridoxal-5'-Phosphate. *J. Am. Chem. Soc.* **2014,** *136*, 12824-12827.

Caulkins, B. G; Yang, C.; Hilario, E.; Fan, L.; Dunn, M. F.; Mueller, L. J. Catalytic Roles of βLys87 in Tryptophan Synthase: ^{15}N Solid State NMR Studies. *BBA – Protein Proteom.* **2015,** *1854*, 1194-1199.

Hilario, E.; **Caulkins, B. G.**; Huang, Y. M.; You, W.; Chang, C. A.; Mueller, L. J.; Dunn, M. F.; Fan, L. Visualizing the Tunnel in Tryptophan Synthase with Crystallography: Insights into a Selective Filter for Accommodating Indole and Rejecting Water. *BBA - Protein Proteom.* **2016**, *1864*, 268-279.

Caulkins, B. G.; Young, R. P.; Kudla, R. A.; Yang, C.; Bittbauer, T. J.; Bastin, B.; Marsella, M. J.; Dunn, M. F.; Mueller, L. J. NMR Crystallography of a Carbanionic Intermediate in Tryptophan Synthase: Chemical Structure, Tautomerization, and Reaction Specificity. *J. Am. Chem. Soc.* **2016**, *138,* 15214-15226.

Dedication

To all the people I love the most. You know who you are.

ABSTRACT OF THE DISSERTATION

Enzymatic Intermediates of Tryptophan Synthase at Atomic Resolution Using Solid-State NMR

by

Bethany Gayle Caulkins

Doctor of Philosophy, Graduate Program in Chemistry
University of California, Riverside, June 2017
Dr. Leonard J. Mueller, Chairperson

The acid-base chemistry that drives catalysis in pyridoxal-5′-phosphate (PLP)-dependent enzymes has been the subject of intense interest and investigation since the initial identification of its role as cofactor in this extensive class of enzymes. X-ray crystallography, optical spectroscopy, and physical-organic studies point to the importance of protonation/deprotonation at ionizable sites on the coenzyme, substrates, and sidechains to activate key steps in the catalytic process. Yet direct characterization remains elusive as these techniques cannot specifically identify proton locations or report unambiguously on local chemical environment. The chemical shift in nuclear magnetic resonance (NMR), however, is an extremely sensitive probe of chemical environment, but a large complex like a protein will give an enormous amount of data that can be inscrutable without guidelines for specific structure determination. The use of computational chemistry aids in the creation of models that rely on specific chemical-level

details and predicts detailed information like chemical shift. We employ NMR crystallography – the synergistic combination of X-ray diffraction, solid-state NMR spectroscopy, and computational chemistry - to define three-dimensional, chemically-detailed structures of the intermediates in the tryptophan synthase cycle under conditions of active catalysis. Together these methods can provide consistent and testable models for structure and function of enzyme active sites. Our results from studies on tryptophan synthase confirm some long-held mechanistic hypotheses, but also point to several novel structural hypotheses.

Table of Contents

List of Figures

List of Tables

List of Schemes

Chapter 1 – Introduction and Background

1.1 Introduction

The atomic-level description of the reactions that transform substrate to product in enzymatic reactions has long been the goal of the field of enzymology. True chemical-level explanation requires detailed structural information about the enzyme active site, including the locations of all protons. X-ray crystallography provides a generous piece of this puzzle by identifying and mapping the electron density of the heavy atoms in the protein, but current resolution of crystal structures does not allow for collection of information about the placement of hydrogen atoms. Nuclear magnetic resonance (NMR) provides a sensitive probe of hybridization and protonation state, but studies on a system the size of a protein will result in more chemical shift data than can be interpreted, and teasing out the signals arising from key nuclei in the active site would be difficult without some guidance. Computational chemistry can provide theoretical chemical shifts for comparison with experimental ones, but it relies on detailed structures with assigned protonation states to make accurate predictions. When used together, these three techniques provide a holistic picture of enzyme catalysis: computational models can be constructed based on X-crystal structures, multiple models with varying protonation states can be built to generate theoretical chemical shifts for each of them, and solid-state NMR provides experimental chemical shifts, which can be used to refine the models until a consistent view of catalysis is achieved. This technique, known as NMR crystallography, has allowed us to define three-dimensional, chemically-detailed structures of the intermediates in the pyridoxal-5′-phosphate (PLP)-dependent tryptophan synthase mechanism under conditions of active catalysis. Our results from

studies on tryptophan synthase confirm some long-held mechanistic hypotheses, but also point to several novel structural hypotheses, helping to rewrite the mechanism for PLP catalysis.

1.2 Pyridoxal-5′-Phosphate

Pyridoxal-5′-phosphate (PLP; figure 1.1), the bioactive form of vitamin B_6, is an essential cofactor found in enzymes that catalyze the non-oxidative metabolism of amino acids and other amine-containing biomolecules.[2,12-14] It is required for the proper function of more than 4% of classified enzymes,[12] and the genes that encode for PLP-dependent enzymes make up 1.5% of the prokaryotic genome.[12] PLP-dependent enzymes are found everywhere, from places as simple as prokaryotic organisms[15] to as complicated as the human brain.[2,16] Two such enzymes are found in all free-living organisms: aspartate aminotransferase and serine hydroxymethyltransferase, underscoring the biological diversity and importance of PLP as a cofactor.[12]

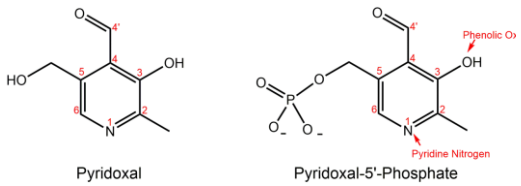

Figure 1.1 Pyridoxal-5′-phosphate (PLP) is the bioactive form of pyridoxal, vitamin B_6.

First isolated and described in 1934,[17] PLP was found to prevent convulsions, dental cavities, and conditions like pellagra and gum disease, while also playing a role in the immune response.[18] Further experiments quickly showed that PLP was the required cofactor in a diverse set of reactions, including decarboxylation, α/β/γ-elimination/replacement, racemization, and transamination. These different reactions occurred in an even more diverse set of enzymes, including racemases, aminotransferases, lyases, decarboxylases, and synthases.[19] Yet despite these rapid

discoveries surrounding the role of the cofactor, the mechanisms for these reactions remained unclear.[13] This changed in 1954 when Metzler *et al.*[8] proposed a general mechanism for B_6-catalyzed reactions, scheme 1.1. Using model compounds chelated with metal ions, these researchers identified three sites on the PLP cofactor that are necessary for catalysis to occur: the pyridine nitrogen (N1), the phenolic oxygen, and the aldehyde functional group at C4′, figure 1.1. The aldehyde carbonyl in particular plays a crucial role in catalysis because it is this site that is attacked by an incoming amino acid substrate to form a Schiff base linkage between the cofactor and the substrate, known as the external aldimine intermediate.[8] The Schiff base is involved in a hydrogen-bond to the phenolic oxygen that helps to stabilize the complex throughout the reaction. Finally, the pyridine nitrogen remains protonated, which withdraws electron density from C4′ and allows for delocalization of electron density throughout the ring structure in a form called the quinonoid intermediate.[8,20] This mechanism was a breakthrough in the chemistry of PLP catalysis and guided the research being done on this cofactor during the next fifty years.

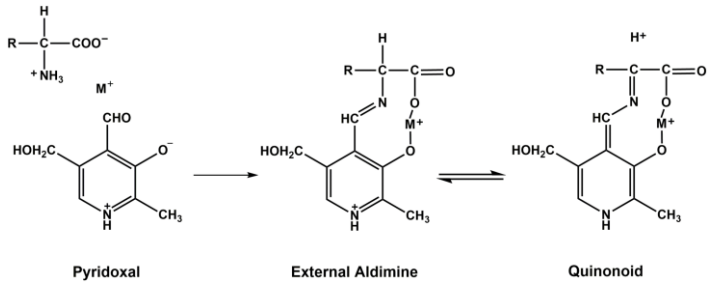

Scheme 1.1 The proposed general mechanism for PLP catalysis. Adapted from Metzler, Ikawa, and Snell, 1954.[8]

During this time, findings from model compound studies started to hint at some of the factors that delineate reaction specificity in PLP-dependent enzymes. Researchers had noted that many of the reactions performed by PLP enzymes could also be performed with pyridoxal (figure 1.1) alone, though at greatly reduced rates.[20-23] Using

methods like UV/vis and IR spectroscopy to determine the structures of PLP-amino acid complexes,[21-25] it was determined that the protonation states of pyridoxal and PLP compounds fluctuate in a pH-dependent manner throughout catalysis, particularly in the form of a tautomeric equilibrium between the Schiff base nitrogen and the phenolic oxygen.[26] These two tautomeric forms were easily identifiable using UV/vis, with the protonated Schiff base form absorbing maximally between 410 and 430 nm and the phenolic form absorbing maximally around 330 nm.[26] Conjugation with the ring nitrogen appeared to be a major feature of these compounds, and the active site residues were thought to encourage the proper tautomeric form for the reaction catalyzed.[26] Further work showed that protonation of the pyridine ring nitrogen made it significantly harder to protonate the phenolic oxygen, suggesting the Schiff base nitrogen should be the protonated species for activity, given the assumed protonation of the pyridine nitrogen.[24] The cationic form of the Schiff base was confirmed in more model compound studies,[27] and it was postulated that this positive nitrogen could stabilize transition states during catalysis, even without the aid of a protonated pyridine nitrogen.[28] Continuing work showed that the zwitterionic form of the complex, consisting of the protonated Schiff base nitrogen and the phenolate oxygen, helped to stabilize transition states in transamination reactions of model compounds.[29,30] Through these studies it became apparent that acid-base equilibria and tautomerization play a large role in the non-enzymatic reactions performed by PLP and pyridoxal.

These findings in model compounds began being applied to the interpretation of the UV/vis results from enzymatic reactions as more and more enzymes were found to be PLP-dependent. Researchers had confirmed that in its resting state, PLP-dependent enzymes use the ε-nitrogen of a lysine side chain in the active site to bind the cofactor in

a Schiff base linkage.[31,32] The protonated Schiff base form of this complex was shown to be much more susceptible to nucleophilic attack by an incoming amino acid substrate, demonstrating the significance of this protonation state at the start of catalysis.[33] This finding helped in determining the sequence of events that occurred next in the reaction mechanism. Key features of catalysis for the proposed mechanism for transamination reactions can be seen in scheme 1.2a,[6,34] and the proposed mechanism for β-elimination and replacement reactions can be seen in Scheme 1.2b.[35] Though these reactions result in different outcomes, they display several common features initially proposed by Snell and Metzler.[8] Both begin in the internal aldimine resting state, E(Ain), and are transformed to an external aldimine species, E(Aex), in a transimination reaction that requires the formation of the transient gem-diamine species, E(GD), for completion. Abstraction of the α-proton results in the quinonoid intermediate, E(Q). In β-elimination/replacement reactions, elimination of a leaving group at C^{β} leads to an aminoacrylate intermediate before addition of the

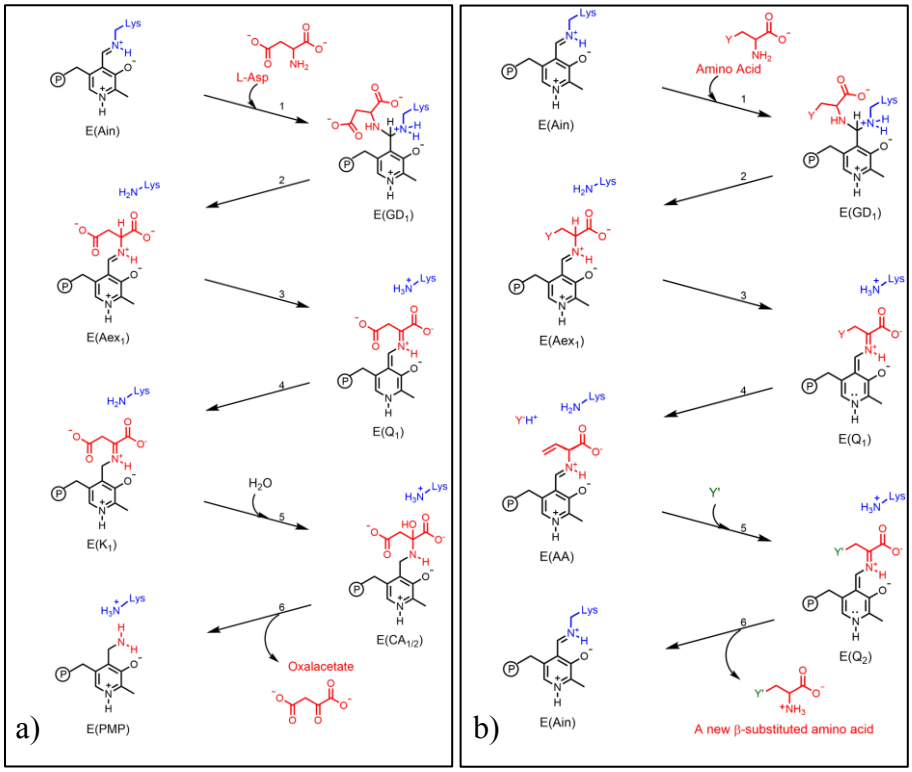

Scheme 1.2 a) The transamination reaction of aspartate aminotransferase. Adapted from Arnone *et al.*[6] b) The β-elimination and replacement reaction. Adapted from Miles *et al.*[2,7]

replacement group leads to the final product. In the transamination reaction, C4′ is reprotonated, leading to a ketimine intermediate, E(K). Addition of water forms a carbinolamine species, E(CA), leading to release of oxalacetate and the reversible formation of pyridoxamine-phosphate (PMP) before the final product is formed. These mechanistic breakthroughs again shed light on what was occurring in these enzyme active sites, but an explanation as to how one cofactor so capably catalyzed such a large number of reactions or performed such varied chemistry was still out of reach.

The first successful explanation of reaction specificity came from H. C. Dunathan.[1] Upon formation of the external aldimine intermediate, cleavage of a bond at C^{α} is required for the reaction to continue. Dunathan noted that the bond that would be cleaved would be the one held perpendicular to the planar ring, R1 in figure 1.2. This would make the bond parallel to the π-molecular orbital system in the complex, and, upon cleavage of a bond at C^{α}, allow the π-system to extend itself by one carbon more when a double bond is created between C^{α} and the Schiff base nitrogen, forming the quinonoid intermediate.[1,15] The electrophilic nature of the cofactor promotes this delocalization into the conjugated π-system of the lone pair electrons by acting as an electron sink and stabilizing the negative charge build-up at C^{α}.[1] Which bond would be broken was determined by the active site residues that held the substrate in the proper conformation for catalysis to occur.[1] So, in enzymes performing a decarboxylase reaction, the carboxylate group of the substrate would be perpendicular to the ring; in racemizations, transaminations, and eliminations, the α-proton would be held perpendicular to the ring.

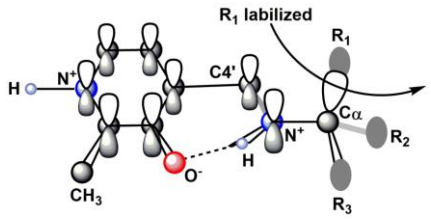

Figure 1.2 The Dunathan Hypothesis explains that the bond parallel to the π-system will be the one initially cleaved. Adapted from Toney.[1,2]

The electron delocalization in the complex would allow the cofactor and active site residues to build up negative or positive charge at specific sites to ensure proper catalysis would occur. Experiments performed on the enzymes α-dialkylamino acid transaminase, glutamate decarboxylase, pyridoxamine-pyruvate transaminase, and hydroxymethylase all supported this stereochemical control theory of reaction specificity in PLP-enzymes,[36-41] while the burgeoning use of nuclear magnetic resonance (NMR) allowed researchers to probe conformational and protonation states of PLP complexes to help investigate this proposed theory. Researchers confirmed the coplanarity of the Schiff base nitrogen with the PLP ring,[42] and others showed the correlation of ^{13}C-chemical shifts in the PLP ring with the protonation states of key sites, like the phenolic oxygen,[43,44] allowing for a probe of the extent of conjugation at the phenolic oxygen site. The Dunathan Hypothesis appeared to explain many of the mysteries of PLP catalysis, and this simple yet elegant theory of reaction specificity coupled with the proposed reaction mechanisms became the dominant view of PLP catalysis for the next several decades.

The determination of the first X-ray crystal structures of PLP-dependent enzymes began to show that the Dunathan Hypothesis was incomplete in its explanation for reaction specificity. The first structure determined for a PLP-dependent enzyme was for aspartate aminotransferase at 2.8 Å resolution,[45] an enzyme that performs a transamination reaction. The structure showed an aspartate residue below the PLP cofactor interacting with the pyridine nitrogen. The acidic nature of the aspartate side chain confirmed the assumption that the pyridine nitrogen is indeed protonated in this enzyme. However, eight years later the second crystal structure of a PLP enzyme was published. The crystal structure of tryptophan synthase was determined at 2.5 Å

resolution.[10] Surprisingly, this enzyme, which performs a β-elimination and replacement reaction, displayed the hydroxyl group of a serine side chain positioned below the pyridine nitrogen. The hydroxyl group would not be a logical proton donor to the pyridine nitrogen, and it was unlikely that both groups contained a proton. When the crystal structure of alanine racemase was solved at 1.9 Å resolution,[46] diffraction data clearly showed a positively charged arginine residue below the ring nitrogen. The positive charge on the side chain would certainly preclude protonation of the pyridine nitrogen. These findings began to call into question the need for a protonated pyridine nitrogen throughout the course of catalysis.

As the sequences and structures of more PLP enzymes became determined, it became clear that a classification system would be needed to keep track of them all. Researchers used comparisons of the numerous published structures to group PLP-dependent enzymes into seven fold types based on their overall sequence, secondary structure, and hydrophobicity profile.[47] Aspartate aminotransferase (AAT), which performs a transamination reaction, is the representative enzyme for fold type I. Fold type I has two major characteristics that stand out. First, the active site lysine follows a hydrophobic β-strand; second, an acidic residue interacts with the pyridine nitrogen and precedes the lysine residue by 20-50 amino acids, as seen in the crystal structures of the aspartate aminotransferases.[47] Fold type II is characterized by a serine, threonine, or cysteine residue interacting with the pyridine nitrogen, and the lysine residue follows a hydrophobic loop structure. The representative enzyme for this fold type is tryptophan synthase (TS).[5,47,48] Fold type III enzymes, represented by alanine racemase (AR), display a positively charged arginine residue below the pyridine nitrogen, and the active site lysine follows a hydrophobic β-strand.[47] Though seven fold types were recognized,

the three listed here comprise the majority of PLP enzymes and the majority of reactions they catalyze. This classification method made it easier for researchers to identify similarities and differences between the various fold types and the representative reactions they catalyze.

The determination of the crystal structures of PLP-dependent enzymes brought the question of reaction specificity in these enzymes back to the forefront. The enzymes displayed many similarities, including a highly conserved binding pocket for the phosphoryl group,[49] several common intermediates,[2,11,50] and catalytic promiscuity.[12] The Dunathan Hypothesis satisfactorily explained why some reactions would occur, but many reactions (transamination, α/β/γ-elimination, racemization) are facilitated by the same α-deprotonation step. There had to be other factors directing reaction outcome.[2,11,50] Researchers now began to return to the acid-base properties of the cofactor-substrate complexes and started to question the protonation states of the ionizable groups on PLP and the amino acid substrate, as well as key active residues near the complex. Perhaps no other group did more to tease out the details of the acid-base chemistry in PLP complexes than the group of Limbach and coworkers.

Limbach recognized that enzyme active sites are often shielded from bulk water, and as a result the conventional ideas about aqueous acid-base equilibria cannot always be applied to enzyme systems.[51] His group employed both solution-state and solid-state NMR to investigate the correlation between the extent of protonation at a particular site and the chemical shift of that nucleus using model compounds with aprotic solvents. Using collidine and carboxylic acid complexes, it was determined that the collidine isotropic ^{15}N chemical shift moves upfield upon protonation, and the distance between the proton and nitrogen atoms in a hydrogen-bonded complex (N···H-X) can be

determined from the measured nitrogen and proton chemical shifts.[51,52] The same correlation was found in solid-state pyridine compounds in an experiment that measured the dipolar interaction between the nitrogen and hydrogen atoms, and hence the distance between them.[53] X-ray crystal structures of benzoic acid derivatives in Schiff base linkages with pyridine-like complexes pointed to both inter- and intramolecular proton transfers as the key to stabilizing these complexes.[54] As seen in figure 1.3, an intermolecular proton transfer is possible between the protonated pyridine nitrogen and the acid group of the benzoic acid derivative, while an intramolecular proton transfer occurs between the Schiff base and the phenolic oxygen of the pyridine compound. These structures also seemed to indicate a coupling of the inter- and intramolecular hydrogen bonds, so that when the pyridine nitrogen was protonated and charged, so was the Schiff base nitrogen. Further work with PLP model systems in the solid-state echoed these findings,[54] while work with PLP model systems in polar solution allowed for the assignment of pk_a to the ionizable sites. Results indicated that at physiological pH, the phosphate group is dianionic and the pyridine nitrogen loses its proton before the proton in the intramolecular bond is lost.[55,56] Furthermore, the zwitterionic form of the intramolecular hydrogen bond is favored before complete deprotonation in that pocket,[56] yet this intramolecular hydrogen bond is lost, and so is any coupling, in aqueous solutions due to solvent interactions with the charged phenolic oxygen and Schiff base nitrogen.[57] Ultimately, Limbach concluded from the model compound studies that these

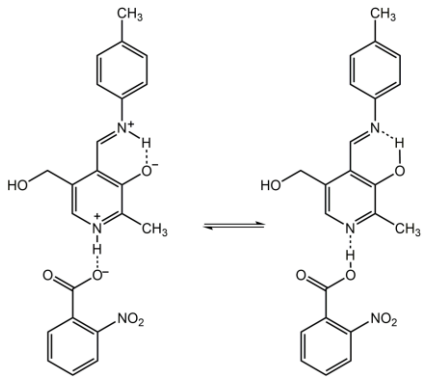

Figure 1.3 One example of a benzoic acid derivative studied by Limbach *et al*. This compound exhibits both inter- and intra-molecular proton transfer.[4]

inter- and intramolecular proton transfers can be seen as coupled low- and high-barrier hydrogen bonds, and the degree of protonation of the heavy atoms can be determined by the distance between the heavy atom and the proton involved in the hydrogen bond, which is determined from the chemical shifts obtained for these sites.[57,58] The solvent plays a large role in which sites are protonated, with the neutral phenolic form dominating in nonpolar environments and the protonated Schiff base/phenolate form dominating in polar environments,[59] but formation of the protonated Schiff base form is always promoted by a protonated pyridine nitrogen.[55]

Limbach then extended his NMR studies to PLP-dependent enzyme systems to see if the generalizations from model compound systems could be applied to the stable intermediates formed throughout catalysis. Focusing on AAT and AR, the researchers synthesized labeled $^{13}C,^{15}N$-PLP in an effort to probe the ionization sites on the complex using solid-state NMR. In AAT, it was confirmed that the pyridine nitrogen is protonated in both the internal aldimine form and the inhibited external aldimine formed with maleate.[60,61] Because the ^{15}N chemical shift of the ε-nitrogen of the catalytic lysine residue in the active site could not be accessed, researchers used poly-L-lysine (PLL) to form an internal aldimine analogue structure to probe the Schiff base linkage in this form. The results supported the finding that the protonated Schiff base is the catalytically active tautomer, and protonation of the pyridine nitrogen promoted protonation of the Schiff base. Yet this study also showed that it is possible to shift protonation to the Schiff base even without protonation of the pyridine nitrogen if the phenolic oxygen is stabilized by hydrogen bonds with the side chains of active site residues or water molecules in the active site.[60] In AR, the deprotonated state of the pyridine nitrogen, long inferred from the crystal structures, was confirmed for the internal aldimine state through the ^{15}N

chemical shift of that site.[60] This was the first direct evidence in a PLP-dependent enzyme that the cofactor could function in an enzyme without the aid of a protonated pyridine nitrogen, and the finding ushered in new level of understanding for PLP catalysis.

Since the work of Limbach and coworkers, the research into reaction specificity in PLP-dependent enzymes has not diminished. Work with deazaPLP, a PLP analogue with the pyridine nitrogen replaced with a carbon atom, figure 1.4b, showed that the loss of the hydrogen bond between the aspartate side chain and the PLP cofactor in AAT

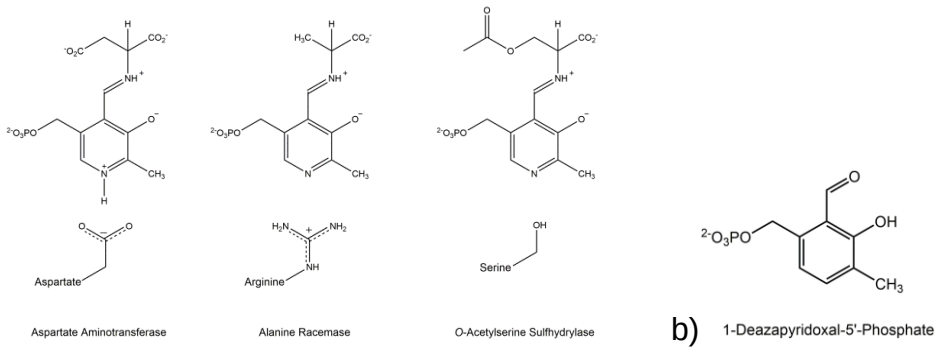

Figure 1.4 a) Three PLP-dependent enzymes from three different fold types and the general structure of their active sites; b) The PLP analogue deazaPLP, which lacks the N1 atom of PLP. Adapted from Griswold.[5]

reduced the activity of the enzyme by greater than 10^9-fold, while in AR activity was reduced ~275-fold, and in the fold type II enzyme O-acetylserine sulfhydralase (OASS), figure 1.4a, activity was reduced ~250-fold.[5] These results demonstrate the necessity of the maximum electron-withdrawing potential of the PLP cofactor in the transamination reactions when compared to racemization and β-elimination/replacement reactions.[62] In the transamination reactions performed by fold type I enzymes, the pyridine nitrogen is protonated due to its interaction with an acidic residue, and this protonation allows the cofactor to act as an electron sink, stabilizing the negative charge that develops at C^{α} by delocalizing it over the entire ring system, forming the quinonoid intermediate, figure

1.5.[11] This delocalization leads to reprotonation at C4′ and formation of the ketimine intermediate proposed by Snell and Jenkins in 1959.[34] The results with the deazaPLP suggest that this delocalization is not required for reactions that do not require reprotonation at C4′, as in the racemization reaction performed by AR and the β-elimination/replacement reaction performed by OASS.[11] Rather, negative charge is

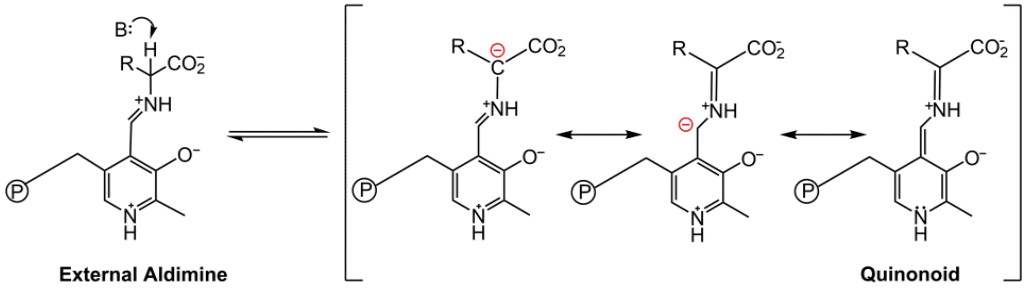

Figure 1.5 The delocalization of negative charge over the PLP ring system leads to the resonance form known as the quinonoid intermediate. Adapted from Toney.[11]

localized more at C^{α} as the reaction proceeds, forming an intermediate better described as a carbanion, figure 1.6.[5,11] Computational experiments echoed these findings,[62-65] and it now appears that reaction specificity in PLP catalysis is controlled by three major factors. First, the stereoelectronics of the active site (the Dunathan Hypothesis) determine which bond on C^{α} will be cleaved. Second, the side chains of the active site residues help to stabilize the intermediates and transition states needed for proper catalysis. Finally, the protonation states of the cofactor-substrate complex ensure the correct acid-base chemistry occurs as the reaction unfolds.[2,11,50,62] It is the final factor that is probed in the following chapters.

1.3 Tryptophan Synthase

The PLP-dependent tryptophan synthase (TS, EC 4.2.1.20) is a fold type II enzyme that performs a β-elimination and replacement reaction in which the β-hydroxyl

group of L-serine is eliminated and replaced with indole to produce tryptophan.[47,66,67] The connection between L-tryptophan and indole had been found in the search for new antibiotics,[68] and the condensation of L-Ser and indole to synthesize L-Trp was revealed soon after.[66] The PLP-dependence of the enzyme was discovered when researchers found that enzymes could not catalyze the conversion of indole and serine to tryptophan unless PLP was added to the solutions of the purified enzyme, which also gave the enzyme a rich yellow color.[67] Shortly thereafter it was shown that the enzyme (which was by now known to be present only in plants, bacteria, yeast, and fungi, not higher order mammals) consisted of two different subunits that catalyzed different reactions, the α- and β-subunits, with the protein activity increased 30-100 fold when the subunits were associated.[69]

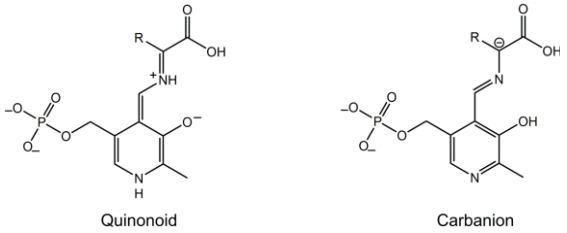

Figure 1.6 The absence of a proton on the pyridine nitrogen precludes formation of a true quinonoid intermediate, instead promoting formation of a carbanionic intermediate.

The finding that the protein is made up of two different subunits allowed researchers to tease out the reactions performed in the individual subunits. It was determined that the α-subunit performed the conversion of indoleglycerol phosphate (IGP) to indole and glyceralehyde 3-phosphate (G3P), while the β-subunit catalyzed the transformation of indole and serine to tryptophan and a water molecule, equations 1.1-1.3.[70] The use of indole produced in the α-reaction as a substrate in the β-reaction, and the lack of free indole in

$$\text{IGP} \longrightarrow \text{Indole} + \text{G3P} \qquad (1.1,\ \alpha\text{-reaction})$$

$$\text{Indole} + \text{L-Ser} \longrightarrow \text{H}_2\text{O} + \text{L-Trp} \qquad (1.2,\ \beta\text{-reaction})$$

$$\text{IGP} + \text{L-Ser} \longrightarrow \text{L-Trp} + \text{G3P} + \text{H}_2\text{O} \qquad (1.3,\ \alpha\beta\text{-reaction})$$

Equations 1.1-1.3 The individual α- and β-reactions, and the overall αβ-reaction in tryptophan synthase.

solution as the reaction progressed led researchers to postulate that the active sites of each subunit are located near each other so the substrate could easily diffuse from one active site to the other.[69,71,72]

Continuing work revealed that the wild type enzyme actually consisted of an $\alpha_2\beta_2$ complex, with the β-subunits tightly associated with one another. The affinity of the β_2-complex for the α-subunits was greatly enhanced by the presence of PLP and serine.[9,73] PLP was bound in the β-subunit in a 1:1 molar ratio, and characteristic absorption bands in the UV/vis agreed well with the work being done on PLP around the same time.[9] As seen in figure 1.7, there is a notable absorption band present at 412 nm, indicative of the protonated Schiff base internal aldimine species formed between the PLP cofactor and the ε-nitrogen of a lysine side chain.[9,31,32] Addition of the nucleophile β-mercaptoethanol and serine to protein solutions with PLP bound in the β-subunit resulted in a strong absorption peak at 468 nm, which researchers could only interpret as showing the subunits were associated at the time, but which also broke down proportionally with the production of the new amino acid *S*-(2-hydroxyethyl)cysteine.[74] Different methods to determine the molecular weight of each of the subunits showed that for the *E. coli* enzyme, the α-subunit weighs about 29 kDa, and the β_2-complex weighs about 86 kDa, for a total molecular weight of about 144 kDa.[75]

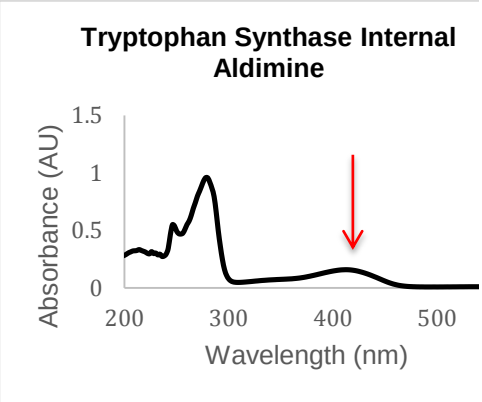

Figure 1.7 Absorption spectrum of the β-subunit in TS. The peak at 412 nm is characteristic of the internal aldimine species in PLP-dependent enzymes.

The discovery that the enzyme is an $\alpha_2\beta_2$ complex helped spur the debate over reaction mechanism in TS. Based on studies suggesting that reactions resulting in an intramolecular dehydration would form an α-aminoacrylate intermediate,[76] researchers had postulated that the PLP-substrate complex must go through such an intermediate in the course of the reaction as a water molecule is one of the products of the reaction.[72,77] The finding that TS could catalyze the deamination of serine to produce pyruvate and ammonia added weight to this idea, as the only explanation for the production of pyruvate involved the α-aminoacrylate intermediate.[78] It was the finding that in the presence of thiols TS can perform either a β-addition or a competing transamination reaction that resulted in the production of pyridoxamine-phosphate (scheme 1.2a) and a completely inactive protein that led to a complete theory of the mechanism in TS, scheme 1.2b.[7,75] This mechanism relied on the electron-withdrawing power of a protonated pyridine nitrogen and the ability of the cofactor to form a quinonoid intermediate, the source of the strong UV/vis peak at 468 nm found earlier when the enzyme was exposed to both serine and β-mercaptoethanol.[74] Each of the different reactions performed by the enzyme could be explained by formation of the α-aminoacrylate intermediate after abstraction of the α-proton and formation of the quinonoid intermediate.[7,75] The mechanism proposed seemed to explain the chemistry performed, and this mechanism became the dominant view of catalysis in TS for the next several decades.

Studies into the structure of TS began to prompt researchers to investigate the nature of the subunit interactions. The lack of free indole in solution during the reaction had initially led researchers to propose the active sites of the two subunits were near each other in the overall protein complex. Continuing work led to the proposal that indole

is actually “channeled” or enzyme-bound throughout the course of the reaction.[79] Separation of the subunits was possible, and the inability of the β_2–complex to synthesize tryptophan without indole being supplied to it supported this channeling theory.[80] Meanwhile, the amino acid sequence of both the α-subunit and β-subunit were determined and published, allowing for initial guesses into the structure of the protein.[81,82] The sequence analysis also included a comparison of the *E. coli* and *S. typhimurium* enzymes, and the two enzymes showed a 75% homology in the α-protein and a 66% homology in the β-protein.[81,82] This allowed the conclusion to be drawn that results obtained on the better-behaved *S. typhimurium* enzyme could be extrapolated to the *E. coli* enzyme. A series of experiments performed to find the quaternary structure of the protein indicated either a linear or spherical arrangement of the subunits and suggested the active sites of the two subunits were actually separated by a significant distance.[83-85] Finally, in 1988, the X-ray crystal structure of TS from *S. typhimurium* was published at 2.5 Å resolution, figure 1.8,[10] only the second crystal structure of a PLP-dependent enzyme to be determined. This structure confirmed the linear arrangement of the subunits in the order αββα. More interesting, though, the structure showed the α- and β- active sites located 25 Å apart from each other and connected by a tunnel that was postulated to allow the free diffusion of indole from the α-active site to the β-active site for the completion of sequential reactions in the biosynthesis of tryptophan. This was the first time that substrate channeling had been

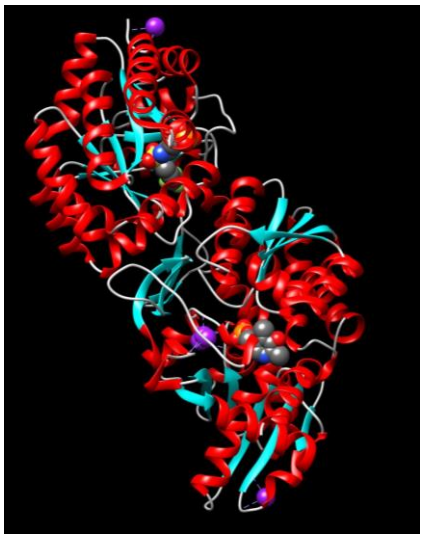

Figure 1.8 The αβ-heterodimer of TS.[10]

definitively shown in an enzyme system, and this finding led to a new level of understanding in the way TS functions.[10] While these breakthroughs into the structure of TS were occurring, other researchers were focused on the catalytic mechanism and the intermediates formed during the β-site reaction. Rapid-scanning stopped-flow (RSSF) experiments performed by the Dunn lab during the same period produced the UV/vis profile of the intermediates formed during the reaction,[86-88] which helped lend credence to the mechanism initially proposed by Miles *et al.* in 1968 for the β-elimination and replacement reaction, scheme 1.3.

Once these initial accomplishments were in place, studies into TS rapidly progressed. Kinetics experiments quickly made it clear that the subunits could be in either an open or closed conformation, with the closed form of the α-subunit associated with movements in residues α176-196 (α-loop L6) that change the conformation of the subunit from disordered/open to ordered/closed, and the closed conformation of the β-subunit occurring when the so-called COMM domain of the subunit moves, forming a salt bridge between residues βArg141 and βAsp305.[89-94] Catalysis requires a switch from the open

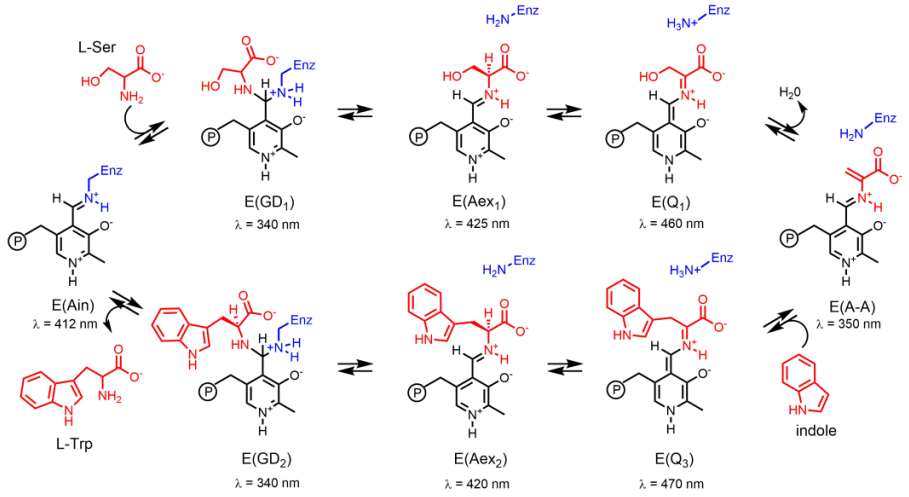

Scheme 1.3 The proposed mechanism for the reaction catalyzed in the β-subunit of TS. The wavelength of maximum absorbance for each intermediate is given for each structure.

to the closed conformations of the subunits for proper formation of the tunnel and to prevent the loss of indole once it is formed in the α-active site.[93,95] These switches in conformation are subject to tight allosteric regulations that rely on communication between subunits in the form of substrate and ligand binding to trigger the conformational switch.[95-97] The kinetics work ultimately led researchers to tease out the order of events in the conformational changes that ensures successful catalysis. In the resting state of the enzyme, both subunits are in the open conformation, and it is possible for either IGP or serine to bind to their respective active sites. Next, binding of IGP to the α-active site closes the α-subunit. This triggers the reaction that occurs in the β-active site to begin by eliminating the β-hydroxyl of serine and forming the α-aminoacrylate intermediate. The formation of the α-aminoacrylate intermediate triggers the α-site reaction, IGP is cleaved, and indole is channeled to the β-subunit, whose closure was also triggered by the formation of this intermediate.[98] The formation of the quinonoid in the β-subunit lowers the affinity of the α-site for G3P, which is then released, opening the α-subunit. The release of G3P prompts the release of tryptophan in the β-site, opening the subunit and returning the protein to its native resting conformation.[91,92,95-97]

Factors other than ligand biding were soon shown to affect the transition from open to closed conformations and the relative stability of intermediates formed during the catalytic transition. The need for a monovalent cation (MVC) to aid in allosteric communication between the subunits had been demonstrated,[96,99-101] and later studies showed while MVCs like Na^+ and K^+, helped to stabilize the open conformation of the enzyme, NH_4^+ and Cs^+ stabilized the closed conformation, allowing for intermediate trapping and leading to greater longevity of intermediates like the α-aminoacrylate.[102-104]

The fact that the α-subunit would close upon binding of the α-site ligand IGP led to the synthesis of novel α-site ligands that promoted the closed conformation of the subunit, but inhibited catalysis.[105] The most effective of these α-site ligands N-(4′-Trifluoromethoxybenzenesulfonyl)-2-aminoethyl phosphate, or F9, had such a stabilizing influence on the α-subunit that it allowed a crystal structure of TS to be collected in which F9 bound at the α-site maintained it in a closed conformation, and the use of Cs^+ and the β-site ligand serine kept the β-subunit in the closed conformation, the first closed crystal structure to not use a mutant. The PLP-serine complex in this structure was clearly in the α-aminoacrylate intermediate form, with the newly formed water molecule seen as a crystallographic water in the structure.[106] This α-site ligand proved so pivotal in the advancement of mechanistic studies that other substrate analogues for serine and indole were sought as a way to extend the lifetimes of intermediates formed during the β-site reaction. Analogues for serine include L-His, D-His, and L-Ala,[107] while analogues for indole that help to stabilize different intermediates include aniline, indoline, and 2-aminophenol.[88,103,104,108,109] The nucleophile benzimidazole (BZI) was initially thought to be a good analogue for indole, but studies showed that it actually acts as an inhibitor, binding in the β-subunit active site and shutting down catalysis, which leads to extended stabilization of the α-aminoacrylate intermediate.[88] These stable intermediates and long-lived complexes provide the opportunity to study reaction mechanism in TS for extended periods of time.

More recent studies on TS have involved more advanced methods like NMR as they have become accessible to such large protein systems. The use of ^{13}C-labeled serine allowed for direct detection of the α-aminoacrylate intermediate and also confirmed the increased affinity of PLP for serine upon binding of the α-site ligand.[110]

Selective labeling of specific amino acids in the tunnel region of the enzyme showed the conformational switch of the subunits upon substrate binding using rotational echo double resonance (REDOR) experiments, which also acted as a probe of the allosteric communication in the enzyme.[111] Further work probed the changes in structure associated with the switching from open to closed conformations using heteronuclear single quantum coherence (HSQC) experiments designed to measure the distance between protons and labeled ^{15}N atoms in residues known to be involved in the stabilization of the closed form of the protein.[102] Fluorine experiments showed the possibility of four combinations of open/closed states over the four subunits, with the ^{19}F signal coming from the F9 inhibitor in the α-subunit.[109] These NMR studies focused on global, large-scale changes in the enzyme that could be probed using methods suitable for measuring dynamics in large protein systems, but did not highlight the reactions occurring in the respective active sites.

The application of NMR crystallography to the TS bienzyme complex reopened the question of reaction specificity in PLP-dependent enzymes. Researchers wanted to probe specifically the idea that the acid-base chemistry in the enzyme active site helped to direct reaction outcome in TS; therefore it was necessary to know the locations of all protons on the ionizable sites throughout the reaction, information that cannot be gained with X-ray crystallography alone. Using a highly complementary combination of X-ray crystallography, computational chemistry, and solid-state NMR, researchers in the

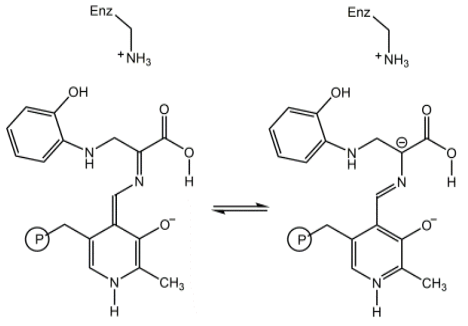

Figure 1.9 The acid form tautomer of the second quinonoid in the PLP-substrate complex in TS.[3]

Mueller lab were able to suggest a mechanism that involved the formation of the acid-form in the second quinonoid intermediate.[3,112] This elegant theory explained that during catalysis a proton in the active site pocket is transferred to the carboxylic acid functional group of the serine substrate, the function of which is to create an electric field gradient and to stabilize negative charge developed over the course of the reaction. This tautomer was postulated to increase the negative charge at C^{α}, helping to direct the proton to that site in the next step of catalysis, while the protonated phenolic tautomer was not present with any appreciable population, figure 1.9.

The acid form theory in TS gave a rationale for the dominance of one tautomer over another in the course of catalysis, and researchers wondered if the same types of tautomerization and acid-base chemistry were responsible for the chemistry that occurred at other steps in the mechanism. Herein, the technique of solid-state NMR (ssNMR) is applied to three stable intermediates in the TS catalytic cycle: the internal aldimine resting form, the α-aminoacrylate intermediate, and the 2-aminophenol quinonoid intermediate. Results from these experiments point to a revised mechanism in the TS β-subunit that explains reaction specificity in this enzyme and also adds to the greater overall understanding of PLP-dependent enzymes. Furthermore, the methods applied here to TS serve as a framework for the investigation of mechanistic pathways in enzymes in general.

1.4 References

(1) Dunathan, H. C. *P Natl Acad Sci USA* **1966**, *55*, 712.

(2) Toney, M. D. *Arch Biochem Biophys* **2005**, *433*, 279.

(3) Lai, J. F.; Niks, D.; Wang, Y. C.; Domratcheva, T.; Barends, T. R. M.; Schwarz, F.; Olsen, R. A.; Elliott, D. W.; Fatmi, M. Q.; Chang, C. E. A.; Schlichting, I.; Dunn, M. F.; Mueller, L. J. *J Am Chem Soc* **2011**, *133*, 4.

(4) Sharif, S.; Powell, D. R.; Schagen, D.; Steiner, T.; Toney, M. D.; Fogle, E.; Limbach, H. H. *Acta Crystallogr B* **2006**, *62*, 480.

(5) Griswold, W. R.; Toney, M. D. *J Am Chem Soc* **2011**, *133*, 14823.

(6) Arnone, A.; Christen, P.; Jansonius, J. N.; Metzler, D. E. In *Transaminases*; Christen, P., Metzler, D. E., Eds.; John Wiley & Sons, Inc.: New York, 1985, p 326.

(7) Miles, E. W.; Hatanaka, M.; Crawford, I. P. *Biochemistry* **1968**, *7*, 2742.

(8) Metzler, D. E.; Ikawa, M.; Snell, E. E. *J Am Chem Soc* **1954**, *76*, 648.

(9) Wilson, D. A.; Crawford, I. P. *J Biol Chem* **1965**, *240*, 4801.

(10) Hyde, C. C.; Ahmed, S. A.; Padlan, E. A.; Miles, E. W.; Davies, D. R. *J Biol Chem* **1988**, *263*, 17857.

(11) Toney, M. D. *BBA - Proteins Proteom* **2011**, *1814*, 1407.

(12) Percudani, R.; Peracchi, A. *EMBO Rep* **2003**, *4*, 850.

(13) Snell, E. E. *Physiol Rev* **1953**, *33*, 509.

(14) Braunstein, A. E. In *The Enzymes Second Edition*; Boyer, P. D., Lardy, H., Myrback, K., Eds.; Academic Press, Inc.: New York, NY, 1960; Vol. 2, p 113.

(15) Schneider, G.; Kack, H.; Lindqvist, Y. *Structure* **2000**, *8*, R1.

(16) Wang, L.; Ota, N.; Romanova, E. V.; Sweedler, J. V. *J Biol Chem* **2011**, *286*, 13765.

(17) Gyorgy, P. *Nature* **1934**, *133*, 498.

(18) *International Symposium on Vitamin B_6*; Harris, R. S.; Wool, I. G.; Loraine, J. A., Eds.; Academic Press, Inc.: New York, NY, 1964.

(19) Wiss, O.; Weber, F. In *International Symposium on Vitamin B_6*; Harris, R. S., Wool, I. G., Loraine, J. A., Eds.; Academic Press: New York, NY, 1964.

(20) Snell, E. E.; Di Mari, S. J. In *The Enzymes Third Edition*; Boyer, P. D., Ed.; Academic Press, Inc.: New York, NY, 1970; Vol. 2, p 335.

(21) Heinert, D.; Martell, A. E. *J Am Chem Soc* **1959**, *81*, 3933.

(22) Nakamoto, K.; Martell, A. E. *J Am Chem Soc* **1959**, *81*, 5857.

(23) Nakamoto, K.; Martell, A. E. *J Am Chem Soc* **1959**, *81*, 5863.
(24) Christensen, H. N. *J Am Chem Soc* **1958**, *80*, 99.

(25) Heinert, D.; Martell, A. E. *J Am Chem Soc* **1963**, *85*, 1334.

(26) Metzler, D. E. *J Am Chem Soc* **1957**, *79*, 485.

(27) Heinert, D.; Martell, A. E. *J Am Chem Soc* **1963**, *85*, 188.

(28) Heinert, D.; Martell, A. E. *J Am Chem Soc* **1963**, *85*, 183.

(29) Auld, D. S.; Bruice, T. C. *J Am Chem Soc* **1967**, *89*, 2090.

(30) Auld, D. S.; Bruice, T. C. *J Am Chem Soc* **1967**, *89*, 2098.

(31) Fischer, E. H.; Kent, A. B.; Snyder, E. R.; Krebs, E. G. *J Am Chem Soc* **1958**, *80*, 2906.

(32) Hughes, R. C.; Jenkins, W. T.; Fischer, E. H. *P Natl Acad Sci USA* **1962**, *48*, 1615.

(33) Cordes, E. H.; Jencks, W. P. *Biochemistry* **1962**, *1*, 773.

(34) Snell, E. E.; Jenkins, W. T. *J Cell Comp Physiol* **1959**, *54*, 161.

(35) Davis, L.; Metzler, D. E. In *The Enzymes Third Edition*; Boyer, P. D., Ed.; Academic Press, Inc.: New York, NY, 1972; Vol. 7, p 33.

(36) Ayling, J. E.; Dunathan, H. C.; Snell, E. E. *Biochemistry* **1968**, *7*, 4537.

(37) Bailey, G. B.; Chotamangsa, O.; Vuttivej, K. *Biochemistry* **1970**, *9*, 3243.

(38) Bailey, G. B.; Kusamrar.T; Vuttivej, K. *Fed Proc* **1970**, *29*, A857.

(39) Dunathan, H. C. *Adv Enzymol Relat Areas Mol Biol* **1971**, *35*, 79.

(40) Sukharev.Bs; Dunathan, H. C.; Braunste.Ae *FEBS Lett* **1971**, *15*, 241.

(41) Voet, J. G.; Hindenlang, D. M.; Blanck, T. J. J.; Ulevitch, R. J.; Kallen, R. G.; Dunathan, H. C. *J Biol Chem* **1973**, *248*, 841.

(42) Tumanyan, V. G.; Mamaeva, O. K.; Bocharov, A. L.; Ivanov, V. I.; Karpeisky, M. Y.; Yakovlev, G. I. *Eur J Biochem* **1974**, *50*, 119.

(43) O'Leary, M. H.; Payne, J. R. *J Biol Chem* **1976**, *251*, 2248.

(44) Harruff, R. C.; Jenkins, W. T. *Org Magn Resonance* **1976**, *8*, 548.

(45) Ford, G. C.; Eichele, G.; Jansonius, J. N. *P Natl Acad Sci USA* **1980**, *77*, 2559.

(46) Shaw, J. P.; Petsko, G. A.; Ringe, D. *Biochemistry* **1997**, *36*, 1329.

(47) Grishin, N. V.; Phillips, M. A.; Goldsmith, E. J. *Protein Sci* **1995**, *4*, 1291.

(48) Griswold, W. R.; Fisher, A. J.; Toney, M. D. *Biochemistry* **2011**, *50*, 5918.

(49) Schnackerz, K. D.; Andi, B.; Cook, P. F. *BBA - Protein Proteom* **2011**, *1814*, 1447.

(50) Hayashi, H. *J Biochem* **1995**, *118*, 463.

(51) Lorente, P.; Shenderovich, I. G.; Golubev, N. S.; Denisov, G. S.; Buntkowsky, G.; Limbach, H.-H. *Magn Reson Chem* **2001**, *39*, S18.

(52) Tolstoy, P. M.; Smirnov, S. N.; Shenderovich, I. G.; Golubev, N. S.; Denisov, G. S.; Limbach, H.-H. *J Mol Struct* **2004**, *700*, 19.

(53) Limbach, H.-H.; Pietrzak, M.; Sharif, S.; Tolstoy, P. M.; Shenderovich, I. G.; Smirnov, S. N.; Golubev, N. S.; Denisov, G. S. *Chem Eur J* **2004**, *10*, 5195.

(54) Sharif, S.; Schagen, D.; Toney, M. D.; Limbach, H.-H. *J Am Chem Soc* **2007**, *129*, 4440.

(55) Chan-Huot, M.; Sharif, S.; Tolstoy, P. M.; Toney, M. D.; Limbach, H. H. *Biochemistry* **2010**, *49*, 10818.

(56) Sharif, S.; Huot, M. C.; Tolstoy, P. M.; Toney, M. D.; Jonsson, K. H.; Limbach, H. H. *J Phys Chem B* **2007**, *111*, 3869.

(57) Sharif, S.; Denisov, G. S.; Toney, M. D.; Limbach, H. H. *J Am Chem Soc* **2007**, *129*, 6313.

(58) Golubev, N. S.; Smirnov, S. N.; Tolstoy, P. M.; Sharif, S.; Toney, M. D.; Denisov, G. S.; Limbach, H. H. *J Mol Struct* **2007**, *844*, 319.

(59) Limbach, H. H.; Chan-Huot, M.; Sharif, S.; Tolstoy, P. M.; Shenderovich, I. G.; Denisov, G. S.; Toney, M. D. *BBA - Proteins Proteom* **2011**, *1814*, 1426.

(60) Chan-Huot, M.; Dos, A.; Zander, R.; Sharif, S.; Tolstoy, P. M.; Compton, S.; Fogle, E.; Toney, M. D.; Shenderovich, I.; Denisov, G. S.; Limbach, H. H. *J Am Chem Soc* **2013**, *135*, 18160.

(61) Sharif, S.; Fogle, E.; Toney, M. D.; Denisov, G. S.; Shenderovich, I. G.; Buntkowsky, G.; Tolstoy, P. M.; Huot, M. C.; Limbach, H. H. *J Am Chem Soc* **2007**, *129*, 9558.

(62) Richard, J. P.; Amyes, T. L.; Crugeiras, J.; Rios, A. *Curr Opin Chem Biol* **2009**, *13*, 475.

(63) Lin, Y. L.; Gao, J. L.; Rubinstein, A.; Major, D. T. *BBA - Proteins Proteom* **2011**, *1814*, 1438.

(64) Major, D. T.; Gao, J. L. *J Am Chem Soc* **2006**, *128*, 16345.

(65) Rubinstein, A.; Major, D. T. *Biochemistry* **2010**, *49*, 3957.

(66) Tatum, E. L.; Bonner, D. *P Natl Acad Sci USA* **1944**, *30*, 30.

(67) Umbreit, W. W.; Wood, W. A.; Gunsalus, I. C. *J Biol Chem* **1946**, *165*, 731.

(68) Fildes, P. *Brit J Exp Pathol* **1941**, *22*, 293.

(69) Crawford, I. P.; Yanofsky, C. *P Natl Acad Sci USA* **1958**, *44*, 1161.

(70) Henning, U.; Helinski, D. R.; Chao, F. C.; Yanofsky, C. *J Biol Chem* **1962**, *237*, 1523.

(71) Yanofsky, C.; Rachmeler, M. *Biochim Biophys Acta* **1958**, *28*, 640.

(72) Demoss, J. A. *Biochim Biophys Acta* **1962**, *62*, 279.

(73) Creighton, T. E.; Yanofsky, C. *J Biol Chem* **1966**, *241*, 980.

(74) Goldberg, M. E.; Baldwin, R. L. *Biochemistry* **1967**, *6*, 2113.

(75) Yanofsky, C.; Crawford, I. P. In *The Enzymes Third Edition*; Boyer, P. D., Ed.; Academic Press, Inc.: New York, NY, 1972; Vol. 7, p 1.

(76) Chargaff, E.; Sprinson, D. B. *J Biol Chem* **1943**, *151*, 273.

(77) Tatum, E. L.; Shemin, D. *J Biol Chem* **1954**, *209*, 671.

(78) Crawford, I. P.; Ito, J. *P Natl Acad Sci USA* **1964**, *51*, 390.

(79) Matchett, W. H. *J Biol Chem* **1974**, *249*, 4041.

(80) Miles, E. W.; Moriguchi, M. *J Biol Chem* **1977**, *252*, 6594.

(81) Nichols, B. P.; Yanofsky, C. *P Natl Acad Sci USA* **1979**, *76*, 5244.

(82) Crawford, I. P.; Nichols, B. P.; Yanofsky, C. *J Mol Biol* **1980**, *142*, 489.

(83) Ibel, K.; May, R. P.; Kirschner, K.; Lane, A. N.; Szadkowski, H.; Dauvergne, M. T.; Zulauf, M. *Eur J Biochem* **1985**, *151*, 505.

(84) Lane, A. N.; Kirschner, K. *Eur J Biochem* **1983**, *129*, 675.

(85) Wilhelm, P.; Pilz, I.; Lane, A. N.; Kirschner, K. *Eur J Biochem* **1982**, *129*, 51.

(86) Drewe, W. F., Jr.; Dunn, M. F. *Biochemistry* **1985**, *24*, 3977.

(87) Drewe, W. F., Jr.; Dunn, M. F. *Biochemistry* **1986**, *25*, 2494.

(88) Roy, M.; Miles, E. W.; Phillips, R. S.; Dunn, M. F. *Biochemistry* **1988**, *27*, 8661.

(89) Dunn, M. F.; Roy, M.; Robustell, B.; Aguilar, V. In *Biochemistry of Vitamin B_6*; Korpela, T., Christen, P., Eds.; Birkhauser Verlag Basel: Switzerland, 1987; Vol. 1, p 171.

(90) Houben, K. F.; Dunn, M. F. *Biochemistry* **1990**, *29*, 2421.

(91) Brzovic, P. S.; Sawa, Y.; Hyde, C. C.; Miles, E. W.; Dunn, M. F. *J Biol Chem* **1992**, *267*, 13028.

(92) Brzovic, P. S.; Hyde, C. C.; Miles, E. W.; Dunn, M. F. *Biochemistry* **1993**, *32*, 10404.

(93) Miles, E. W. *J Biol Chem* **1991**, *266*, 10715.

(94) Kirschner, K.; Lane, A. N.; Strasser, A. W. *Biochemistry* **1991**, *30*, 472.

(95) Brzovic, P. S.; Ngo, K.; Dunn, M. F. *Biochemistry* **1992**, *31*, 3831.

(96) Leja, C. A.; Woehl, E. U.; Dunn, M. F. *Biochemistry* **1995**, *34*, 6552.

(97) Peracchi, A.; Bettati, S.; Mozzarelli, A.; Rossi, G. L.; Miles, E. W.; Dunn, M. F. *Biochemistry* **1996**, *35*, 1872.

(98) Dunn, M. F.; Aguilar, V.; Brzovic, P.; Drewe, W. F.; Houben, K. F.; Leja, C. A.; Roy, M. *Biochemistry* **1990**, *29*, 8598.

(99) Woehl, E.; Dunn, M. F. *Biochemistry* **1999**, *38*, 7131.

(100) Woehl, E.; Dunn, M. F. *Biochemistry* **1999**, *38*, 7118.

(101) Weber-Ban, E.; Hur, O.; Bagwell, C.; Banik, U.; Yang, L. H.; Miles, E. W.; Dunn, M. F. *Biochemistry* **2001**, *40*, 3497.

(102) Ferrari, D.; Niks, D.; Yang, L. H.; Miles, E. W.; Dunn, M. F. *Biochemistry* **2003**, *42*, 7807.

(103) Dierkers, A. T.; Niks, D.; Schlichting, I.; Dunn, M. F. *Biochemistry* **2009**, *48*, 10997.

(104) Harris, R. M.; Dunn, M. F. *Biochemistry* **2002**, *41*, 9982.

(105) Ngo, H.; Harris, R.; Kimmich, N.; Casino, P.; Niks, D.; Blumenstein, L.; Barends, T. R.; Kulik, V.; Weyand, M.; Schlichting, I.; Dunn, M. F. *Biochemistry* **2007**, *46*, 7713.

(106) Ngo, H.; Kimmich, N.; Harris, R.; Niks, D.; Blumenstein, L.; Kulik, V.; Barends, T. R.; Schlichting, I.; Dunn, M. F. *Biochemistry* **2007**, *46*, 7740.

(107) Houben, K. F.; Kadima, W.; Roy, M.; Dunn, M. F. *Biochemistry* **1989**, *28*, 4140.

(108) Hur, O.; Niks, D.; Casino, P.; Dunn, M. F. *Biochemistry* **2002**, *41*, 9991.

(109) Niks, D.; Hilario, E.; Dierkers, A.; Ngo, H.; Borchardt, D.; Neubauer, T. J.; Fan, L.; Mueller, L. J.; Dunn, M. F. *Biochemistry* **2013**, *52*, 6396.

(110) Mcdowell, L. M.; Lee, M. S.; Schaefer, J.; Anderson, K. S. *J Am Chem Soc* **1995**, *117*, 12352.

(111) McDowell, L. M.; Lee, M. S.; McKay, R. A.; Anderson, K. S.; Schaefer, J. *Biochemistry* **1996**, *35*, 3328.

(112) Mueller, L. J.; Dunn, M. F. *Acc Chem Res* **2013**, *46*, 2008.

Chapter 2 – A Brief Introduction to Nuclear Magnetic Resonance

2.1 Introduction

The theory of nuclear magnetic resonance (NMR) has been extensively developed and is covered in several classic texts.[1-4] Below, I highlight the aspects most pertinent to this thesis.

The nuclei of many atoms possess an intrinsic property known as "spin" and are described by a spin quantum number, I. A nucleus with spin angular momentum, $\mathbf{I}$, has an associated magnetic dipole moment, **μ**, modulated by the isotope-specific gyromagnetic ratio, γ:

$$\hat{\boldsymbol{\mu}} = \gamma\hat{\mathbf{I}} = \gamma\hbar[I(I+1)]^{1/2} \ , \qquad \text{(Equation 2.1)}$$

where I is a half-integer value representing the quantization of rotational energy levels in a given system. The gyromagnetic ratio is a way of measuring how magnetic a given isotope is. A nucleus with a nonzero I-value is considered NMR active and will display (2I + 1) degenerate spin states whose degeneracy is broken when placed in an external magnetic field, $\mathbf{B_0}$. For a spin-1/2 nucleus, the only type considered herein, the system will split into two spin states, known as the Zeeman splitting, one with lower energy aligned with the field, $|\alpha\rangle$, and one with higher energy aligned against the field, $|\beta\rangle$, figure 2.1, for isotopes with a positive value of γ. The majority of biologically relevant atoms possess at least one isotope with spin-1/2, including ^{1}H, ^{13}C, ^{15}N, and

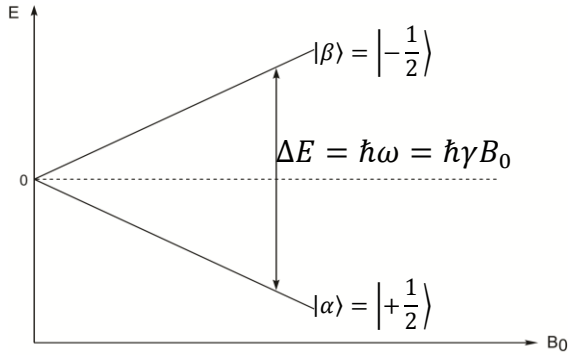

Figure 2.1 The Zeeman splitting exhibited by a spin-1/2 nucleus in a magnetic field.

^{31}P. At natural abundance, nearly 100% of ^{1}H and ^{31}P atoms are NMR active, while ^{13}C and ^{15}N are far more scarce, at 1.11% and 0.37%, respectively, of their respective nuclei.

The effect of a magnetic field on the magnetic moment is to produce a torque on the magnetic moment, leading to a rotation about the field, conventionally defined as the positive z-direction, figure 2.2. This rotation is called free precession, and the rate of rotation, or angular velocity, ω_0, is known as the Larmor frequency, equation 2.2. The Larmor frequency is related to the energy splitting

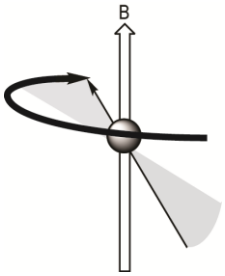

Figure 2.2 A spin-1/2 nucleus in an external magnetic field, B, will experience free precession about the field. Adapted from Levitt.[4]

$$\omega_0 = -\gamma B_0 \qquad \text{(Equation 2.2)}$$

between the spin states, which in terms of the Hamiltonian for the quantum mechanical treatment of the system can be written as shown in equation 2.3.The signal in NMR is generated when a nucleus is hit with a

$$\widehat{H_0^{static}} = \omega_0 \widehat{I_z} \qquad \text{(equation 2.3)}$$

$$\widehat{H_0}|\alpha\rangle = +\frac{\hbar}{2}\omega_0|\alpha\rangle$$

$$\widehat{H_0}|\beta\rangle = -\frac{\hbar}{2}\omega_0|\beta\rangle$$

photon of energy $\hbar\omega_0$ that matches the energy difference between the α- and β-spin

$$\Delta E = \hbar\omega_0 = \hbar\gamma B_0 \qquad \text{(Equation 2.4)}$$

states, figure 2.1 and equation 2.4. Because the α-spin state has slightly lower energy than the β-spin state, the α-state has a higher population, N, resulting in a population difference between the states governed by the Boltzmann constant and temperature, equation 2.5. At equilibrium, this population difference creates a bulk magnetization $\mathbf{M_0}$

in the sample (even a dilute NMR sample still has ~10^{17} spins) that is aligned along the

$$\frac{N_\alpha}{N_\beta} = e^{\frac{\Delta E}{k_B T}} \qquad \text{(Equation 2.5)}$$

z-axis. It is this bulk magnetization upon which NMR experiments are performed.

As seen in equation 2.2, the Larmor frequency is directly proportional to the magnetic field at which experiments are being performed, creating complications when comparing data recorded at different magnetic field strengths. NMR absorptions are typically reported in units of ppm based on the B_0-independent chemical shift scale. The ppm scale relies on a reference compound whose resonance is set to an agreed-upon value. All other signals are reported in relation to the reference compound. To convert the angular frequency to ppm, the following expression is used:

$$\delta(ppm) = 10^6 \times \frac{\omega - \omega_{ref}}{\omega_{ref}} \qquad \text{(Equation 2.6)}$$

The chemical shift scale allows for comparison of different types of the same nucleus. For example, a methyl carbon will have a very different resonance than a carbonyl carbon. A single spectrum will have signals from all the different types of nuclei, and the chemical shift scale provides a convenient, field independent way to report these differences.

To observe magnetization and perform useful experiments, the magnetization of the sample must be brought into the transverse plane, as magnetization along the z-axis is not detectable. This is accomplished by irradiating the sample with radiofrequency waves for a set amount of time. The rf pulse, as it is called, rotates the sample magnetization with angular frequency ω_1 into the transverse plane. A 90° pulse along the x-axis, for example, will result in magnetization being rotated to the –y-axis, while a 180° pulse puts magnetization along the –z-axis, which would again be undetectable.

Quantum mechanically, the effect of an x- or y-pulse is to create coherent superpositions of spin states that are no longer eigenstates of the Hamiltonian and therefore evolve in time as described by the time-dependent Schrodinger equation. Again, it is the energy difference between the eigenstates that governs this time-evolution. At the same time, the non-equilibrium magnetization relaxes slowly back to equilibrium, and the rate of return is exploited regularly to determine dynamics of chemical systems.

In multi-spin systems, the nuclei can interact, or couple, with each other in two different ways: J-coupling and dipolar coupling. J-coupling is also known as through-bond coupling, and all the experiments discussed herein employ high-power proton decoupling[8] to eliminate both the effects of J-coupling and dipolar coupling due to protons from the spectrum. Dipolar coupling is a through-space magnetic-dipole – magnetic-dipole interaction that describes how the magnetic dipole field of one nucleus influences the total magnetic field felt by its neighboring nuclei. This interaction is distance dependent, falling off with the cube of the distance between the two nuclei, and is inherently anisotropic. In a solution state sample, rapid isotropic tumbling averages out this interaction. A static solid-state sample, however, will exhibit significant line-broadening due to the orientationally-dependent dipolar coupling. In polycrystalline or powdered samples, each orientation would have a unique dipolar coupling and the sum of the resulting spectra for the different spatial orientations of the sample gives rise to a characteristically broad peak known as

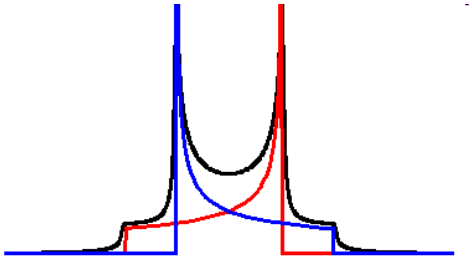

Figure 2.3 A Pake doublet forms due to dipolar coupling.

a Pake doublet,[9] figure 2.3. In the case of heteronuclear dipolar coupling, the only case considered herein, only the z-component of the spin angular momentum **I** plays a role in the interaction, equation 2.7. In this equation, Θ_{jk} is the angle of the internuclear vector

$$\hat{H}_{jk}^{DD}(\Theta_{jk}) = d_{jk} 2\hat{I}_{jz}\hat{I}_{kz}, \qquad \text{(Equation 2.7)}$$
$$where\ d_{jk} = b_{jk}\frac{1}{2}\left(3\cos^2\Theta_{jk} - 1\right),$$
$$and\ b_{jk} = -\frac{\mu_0}{4\pi}\frac{\gamma_j\gamma_k\hbar}{r_{jk}^3}$$

with respect to the z-axis, figure 2.4, and b_{jk} is the dipole-dipole coupling constant, which depends on the distance between the spins.

Dipolar coupling is not the only parameter to have adverse effects line shapes in the solid state. The chemical shift parameter is also anisotropic, and in the absence of rapid tumbling, the chemical shift anisotropy (CSA) contributes significant line broadening to the signal, a consequence of multiple orientations of the solid being present in the sample. Each orientation leads to a unique chemical shift, only slightly different than all the others, and the sum of these signal results in a powder pattern line shape, figure 2.5. The chemical shift Hamiltonian can be seen in equation 2.8:

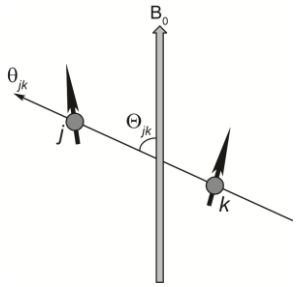

Figure 2.4 Schematic depicting the internuclear dipolar coupling vector. Adapted from Levitt.[4]

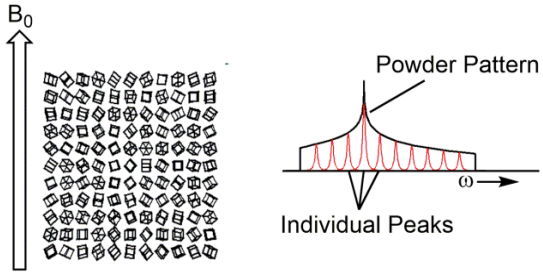

Figure 2.5 A solid powder sample will exhibit a broad powder pattern as a result of each possible crystallite orientation. Reprinted from Levitt.[4]

$$\hat{H}_j^{CS} = -\gamma_j\overline{\delta_{zz}^J(\Theta)}B_0\hat{I}_{jz}\ , \qquad \text{(Equation 2.8)}$$

which explicitly shows the dependence of the shift on the orientation of the crystal with respect to the magnetic field.

2.2 Magic Angle Spinning (MAS)

The broad powder patterns associated with solid-state NMR diminish resolution and, ultimately, the amount of useful information that can be extracted from these spectra in multi-spin systems. However, inspection of equation 2.7 reveals that there should be some value of Θ_{jk} that makes the expression $\left(3\cos^2\Theta_{jk} - 1\right)$ equal to zero. Indeed, that is that case. When Θ_{jk} is set to the "magic angle" of 54.74°, the dipolar interaction is averaged to zero, much as in a rapidly tumbling solution-state sample, helping to narrow the linewidth due to the elimination of this interaction. Furthermore, when the sample is rotated at the magic angle, a process known as magic angle spinning (MAS), faster than the magnitude of anisotropic interactions, the spectrum collapses into a narrow isotropic peak with a manifold of spinning side bands that appear at integer intervals of the spinning speed.[10-12] The act of spinning introduces symmetry to the sample, simulating the solution state environment and drastically reducing line width in solid samples by removing anisotropic interactions from the spectrum.

2.3 Rotational Echo Double Resonance (REDOR) Experiments

While magic angle spinning significantly reduces line width in solid-state samples, the concomitant loss of all anisotropic information is not always desirable. For example, the dipolar coupling interaction is dependent on the inverse of cube of the distance between the coupled nuclei. Loss of information about the dipolar interaction also leads to loss of important structural information. Fortunately, experiments have been developed that reintroduce the effects of these interactions to the spectrum. Rotational echo double resonance (REDOR) experiments reintroduce the dipolar interaction between two nuclei to the spectrum, resulting in the dephasing of the signal

corresponding to the dipolar-coupled nucleus.[6] The pulse sequence for the REDOR experiment can be seen in figure 2.6. If we consider only what occurs on the carbon and nitrogen nuclei, we see that after a period of time, a 180° pulse is given on the carbon channel to refocus the magnetization. This is the classic spin echo experiment, and it has the effect of eliminating any inhomogeneity and heteronuclear coupling in the system.[2-4] Meanwhile, the nitrogen nucleus is subjected to a series of rotor-synchronized π-pulses, the effects of which are to reintroduce the dipolar coupling to the spectrum, resulting in a decrease of the intensity of the dipolar-coupled peak.

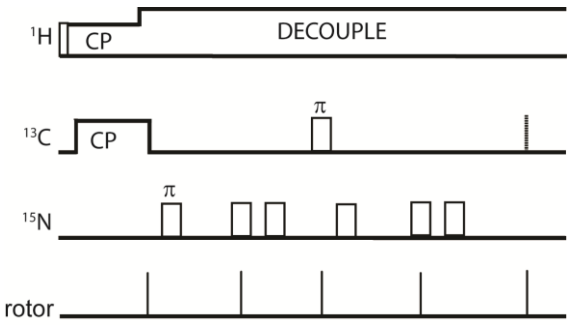

Figure 2.6 The pulse sequence for the REDOR experiment. Adapted from Gullion and Schaefer.[6]

As an example, consider a sample of glycine labeled at the nitrogen and the α-carbon positions. These two nuclei are very near in space, with a bond length

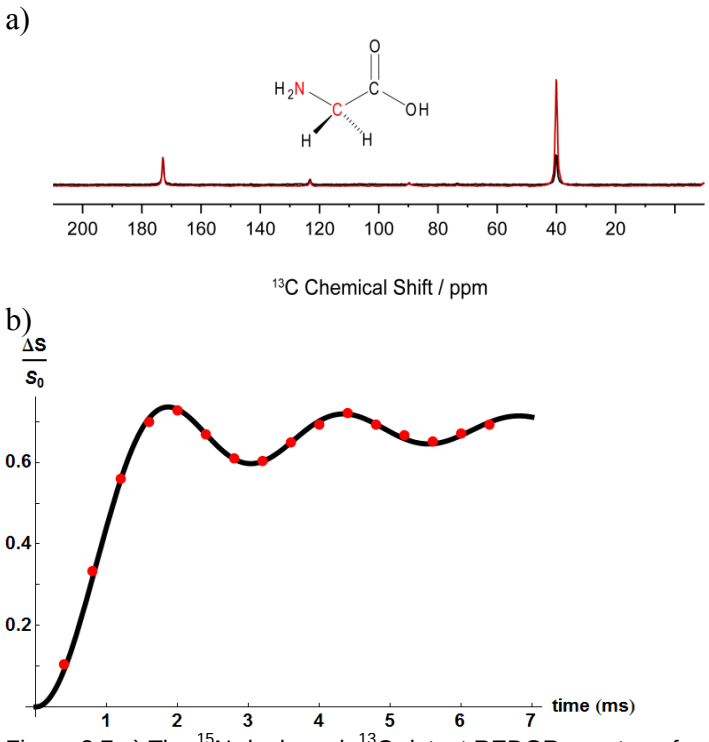

Figure 2.7 a) The ^{15}N-dephased, ^{13}C-detect REDOR spectrum for 2-^{13}C-glycine. There is dephasing of a single resonance at 40 ppm. b) Full dephasing is accomplished after only 2 ms, corresponding to a dipolar coupling constant of 896 Hz and a bond length of 1.5 Å.[7]

of 1.5 Å. The ^{13}C NMR spectrum of this sample can be seen in figure 2.7a. The red spectrum was acquired without the π-pulses on nitrogen, while the black spectrum was recorded after the π-pulses had been applied to nitrogen. The intensity of the peak at 40 ppm corresponding to C^{α} is greatly reduced in the black spectrum due to the reintroduction of dipolar coupling to the system. 2.7b shows the amount of time it takes to reintroduce this interaction to the system.[7] With the proximity of the nitrogen and carbon atoms, it takes only 2 ms to dephase the carbon magnetization, a time correlated with a dipolar coupling of 896 Hz. Figure 2.8a shows glycine labeled on the nitrogen and carbonyl carbon. These atoms are farther apart, separated by a distance of 2.5 Å. Selective dephasing of the carbonyl peak is seen in the black spectrum, though figure 2.8b shows that it took almost 7 ms to achieve this dephasing, consistent with a dipolar interaction of 186 Hz. This is due to the greater distance between the nuclei and the smaller dipolar interaction that exists between them. The

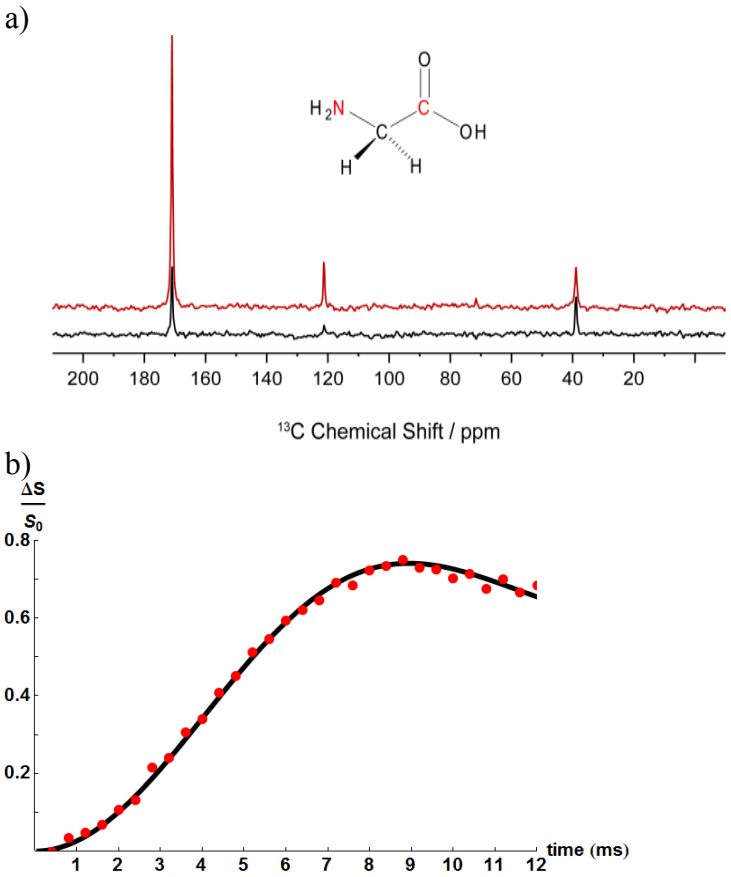

Figure 2.8 a) The ^{15}N-dephased, ^{13}C-detect REDOR spectrum for 1-^{13}C-glycine. There is dephasing of a single resonance at 170 ppm. b) Full dephasing is accomplished after 7 ms, corresponding to a dipolar coupling constant of 186 Hz and a separation of 2.5 Å.[7]

REDOR experiment is one important example of how anisotropic information can be reintroduced even under MAS conditions and how these can lead to greater structural insight.[6]

2.4 Cross Polarization (CP)

The dipolar coupling interaction can also be used to transfer magnetization from one spin type to another in a technique referred to as cross polarization (CP).[13,14] CP is often exploited to observe dilute spins such as ^{13}C and ^{15}N with higher sensitivity. CP begins with an initial 90° pulse on the protons, and the magnetization is then transferred to the carbon nuclei by reintroducing the dipolar coupling between them with simultaneous spin locks on both nuclei, figure 2.6. The major benefit of CP is the increase in signal in the carbon spectrum, but an added benefit is the repetition time of the experiment is now set by the proton relaxation time, which is typically shorter than that for carbon nuclei, greatly speeding up the rate at which experiments can be repeated. Importantly, magnetization can only be transferred between nuclei that are dipolar coupled. In the solid state, this tells us that only nuclei that are not undergoing rapid motion will be able to transfer or receive magnetization effectively. When CP is coupled with MAS (CPMAS), the resulting solid-state spectrum has resolution and sensitivity rivalling (and sometimes exceeding) solution state experiments.[15,16]

2.5 Conclusion

The preceding ideas and techniques will come up repeatedly in the following chapters. This is hardly an exhaustive overview of the topic, rather a brief introduction to some of the concepts mentioned in later chapters. As will be seen, the application of CPMAS to catalytically active tryptophan synthase microcrystals has ushered in a new

understanding of catalysis in that enzyme, underscoring the power of ssNMR as an investigative tool.

2.6 References

(1) Apperley, D. C.; Harris, R. K.; Hodgkinson, P. *Solid State NMR Basic Principles & Practice*; Momentum Press, LLC: New York, 2012.

(2) Claridge, T. D. W. *High Resolution NMR Techniques in Organic Chemistry*; Second ed.; Elsevier, Ltd.: United Kingdom, 2009; Vol. 27.

(3) Keeler, J. *Undestanding NMR Spectroscopy*; Second ed.; John Wiley & Sons, Ltd: United Kingdom, 2010.

(4) Levitt, M. H. *Spin Dynamics: Basics of Nuclear Magnetic Resonance*; Second ed.; John Wiley & Sons, Ltd: United Kingdom, 2008.

(5) Duer, M. J. *Solid-State NMR Spectroscopy Principles and Applications*; Blackwell Science: United Kingdom, 2002.

(6) Gullion, T.; Schaefer, J. *J Magn Reson* **1989**, *81*, 196.

(7) Mueller, K. T. *J Magn Reson, Ser A* **1995**, *113*, 81.

(8) Fung, B. M.; Khitrin, A. K.; Ermolaev, K. *J Magn Reson* **2000**, *142*, 97.

(9) Gutowsky, H. S.; Pake, G. E. *J Chem Phys* **1950**, *18*, 162.

(10) Lowe, I. J. *Phys Rev Lett* **1959**, *2*, 285.

(11) Mehring, M.; Waugh, J. S. *Physical Review B* **1972**, *5*, 3459.

(12) Andrew, E. R. *Prog Nucl Magn Reson Spectrosc* **1971**, *8*, 1.

(13) Pines, A.; Gibby, M. G.; Waugh, J. S. *J Chem Phys* **1973**, *59*, 569.

(14) Pines, A.; Waugh, J. S.; Gibby, M. G. *J Chem Phys* **1972**, *56*, 1776.

(15) Schaefer, J.; Stejskal, E. O. *J Am Chem Soc* **1976**, *98*, 1031.

(16) Stejskal, E. O.; Schaefer, J.; Waugh, J. S. *J Magn Reson* **1977**, *28*, 105.

Chapter 3 – The Internal Aldimine

3.1 Introduction

Pyridoxal-5'-phosphate (PLP), the bioactive form of vitamin B_6, acts as coenzyme in multiple amino acid transformations, including α/β/γ elimination/replacement, racemization, transamination, and decarboxylation.[1,2] At the start of the catalytic cycle, the cofactor is covalently attached to the enzyme through an imine bond to the ε-nitrogen of a lysine sidechain, giving a secondary aldimine, or Schiff base, species referred to as the "internal aldimine," figure 3.1. It has been proposed that a positively charged, protonated Schiff base (PSB) tautomer activates catalysis at this point by forming a significantly more reactive target for nucleophilic attack than the neutral imine,[3-5] while the protonation states of other sites on the coenzyme – the phenolic oxygen and PLP ring nitrogen in particular – are thought to be critical in establishing the specificity of the reaction pathway.[2,6-8] The experimental determination of protonation states within PLP active sites is typically indirect; the two most common methods of characterization, X-ray crystallography and optical spectroscopy, cannot specifically identify proton locations or report unambiguously on the local chemical environment of individual atoms. Nuclear magnetic resonance (NMR) spectroscopy can provide atomic-resolution characterization, but to date only a handful

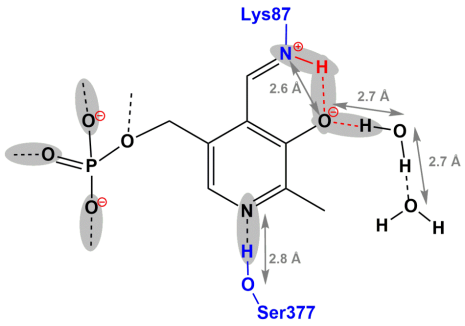

Figure 3.1 Schematic of PLP covalently bound to βLys87 in the β-subunit active site of tryptophan synthase. Distances and water molecules are from the X-ray crystal structure of the S. typhimurium TS internal aldimine state (PDB: 4HT3). The experimentally determined protonation states from solid-state NMR are highlighted in red. Protein residue fragments are shown in blue and PLP and water in black.

of NMR studies have been reported for PLP-dependent enzyme active sites.[9-13] Here we detail the first ^{15}N NMR chemical shift measurements of the Schiff base linkage in the resting holoenzyme state of a PLP-dependent enzyme, the tryptophan synthase internal aldimine complex; these provide the first atomic-resolution observation of the protonated Schiff base tautomer, while additional ^{13}C, ^{15}N, and ^{31}P chemical shift measurements on the coenzyme allow a chemically-detailed model – including all coenzyme protonation states – to be established.

The tryptophan synthase (TS) $\alpha_2\beta_2$ bienzyme complex relies on PLP to bring together indole and L-serine to form L-tryptophan, scheme 3.1.[15-18] Figure 3.1 shows a schematic of the β-subunit active site for the internal aldimine state, E(Ain), with PLP

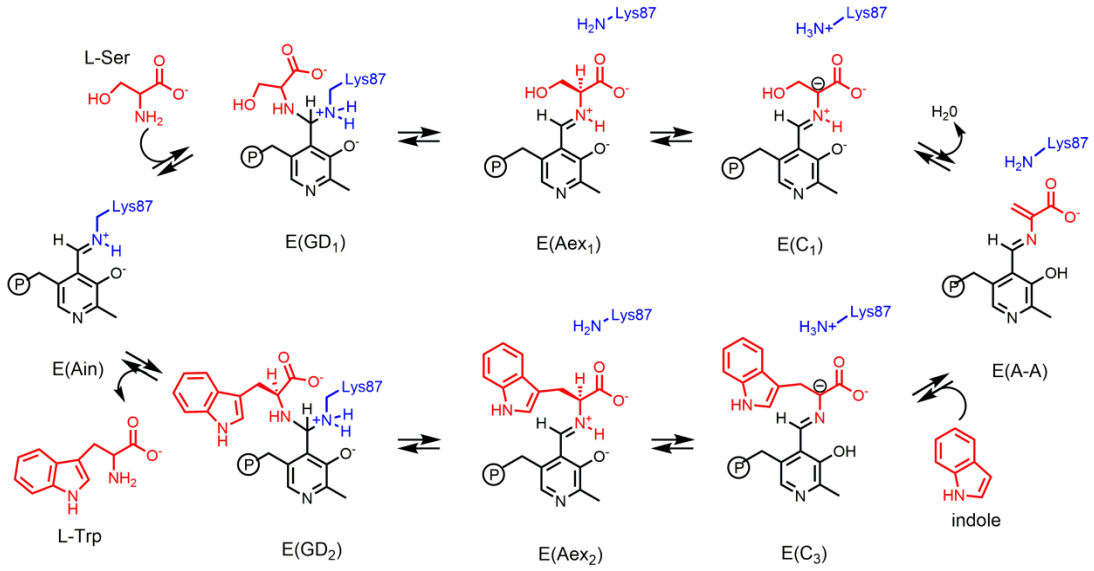

Scheme 3.1 The tryptophan synthase β-site reaction.

covalently bound to βLys87. In TS (as with the vast majority of PLP-dependent enzymes), the first step in catalysis is a transimination reaction in which an amino acid substrate makes a nucleophilic attack at C4' of PLP; this step exchanges the PLP Schiff

base linkage to the protein with one to the substrate. The PSB hypothesis posits that the imine nitrogen should be protonated for reactivity toward nucleophiles at the Schiff base carbon, a hypothesis first proposed to explain the remarkable acceleration of enzyme catalyzed reactions compared to PLP catalyzed reactions in solution.[3]

UV/vis optical spectroscopy of TS supports the PSB hypothesis. Studies of enzyme internal aldimine states and model compounds with Schiff base linkages to peptides and amino acids in polar, aprotic solvents indicate a conjugation best explained by a protonated Schiff base nitrogen.[4,5,19] The internal aldimine complexes of most PLP enzymes give absorption maxima in the 420 to 430 nm range, and the 412 nm λ_{max} exhibited by the TS E(Ain), both in solution and in single crystals, correlates well with the postulate of a Schiff base structure conjugated with the PLP π-system.[20] The UV/vis spectrum of TS is independent of pH over the range 5.8 – 10.4,[20-22] and consequently there is a single ionic form of the E(Ain) β-site and no change in the distribution of tautomeric structures in this pH range.[23] Deprotonation of PLP enzyme Schiff bases causes shifts to shorter wavelength (~360 nm),[24] while deprotonation of the internal aldimine PLP ring nitrogen has only minor effects on the UV/vis spectrum.[25]

The X-ray crystal structures of TS internal aldimine complexes show the Schiff base nitrogen in close proximity to the 3' oxygen of the PLP ring.[26-31] Key distances from the 1.30 Å resolution X-ray crystal structure of the *S. typhimurium* TS E(Ain) (PDB accession code 4HT3[31]) are shown in figure 3.1. The 2.6 Å N-O distance is fully consistent with the presence of a proton in an N-H-O hydrogen bond, but the assignment of donor and acceptor in this bonding system cannot be established directly from the crystal structure. Also apparent, the Schiff base nitrogen is twisted slightly out of the PLP plane, with a C3-C4-C4'-N dihedral angle of 27.2°, and the phenolic oxygen is involved

in a hydrogen bonding network with two crystallographically observed water molecules, indicated in the figure.

While X-ray crystallography and UV/vis spectroscopy suggest a protonated Schiff base form, atomic-resolution probes, such as NMR spectroscopy, have not been applied to directly characterize the linking lysine ε-nitrogen in a PLP-dependent enzyme. NMR chemical shifts are particularly sensitive to local chemical structure; protein and model compound Schiff base nitrogen atoms show changes in chemical shifts greater than 100 ppm upon protonation.[32] NMR spectroscopy on PLP model compounds by Limbach and co-workers has demonstrated that the tautomeric form favored can depend upon the substituent on the Schiff base nitrogen, solute-solvent interactions, the protonation state of the pyridine nitrogen, and hydrogen bonding to the phenolic oxygen.[32-35] For PLP-dependent enzymes, pyridine nitrogen and select carbon atom chemical shifts have been reported for internal aldimines of alanine racemase and aspartate aminotransferase,[11,13] and nitrogen linkages to covalently bound substrates in TS[12] and alanine racemase.[9] Yet no chemical shift measurement for a linking Schiff base nitrogen has been reported for any internal aldimine complex. The challenge to interrogating the Schiff base nitrogen is resolution of this single site within the forest of other peaks. Substrate and coenzyme studies rely on the selective introduction of ^{13}C and ^{15}N-isotopically enriched components to achieve specificity, an approach that is not generally applicable to sidechain sites. Fortunately, the distinct ε-nitrogen chemical shift of a lysine residue covalently bound to the coenzyme can provide resolution of this single site in labeled protein preparations, an approach exploited to study the Schiff base linkage to retinal in bacteriorhodopsin.[36]

3.2 Experimental Details

Preparation of ε-^{15}N-Lys TS and U-^{15}N TS

Tryptophan synthase was expressed and purified as previously described,[37,38] with the following modifications. Bacteria were grown in LB containing tryptone (10 g/L), NaCl (10 g/L), yeast extract (5 g/L), and ampicillin (50 mg/L) until the late log phase (~6 hours, 37 °C) when cells were harvested and transferred to minimal media. Expression was induced through addition of isopropyl β-D-1-thiogalactopyranoside (IPTG) to a final concentration of 0.2 mM in minimal media enriched with 2 g L^{-1} $^{15}NH_4Cl$ (U-^{15}N labeled sample only, Cambridge Isotope Laboratories (CIL)) for 12 hours at 25 °C. Minimal media for unlabeled and ε-15N-Lys TS samples were supplemented with 40 mL unlabeled 10x BioExpress Cell Growth Media (CIL), while U-^{15}N TS samples were supplemented with 40 mL 10x U-^{15}N BioExpress Cell Growth Media (CIL). ε-^{15}N-Lys TS was prepared by addition of 250 mg L-ε-^{15}N-Lys hydrochloride (CIL) to unlabeled minimal media. Microcrystals were prepared by diluting enzyme solution 1:1 with 50 mM Cs-bicine buffer, pH = 7.8 containing 14% PEG-8000 and 3.0 mM spermine as described previously.[37] Microcrystals were collected and washed with 50 mM Cs-bicine, pH 7.8 containing 8% PEG-8000, 1.8 mM spermine, and 3 mM N-(4'-trifluoromethoxybenzenesulfonyl)-2-aminoethyl phosphate (F9; a high affinity alpha site ligand). Magic-angle-spinning rotors were packed at 10,000 rpm, and each rotor contained approximately 25-30 mg of protein.

Preparation of U-^{15}N TS/2,2',3-^{13}C3;^{15}N-PLP

Tryptophan synthase $\alpha_2\beta_2$ subunits were dissociated and reconstituted with labeled PLP as previously described[39] with attention called to the following details. Addition of potassium thiocyanate (KSCN) to a final concentration of 1 M to the enzyme

solution was followed by a five minute wait at room temperature until reaction initiation. Hydroxylamine was then added to a final concentration of 10 mM, followed by five more minutes at room temperature, completing oxime formation. Dissociation was completed with dialysis against Cs-bicine, pH 7.8, containing 1 M KSCN for four hours at 4 °C. This was followed by two more dialyses against plain 50 mM Cs-bicine, pH 7.8, at 4 °C. UV/vis tests on the apoenzyme showed no activity in the presence of substrates. The holoenzyme was resolved by addition of 2,2',3-^{13}C3;^{15}N-PLP, synthesized by our organic collaborators,[40] to the dialyzed protein so the final PLP concentration was three times greater than the protein concentration. This solution was incubated in a water bath at 35 °C for 10 minutes. Re-association of the subunits was completed with direct addition of L-serine to the solution for a final concentration of 15 mM. The enzyme solution was allowed to sit for 10 more minutes in the warm water bath. Final resolution of the enzyme was achieved by then cooling the solution in an ice bath for 30 minutes and dialyzing twice against 50 mM Cs-bicine, pH 7.8, at 4 °C. UV/vis activity tests performed on the reconstituted holoenzyme showed fully active enzyme with 70% recovery of the initial concentration, and incorporation of the 2,2',3-^{13}C3;^{15}N-PLP into the enzyme was verified with both ^{13}C and ^{15}N ssNMR.

Microcrystalline Protein Samples for Solid-State NMR

Microcrystalline samples of TS were prepared by diluting enzyme solution 1:1 with 50 mM Cs-bicine buffer, pH 7.8, containing 14% PEG-8000 and 3.0 mM spermine as previously described.[12] Microcrystals were collected and washed with 50 mM Cs-bicine, pH 7.8, containing 8% PEG-8000, 1.8 mM spermine, and 3 mM N-(4'-trifluoromethoxybenzenesulfonyl)-2-aminoethyl phosphate (F9; a high affinity alpha site ligand and analogue of the natural α-site substrate 3-idole-D-glycerol-3'-phosphate

(IGP)). The crystals were packed at 10,000 rpm into a Bruker 4 mm magic-angle spinning (MAS) rotor with an approximate volume of 80 µL; each rotor contained 25-30 mg of protein.

Chemical Shift Referencing

Solid-state ^{13}C and ^{15}N chemical shifts were indirectly referenced to TMS and liquid-NH_3 following the recommendations outlined in Morcombe and Zilm[41] and Markley *et al*.[42] In brief, the downfield ^{13}C CPMAS peak of solid adamantane was set to 38.48 ppm; this defines a scale on which the corresponding methyl resonance of neat TMS is 0 ppm. The ^{15}N resonance of liquid ammonia was then calculated as the ^{13}C 0 ppm reference frequency multiplied by 10.1329118/25.1450038. On this scale, solid $^{15}NH_4Cl$ was found to resonate at an offset of 39.2 ppm.

Solid-state ^{31}P was indirectly referenced to 85% H_3PO_4 (capillary) following the procedure outlined in Maurer and Kalbitzer.[43] This scale was chosen for direct comparison with the PLP titration results of Schnackerz et al.[44-46] A MAS rotor was first loaded with a 1% solution of DSS in D_2O to determine 0 ppm ^1H (DSS). This frequency was multiplied by 0.404807210 to define the ^{31}P 0 ppm point, corresponding to 85% H_3PO_4 (capillary). For comparison, δ[85% H_3PO_4 (capillary)] = δ[85% H_3PO_4 (sphere)] +0.36 ppm.

NMR Experiments

^{13}C and ^{15}N Solid-State NMR Spectroscopy: ^{13}C and ^{15}N cross-polarization (CP) magic-angle-spinning (MAS) experiments were performed at 9.4 T (400.37 MHz ^1H, 100.69 MHz ^{13}C, 40.57 MHz ^{15}N) on a Bruker AVIII spectrometer equipped with a double resonance, 4 mm MAS probe, spinning at MAS rates of 8 kHz; the bearing gas was cooled to -15 °C, giving an effective sample temperature of ~-5 °C. Cross-polarization

was accomplished at a ^{1}H spin-lock field of 45 kHz and a $^{13}C/^{15}N$ spin-lock of 54 kHz (^{13}C) and 37 kHz (^{15}N) (ramped +/- 2 kHz); 85 kHz Spinal64 ^{1}H decoupling[47] was used throughout. Standard ^{13}C spectra consist of the sum of 16,384 transients acquired with a relaxation delay of 4 s, for a total acquisition time of 18.3 h. ^{13}C chemical shifts were referenced indirectly to neat TMS via an external solid-state sample of adamantane with the downfield-shifted peak set to 38.48 ppm.[41,48] Standard ^{15}N spectra consist of the sum of 81,920 transients acquired with a relaxation delay of 4 s, for a total acquisition time of 3 d 19 h.

The acquisition of solid-state NMR spectra was interleaved with single pulse, low-power decoupling experiments (64 scans ^{13}C, 256 scans ^{15}N) reporting predominantly on free ligand and reaction products in solution (mother liquor). Acquisition of solid-state NMR spectra for the intermediate was halted before reactant concentrations in solution fell to zero.

^{31}P Solid-State NMR Spectroscopy: ^{31}P CPMAS experiments were performed at 14.1 T (600.01 MHz ^{1}H, 242.89 MHz ^{31}P) on a Bruker AVIII spectrometer equipped with a ^{1}H-X double resonance 4 mm MAS probe, spinning at a MAS rate of 10 kHz. The bearing gas was cooled to -15 °C, giving an effective sample temperature of -5 °C. Cross-polarization was accomplished with a ^{1}H spin-lock field of 45 kHz and a ^{31}P spin-lock of 47 kHz (ramped +/- 5 kHz); 58 kHz Spinal64 ^{1}H decoupling[47] was used during detection. The ^{31}P spectra consist of the sum of 4,096 transients acquired with a relaxation delay of 3 s, for a total acquisition time of 3.4 h. ^{31}P chemical shifts were indirectly referenced to 85% H_3PO_4 (MAS). For comparison to measurements in solution, δ[85% H_3PO_4 (capillary)] = δ[85% H_3PO_4 (sphere/MAS)] + 0.36 ppm.

^{15}N-observe, ^{13}C-dephased Rotational Echo Double Resonance (REDOR) Experiments: ^{15}N{^{13}C}-REDOR[49] experiments were performed at 9.4 T (400.37 MHz for ^{1}H, 100.69 MHz for ^{13}C, 40.57 MHz for ^{15}N) on a Bruker AVIII spectrometer equipped with a ^{1}H−^{13}C−^{15}N triple resonance 4 mm MAS probe spinning at a MAS rate of 8 kHz The bearing gas was cooled to -15 °C, giving an effective sample temperature of -5 °C. Cross-polarization was accomplished at a ^{1}H spin-lock field of 45 kHz, ^{15}N spin-lock of 37 kHz (ramped +/- 2 kHz), and a 2 ms contact time; 100 kHz Spinal64 ^{1}H decoupling[47] was used throughout. A single 14 μs π pulse was applied to ^{15}N at the center of the 10 ms echo period, while a series of 14 μs π pulses at half rotor intervals was applied to ^{13}C during the dephasing (*S*) experiments. The REDOR *S* and S_o spectra were acquired in an interleaved fashion, and each spectrum consists of the sum of 81,920 transients acquired with a relaxation delay of 4 s, for a total acquisition time of 3 days 19 h.

3.3 Results and Discussion

Figure 3.2 shows ^{15}N solid-state NMR spectra of catalytically-active *S. typhimurium* tryptophan synthase microcrystals prepared under the following four conditions: (3.2a) natural abundance isotopomer concentration, (3.2b) selectively ^{15}N-enriched at lysine ε-nitrogen sites (ε-^{15}N-Lys TS), (3.2c) selectively ^{13}C/^{15}N enriched at C2, C2', C3 and N1 of the PLP coenzyme (TS/2,2',3-$^{13}C_3$;^{15}N-PLP), and (3.2d/3.2e) uniformly-^{15}N-enriched at protein sites and selectively ^{13}C/^{15}N enriched at C2, C2', C3 and N1 of the PLP coenzyme (U-^{15}N-TS/2,2',3-$^{13}C_3$;^{15}N-PLP). At natural abundance, only signal from the large number of protein backbone nitrogens is observed. Upon incorporation of selectively enriched ε-^{15}N-Lys, two new spectral features are revealed: a large number of mostly overlapped resonances centered at 33 ppm (δ[NH_3(l)] scale), and a single

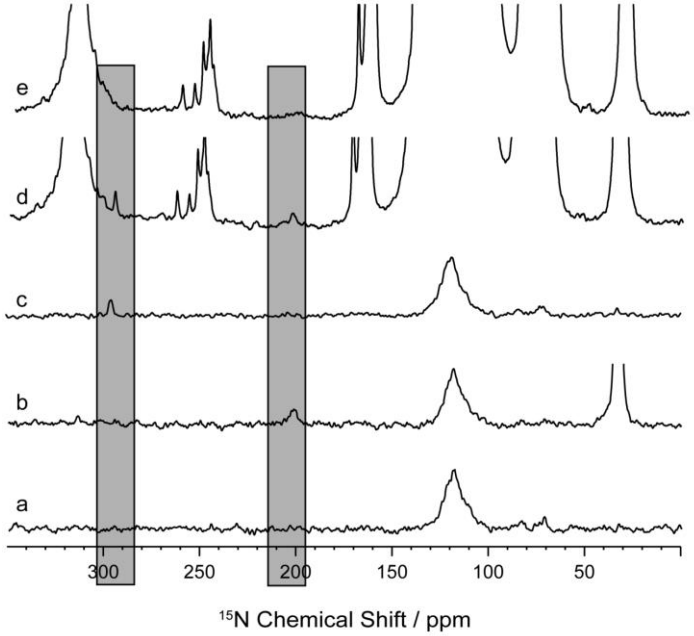

Figure 3.2 ^{15}N-solid-state NMR cross-polarization magic-angle-spinning (CPMAS) spectra of the tryptophan synthase internal aldimine complex used to assign ^{15}N chemical shifts to the linking lysine ε-imine nitrogen (202.3 ppm) and N1 of PLP (294.7 ppm). Data were acquired on microcrystalline samples of S. typhimurium TS prepared with (a) TS at natural abundance isotopomer concentration, (b) ε-^{15}N-Lys TS, (c) natural abundance TS/2,2',3-^{13}C3;^{15}N PLP and (d/e) U-^{15}N TS/2,2',3-^{13}C3;^{15}N PLP. a, b, and c correspond to direct observation after cross-polarization from ^{1}H to ^{15}N, while d and e form a ^{15}N{^{13}C}-REDOR pair; both have a 10 ms echo period after cross-polarization, but differ in the application of π pulses to ^{13}C (at the quarter and three-quarter mark of each rotor period) in e. Spectra acquired at 9.4 T and 8 kHz MAS.

resonance at 202.3 ppm. The former correspond to charged ε-amino groups on the labeled lysine residues that have been incorporated into the protein, whereas the latter resonates at the position of a protonated Schiff base[32] and is tentatively assigned to N$^{\varepsilon}$ of βLys87, the active-site residue that covalently binds PLP. This assignment is confirmed in two ways. First, the Schiff base linkage to βLys87 is broken by addition of the substrate L-serine, which reacts to form an external aldimine intermediate that subsequently loses water to give an aminoacrylate species;[15] upon addition of 5 μL of 1.2 M serine directly to the microcrystalline sample used to obtain the spectrum in figure 3.2b, the peak at 202.3 ppm is lost and a new peak at 24.2 ppm appears, suggestive of a neutral amino lysine sidechain for the aminoacrylate intermediate, figure 3.3. Second, rotational echo double resonance (REDOR)[49] experiments are used to specifically edit out (dephase) ^{15}N resonances that are dipolar coupled to ^{13}C atoms at the 2, 2', and 3

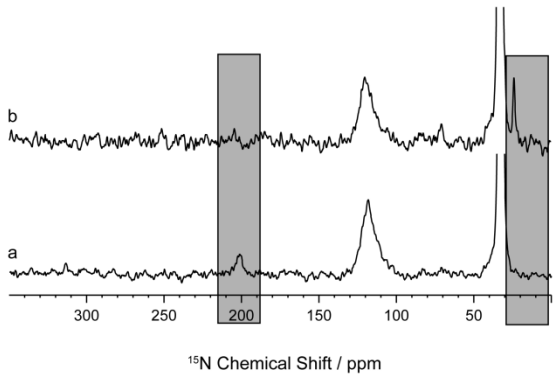

Figure 3.3 ^{15}N ssNMR spectra of the reaction of ε-^{15}N-Lys tryptophan synthase microcrystals and (a) no serine and (b) 75 mM L-Ser. The conditions in (b) give rise to the aminoacrylate intermediate in which the Schiff base resonance at 202.3 ppm is lost and a new peak at 24.2 ppm appears, suggestive of a neutral amino lysine sidechain for the aminoacrylate intermediate. Spectra acquired at 9.4 T and 8 kHz MAS.

positions on the PLP ring. As the dipolar coupling falls off as the inverse cube of the interatomic distance, the ^{15}N{^{13}C}-REDOR editing used here (with 10 ms of dipolar dephasing) is selective for nitrogen atoms within ~3-4 Å of the PLP ^{13}C atoms. The spectra in figure 3.2d and 3.2e form a REDOR S_o and S pair: both have a 10 ms echo period on ^{15}N before detection, but differ in the application of dipolar dephasing to ^{13}C for the latter. As expected, there are considerably more peaks in U-^{15}N-TS spectra than in the ε-^{15}N-Lys TS spectrum; there is also remarkable resolution of many individual nitrogen sites. The peak at 202.3 ppm is evident in the REDOR S_o spectrum, but is selectively dephased under dipolar couplings to ^{13}C in S. As this peak arises from a lysine ε-nitrogen, we can conclude that this is the resonance of the Schiff base linkage to PLP and, based on its chemical shift,[32] that it is protonated.

Examination of spectra 3.2d and 3.2e show a second peak at 294.7 ppm that is also dephased in the REDOR experiment. This peak is not in spectrum 3.2b, so does not arise from an ε-nitrogen label, but as shown in figure 3.2c correlates with the introduction of ^{15}N-labeled PLP; this peak is assigned to the PLP pyridine nitrogen, N1. As expected, strong dipolar coupling of N1 to its directly bonded neighbor, C2, leads to efficient REDOR dephasing. This chemical shift of N1 reports that the pyridine nitrogen is deprotonated.[32] Additional chemical shift measurements, figures 3.4 and 3.5, for

carbons C2 and C3, 158.4 ppm and 168.6 ppm (δ[TMS(l)] scale), respectively, and the phosphorus of the PLP phosphoryl, 4.3 ppm (δ[H_3PO_4(85%)] scale), help complete the assignment of ionization states for the coenzyme. For the former, ^{13}C NMR spectroscopy of model Schiff base compounds[50] under conditions in which the protonated Schiff base form dominates[51] assists in identifying the chemical shifts of C2 and C3 as those for PLP with a deprotonated phenolic oxygen. For the latter, the ^{31}P chemical shift of the phosphoryl definitively reports a dianionic group, figure 3.5.[46] The experimentally determined protonation states are shown in figure 3.6. We note that neither N1 of PLP nor N^{ε} of βlys87 is at the extreme chemical shift value anticipated for a fully deprotonated or fully protonated nitrogen;[13] this may indicate hydrogen bonding interactions or equilibria between tautomeric forms that, though present, strongly favor the form shown.

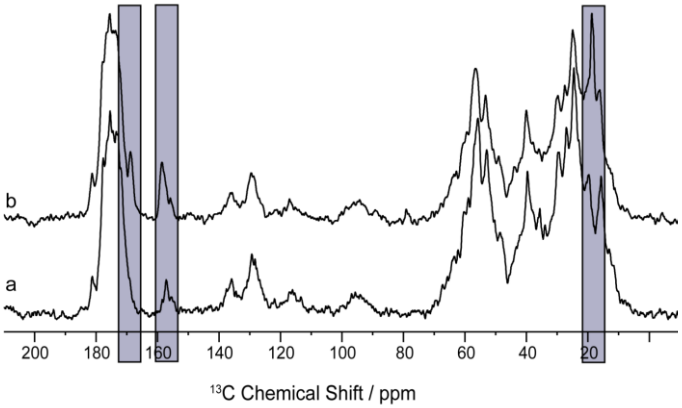

Figure 3.4 ^{13}C-solid-state NMR cross-polarization magic-angle-spinning (CPMAS) spectra of the tryptophan synthase internal aldimine complex used to assign the ^{13}C chemical shifts for C2 and C3 of PLP. Data were acquired on microcrystalline samples of S. typhimurium TS prepared with (a) natural abundance TS/natural abundance PLP and (b) natural abundance TS/2,2',3-$^{13}C3$;^{15}N-PLP. Spectra acquired at 9.4 T and 8 kHz MAS.

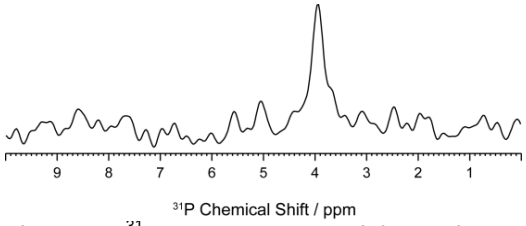

Figure 3.5 ^{31}P ssNMR spectra of the TS internal aldimine. The istotropic chemical shift confirms a dianionic state for the phosphoryl group. Spectrum acquired at 14.1 T and 10 kHz MAS.

The ^{15}N solid-state NMR chemical shift of the Schiff-base nitrogen supports the PSB hypothesis for the internal aldimine state of tryptophan synthase. At the same time,

^{13}C, ^{15}N and ^{31}P chemical shifts on PLP establish that the phosphoryl group, phenolic oxygen, and pyridine ring nitrogen are deprotonated. The pyridine nitrogen in tryptophan synthase interacts with the hydroxyl of βSer377 and, in the absence of an additional proton, would be incapable of assuming the role of hydrogen bond donor. It has been proposed that the protonation state of the pyridine nitrogen plays an important role in steering later reaction specificity for PLP-dependent enzymes: a protonated pyridine nitrogen enhances electrophilic addition at C4', while a deprotonated pyridine favors reaction at the substrate C^{α}.[2,6-8,52] The deprotonated pyridine nitrogen in TS, assuming it is maintained during the catalytic cycle, is consistent with its catalytic role on the β-replacement pathway that takes serine to tryptophan. Yet protonation of the PLP nitrogen has been shown to promote proton transfer from the phenolic oxygen to the Schiff-base nitrogen,[32,53] a defining aspect of the PSB hypothesis. Effecting this transfer for the unprotonated PLP nitrogen clearly requires a different mode of activation. Recent work by Toney and Limbach suggests that the formation of the Zwitterionic species can be triggered by hydrogen bonding of water molecules to the PLP phenolic oxygen.[2,13] In the active site of TS, there are indeed two crystallographically-observed water molecules that form a hydrogen bonded chain to the phenolic oxygen. Molecular dynamics simulations

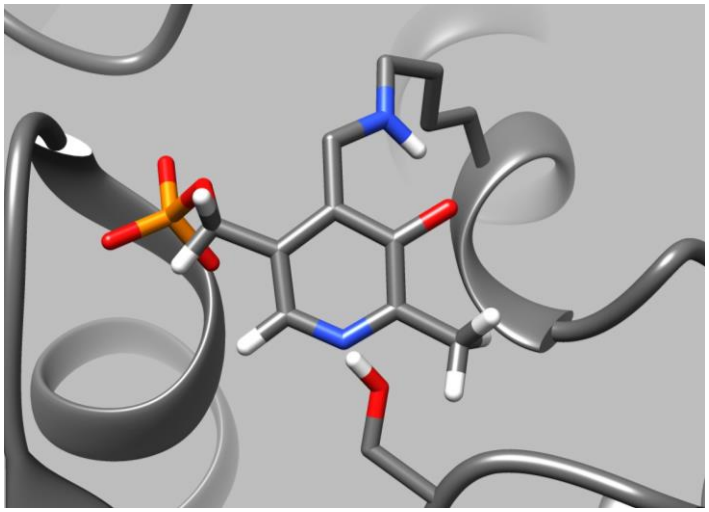

Figure 3.6 Protonation states and hydrogen bonding interactions revealed by NMR crystallography in the tryptophan synthase β-subunit active site for the internal aldimine resting form. Image rendered in UCSF Chimera.[14]

undertaken in response to these NMR findings[40,54] indicate that the pocket adjacent to the phenolic oxygen contains a network of water molecules that maintain persistent hydrogen bonding interactions with the phenolic oxygen for the internal aldimine state. The concluded protonation states agree with the proposal that hydrogen bonding of water to the phenolic oxygen is sufficient for activation of catalysis by proton transfer to the Schiff base nitrogen.

The measurement of chemical shifts in the enzyme active site of tryptophan synthase provides a snapshot of protonation states critical for initiating catalysis in this PLP-dependent enzyme. The ^{15}N chemical shift for the linking lysine ε-nitrogen confirms a protonated Schiff base tautomer for the internal aldimine state, while ^{13}C, ^{15}N, and ^{31}P chemical shifts on PLP report that the phosphoryl group, phenolic oxygen, and pyridine ring nitrogen are deprotonated. These results are consistent both with the PSB hypothesis for PLP activation and the role of β-elimination/replacement catalyst played by tryptophan synthase. Looking forward, as sensitivity continues to increase in solid-state NMR spectroscopy due to advances in sample preparation, hardware design, and techniques such as dynamic nuclear polarization (DNP), the resulting atomic-resolution models of active sites (and entire proteins) will permit an unprecedented, chemically-detailed view of mechanism in functioning enzyme systems such as tryptophan synthase.

3.4 References

(1) Metzler, D. E.; Ikawa, M.; Snell, E. E. *J Am Chem Soc* **1954**, *76*, 648.

(2) Toney, M. D. *Biochim Biophys Acta* **2011**, *1814*, 1407.

(3) Cordes, E. H.; Jencks, W. P. *Biochemistry* **1962**, *1*, 773.

(4) Heinert, D.; Martell, A. E. *J Am Chem Soc* **1963**, *85*, 183.

(5) Metzler, D. E. *J Am Chem Soc* **1957**, *79*, 485.

(6) Crugeiras, J.; Rios, A.; Riveiros, E.; Richard, J. P. *J Am Chem Soc* **2011**, *133*, 3173.

(7) Major, D. T.; Gao, J. L. *J Am Chem Soc* **2006**, *128*, 16345.

(8) Major, D. T.; Nam, K.; Gao, J. *J Am Chem Soc* **2006**, *128*, 8114.

(9) Copie, V.; Faraci, W. S.; Walsh, C. T.; Griffin, R. G. *Biochemistry* **1988**, *27*, 4966.

(10) Mcdowell, L. M.; Lee, M. S.; Schaefer, J.; Anderson, K. S. *J Am Chem Soc* **1995**, *117*, 12352.

(11) Sharif, S.; Fogle, E.; Toney, M. D.; Denisov, G. S.; Shenderovich, I. G.; Buntkowsky, G.; Tolstoy, P. M.; Huot, M. C.; Limbach, H. H. *J Am Chem Soc* **2007**, *129*, 9558.

(12) Lai, J. F.; Niks, D.; Wang, Y. C.; Domratcheva, T.; Barends, T. R. M.; Schwarz, F.; Olsen, R. A.; Elliott, D. W.; Fatmi, M. Q.; Chang, C. E. A.; Schlichting, I.; Dunn, M. F.; Mueller, L. J. *J Am Chem Soc* **2011**, *133*, 4.

(13) Chan-Huot, M.; Dos, A.; Zander, R.; Sharif, S.; Tolstoy, P. M.; Compton, S.; Fogle, E.; Toney, M. D.; Shenderovich, I.; Denisov, G. S.; Limbach, H. H. *J Am Chem Soc* **2013**, *135*, 18160.

(14) Pettersen, E. F.; Goddard, T. D.; Huang, C. C.; Couch, G. S.; Greenblatt, D. M.; Meng, E. C.; Ferrin, T. E. *J Comput Chem* **2004**, *25*, 1605.

(15) Dunn, M. F.; Niks, D.; Ngo, H.; Barends, T. R. M.; Schlichting, I. *Trends Biochem Sci* **2008**, *33*, 254.

(16) Yanofsky, C.; Crawford, I. P. In *The Enzymes Third Edition*; Boyer, P. D., Ed.; Academic Press, Inc.: New York, NY, 1972; Vol. 7, p 1.

(17) Miles, E. W. *Adv Enzymol Relat Areas Mol Biol* **1979**, *49*, 127.

(18) Lane, A. N.; Kirschner, K. *Eur J Biochem* **1983**, *129*, 571.

(19) Christensen, H. N. *J Am Chem Soc* **1958**, *80*, 99.

(20) Peracchi, A.; Bettati, S.; Mozzarelli, A.; Rossi, G. L.; Miles, E. W.; Dunn, M. F. *Biochemistry* **1996**, *35*, 1872.

(21) Goldberg, M. E.; Baldwin, R. L. *Biochemistry* **1967**, *6*, 2113.

(22) Hur, O.; Niks, D.; Casino, P.; Dunn, M. F. *Biochemistry* **2002**, *41*, 9991.

(23) Bazhulina, N. P.; Morozov, Y. V.; Papisova, M. I.; Demidkina, T. V. *Eur J Biochem* **2000**, *267*, 1830.

(24) Arnone, A.; Christen, P.; Jansonius, J. N.; Metzler, D. E. In *Transaminases*; Christen, P., Metzler, D. E., Eds.; John Wiley & Sons, Inc.: New York, 1985, p 326.

(25) Metzler, C. M.; Cahill, A.; Metzler, D. E. *J Am Chem Soc* **1980**, *102*, 6075.

(26) Hyde, C. C.; Ahmed, S. A.; Padlan, E. A.; Miles, E. W.; Davies, D. R. *J Biol Chem* **1988**, *263*, 17857.

(27) Sachpatzidis, A.; Dealwis, C.; Lubetsky, J. B.; Liang, P. H.; Anderson, K. S.; Lolis, E. *Biochemistry* **1999**, *38*, 12665.

(28) Kulik, V.; Weyand, M.; Seidel, R.; Niks, D.; Arac, D.; Dunn, M. F.; Schlichting, I. *J Mol Biol* **2002**, *324*, 677.

(29) Weyand, M.; Schlichting, I.; Marabotti, A.; Mozzarelli, A. *J Biol Chem* **2002**, *277*, 10647.

(30) Ngo, H.; Harris, R.; Kimmich, N.; Casino, P.; Niks, D.; Blumenstein, L.; Barends, T. R.; Kulik, V.; Weyand, M.; Schlichting, I.; Dunn, M. F. *Biochemistry* **2007**, *46*, 7713.

(31) Niks, D.; Hilario, E.; Dierkers, A.; Ngo, H.; Borchardt, D.; Neubauer, T. J.; Fan, L.; Mueller, L. J.; Dunn, M. F. *Biochemistry* **2013**, *52*, 6396.

(32) Limbach, H. H.; Chan-Huot, M.; Sharif, S.; Tolstoy, P. M.; Shenderovich, I. G.; Denisov, G. S.; Toney, M. D. *Biochim Biophys Acta* **2011**, *1814*, 1426.

(33) Chan-Huot, M.; Sharif, S.; Tolstoy, P. M.; Toney, M. D.; Limbach, H. H. *Biochemistry* **2010**, *49*, 10818.

(34) Sharif, S.; Denisov, G. S.; Toney, M. D.; Limbach, H. H. *J Am Chem Soc* **2007**, *129*, 6313.

(35) Sharif, S.; Schagen, D.; Toney, M. D.; Limbach, H.-H. *J Am Chem Soc* **2007**, *129*, 4440.

(36) Harbison, G. S.; Herzfeld, J.; Griffin, R. G. *Biochemistry* **1983**, *22*, 1.

(37) Tian, Y.; Chen, L.; Niks, D.; Kaiser, J. M.; Lai, J.; Rienstra, C. M.; Dunn, M. F.; Mueller, L. J. *PCCP* **2009**, *11*, 7078.

(38) Yang, L.; Ahmed, S. A.; Miles, E. W. *Protein Expr Purif* **1996**, *8*, 126.

(39) Miles, E. W.; Moriguchi, M. *J Biol Chem* **1977**, *252*, 6594.

(40) Caulkins, B. G.; Bastin, B.; Yang, C.; Neubauer, T. J.; Young, R. P.; Hilario, E.; Huang, Y. M.; Chang, C. E.; Fan, L.; Dunn, M. F.; Marsella, M. J.; Mueller, L. J. *J Am Chem Soc* **2014**, *136*, 12824.

(41) Morcombe, C. R.; Zilm, K. W. *J Magn Reson* **2003**, *162*, 479.

(42) Markley, J. L.; Bax, A.; Arata, Y.; Hilbers, C. W.; Kaptein, R.; Sykes, B. D.; Wright, P. E.; Wuthrich, K. *Pure Appl Chem* **1998**, *70*, 117.

(43) Maurer, T.; Kalbitzer, H. R. *J Magn Reson, Ser B* **1996**, *113*, 177.

(44) Schnackerz, K. D.; Mozzarelli, A. *J Biol Chem* **1998**, *273*, 33247.

(45) Schnackerz, K. D.; Keller, J.; Phillips, R. S.; Toney, M. D. *BBA - Protein Proteom* **2006**, *1764*, 230.

(46) Schnackerz, K. D.; Andi, B.; Cook, P. F. *BBA - Protein Proteom* **2011**, *1814*, 1447.

(47) Fung, B. M.; Khitrin, A. K.; Ermolaev, K. *J Magn Reson* **2000**, *142*, 97.

(48) Harris, R. K.; Becker, E. D.; De Menezes, S. M. C.; Granger, P.; Hoffman, R. E.; Zilm, K. W. *Pure Appl Chem* **2008**, *80*, 59.

(49) Gullion, T.; Schaefer, J. *J Magn Reson* **1989**, *81*, 196.

(50) O'Leary, M. H.; Payne, J. R. *J Biol Chem* **1976**, *251*, 2248.

(51) Sharif, S.; Huot, M. C.; Tolstoy, P. M.; Toney, M. D.; Jonsson, K. H.; Limbach, H. H. *J Phys Chem B* **2007**, *111*, 3869.

(52) Casasnovas, R.; Adrover, M.; Ortega-Castro, J.; Frau, J.; Donoso, J.; Munoz, F. *J Phys Chem B* **2012**, *116*, 10665.

(53) Sharif, S.; Powell, D. R.; Schagen, D.; Steiner, T.; Toney, M. D.; Fogle, E.; Limbach, H. H. *Acta Crystallogr Sect B: Struct Sci* **2006**, *62*, 480.

(54) Huang, Y. M.; You, W.; Caulkins, B. G.; Dunn, M. F.; Mueller, L. J.; Chang, C. E. *Protein Sci* **2016**, *25*, 166.

Chapter 4 – The Aminoacrylate

4.1 Introduction

The power of pyridoxal-5′-phosphate (PLP), figure 4.1, as a cofactor comes from its ability to behave as an electron sink during catalysis, allowing for stabilization of carbanionic intermediates generated in virtually all PLP-dependent enzyme mechanisms.[1-3] Yet one more subtle aspect of PLP catalysis is the ability of the cofactor to reverse polarity at the β-carbon of amino acids, allowing the site to alternate between nucleophile and electrophile as the reaction unfolds.[3] The electrostatic environment of the active site ensures the proper ionization states on the cofactor, substrate, and active site residues to support the necessary charge delocalization and polarity reversal to guarantee a given reaction.[4-9] In this chapter, it is shown using solid-state NMR (ssNMR) that the α-aminoacrylate intermediate formed in the PLP-dependent enzyme tryptophan synthase exploits this aspect of the cofactor to ensure the β-elimination and replacement reaction pathway. Furthermore, we show that for the α-aminoacrylate complexed with the inhibitor benzimidazole (BZI), figure 4.1c, the electrostatic environment prevents reaction of the nucleophile with the complex. X-ray crystal structures help build a fuller model of this intermediate and support our conclusions about the differing protonation states for each of these complexes. Our results underscore the influence of ionization states on reaction specificity in PLP-

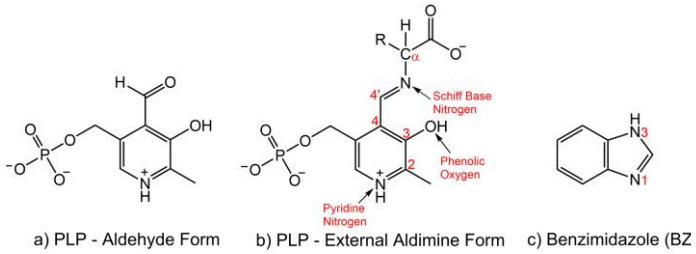

Figure 4.1 Pyridoxal-5′-phosphate (PLP) in both its (a) aldehyde and (b) external aldimine forms. (c) β-reaction inhibitor benzimidazole (BZI).

dependent enzymes and highlight the power of ssNMR as an interrogative tool for the investigation of enzyme active sites.

The vast majority of known PLP-dependent enzymes begin catalysis with the cofactor covalently bound to the enzyme through a catalytically essential lysine residue in the active site.[11,12] In tryptophan synthase from *S. typhimurium* this lysine residue is βLys87, scheme 4.1.[13] Tryptophan synthase (TS; 4.2.1.20) is a 143 kDa $\alpha_2\beta_2$ bienzyme

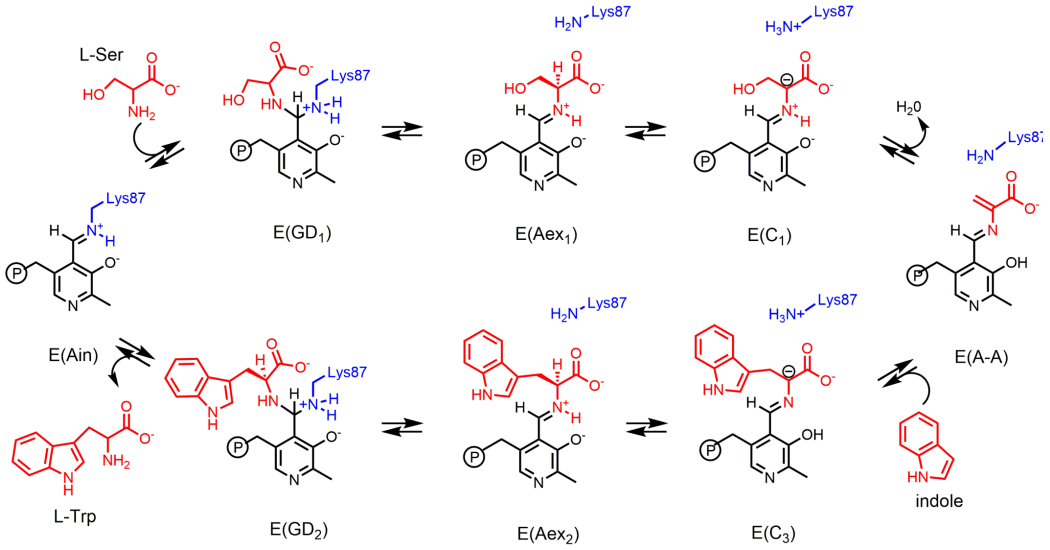

Scheme 4.1 The β-subunit reaction in TS.

complex that catalyzes the PLP-dependent β-elimination and replacement of the hydroxyl group on L-Ser by indole to ultimately produce L-Trp, scheme 4.1.[14-17] Reaction of L-Ser with the internal aldimine resting form, E(Ain), results in a nucleophilic attack at C4′ of PLP, displacing the covalent bond between the cofactor and Lys87 and generating the first the transient gem-diamine, $E(GD_1)$, then the short-lived external aldimine intermediate, $E(Aex_1)$, in which L-Ser forms the Schiff base linkage to PLP. Abstraction of the α-proton of L-Ser results in the first carbanionic intermediate, $E(C_1)$, and elimination of the β-hydroxyl group releases a water molecule and forms the α-

aminoacrylate intermediate, E(A-A).[14] At this step, indole is channeled to the β-subunit from the α-subunit through a 25 Å-long tunnel connecting the α- and β-subunits.[13,14,18-21] A carbon-carbon bond is created between the C^{β} of serine and C3 of indole, resulting in the second and third carbanionic intermediates, E(C_2) and E(C_3). Reprotonation of the α-carbon of E(C_3) forms the second external aldimine intermediate, E(Aex_2), βLys87 then reacts to form the second gem-diamine, E(GD_2), and finally L-Trp is released as the internal aldimine resting state is regenerated.[18]

The α-aminoacrylate intermediate signifies a major divergent step in PLP chemistry, as only the enzymes that perform β-elimination reactions generate this species, providing a tantalizing opportunity to probe the electrostatic environment in the active site and delineate the factors that uniquely lead to this structure.[22-26] Formation of the α-aminoacrylate intermediate in tryptophan synthase is characterized by adoption of closed conformations by both the α-subunit and the β-subunit. Closure of the α-subunit is enhanced by binding of an α-site ligand,[27] and the α-subunit is considered to be in its closed conformation when a salt bridge forms between αAsp56 and βLys167, decreasing the distance between hydrogen-bonded partners from 4.10 Å in the open conformation to 2.79 Å in the closed structure.[18,27,28] Adoption of an ordered conformation by α-loop2 (residues α-53-60) and α-loop6 (residues α179-193, the “lid” of the tunnel) further defines the closed form of the α-subunit.[18,29,30] The β-subunit is considered closed when a hydrogen-bonded salt bridge forms between residues βAsp305 and βArg141, decreasing the distance between heavy atoms from 11.0 Å in the open structure to 2.88 Å in the closed structure.[18,27,31,32] The switch in conformation from open to closed occurs when L-Ser reacts with the PLP cofactor to produce the α-aminoacrylate species, which stimulates the α-site reaction by at least 30-fold, as the β-

subunit active site becomes poised to fuse indole to the PLP-substrate complex.[18,27,33] The closed conformation has been shown to prevent the escape of indole when it is channeled to the β-subunit,[13,14,18,20,28] and our previous work has shown that small nonpolar molecules can easily bind in the tunnel, which acts a dewetted nanotube, preventing water from entering the β-subunit active site and performing a deleterious side reaction that results in pyruvate and ammonia.[19] BZI is a nitrogen isostere of indole and was found to be an unreactive substrate analogue of indole.[20] The physical-chemical basis for the potent inhibition by BZI remains a topic of intense interest.

Examination of the aminoacrylate crystal structures with and without BZI in the active site allows us to trace the fate of the hydroxyl leaving group. The WT AA structure (PDBID: 4HN4) shows a crystallographic water in the just-cleaved position from the PLP-substrate complex. With BZI (PDBID:4HPX) we see the attack position of the incoming nucleophile, which has also displaced this crystallographic water molecule. Here we argue that it is the unique electronic structure of BZI compared to indole that prevents further reaction, while perturbations to key ionizable sites, measured with ssNMR, stabilize the complex and ensure the inhibition of the complex.

4.2 Experimental Details

Protein Preparation

Tryptophan synthase was prepared by overexpression of *S. typhimurium* TS in *E. coli* as previously described.[6,7] Samples were prepared with the following isotopic labeling schemes for the cofactor and protein components: (1) Protein and cofactor unlabeled/natural abundance isotopomer concentration; (2) Protein ^{15}N-labeled at lysine ε-nitrogen sites; PLP unlabeled (ε-^{15}N-Lys TS); (3) PLP cofactor selectively ^{13}C enriched

at carbon sites C2, C2', and C3 and ^{15}N enriched at the pyridine ring nitrogen; protein unlabeled (2,2',3-13C3,^{15}N-PLP TS); and (4) PLP cofactor selectively ^{13}C,^{15}N enriched; protein uniformly ^{15}N-labeled (2,2',3-^{13}C3,^{15}N-PLP; U-^{15}N TS).

Microcrystalline Protein Samples for Solid-State NMR

Microcrystalline samples of TS were prepared by diluting enzyme solution 1:1 with 50 mM Cs-bicine buffer, pH 7.8, containing 14% PEG-8000 and 3.0 mM spermine as previously described.[6-8] Microcrystals were collected and washed with 50 mM Cs-bicine, pH 7.8, containing 8% PEG-8000, 1.8 mM spermine, and 3 mM N-(4'-trifluoromethoxybenzenesulfonyl)-2-aminoethyl phosphate (F9; a high affinity alpha site ligand and analogue of the natural α-site substrate 3-idole-D-glycerol-3'-phosphate (IGP)). Microcrystals containing the unlabeled inhibitor benzimidazole (BZI) were prepared in the same manner, with BZI added to the wash for a final concentration of 20 mM. The crystals were packed at 10,000 rpm into a Bruker 4 mm magic-angle spinning (MAS) rotor with an approximate volume of 80 µL; each rotor contained 25-30 mg of protein. To form the α-aminoacrylate intermediate, serine was introduced by direct addition of 5 µL of 1.2 M L-Ser to the packed MAS rotor. Samples containing ^{15}N-BZI were formed by direct addition of ^{15}N-BZI, prepared by our organic collaborators using literature protocols,[34,35] dissolved in ethanol to the packed MAS rotor for a final concentration of 20 mM. Stabilization of the α-aminoacrylate and BZI-aminoacrylate species is enhanced by low temperature (-5 °C), the use of the tight binding α-subunit ligand F9, and the presence of Cs^+,[32] which binds to the monovalent cation site in the β-subunit.

NMR Spectroscopy

^{13}C and ^{15}N Solid-State NMR Spectroscopy: ^{13}C and ^{15}N cross-polarization (CP) magic-angle-spinning (MAS) experiments were performed at 9.4 T (400.37 MHz ^{1}H, 100.69 MHz ^{13}C, 40.57 MHz ^{15}N) on a Bruker AVIII spectrometer equipped with a double resonance, 4 mm MAS probe, spinning at MAS rates of 8 kHz; the bearing gas was cooled to -15 °C, giving an effective sample temperature of -5 °C in both cases. Cross-polarization was accomplished at a ^{1}H spin-lock field of 45 kHz and a ^{13}C/^{15}N spin-lock of 54 kHz (^{13}C) and 37 kHz (^{15}N) (ramped +/- 2 kHz); 85 kHz Spinal64 ^{1}H decoupling[36] was used throughout. Standard ^{13}C spectra consist of the sum of 16,384 transients acquired with a relaxation delay of 4 s, for a total acquisition time of 18.3 h. ^{13}C chemical shifts were referenced indirectly to neat TMS via an external solid-state sample of adamantane with the downfield-shifted peak set to 38.48 ppm.[37,38] Standard ^{15}N spectra consist of the sum of 81,920 transients acquired with a relaxation delay of 4 s, for a total acquisition time of 3 d 19 h. ^{15}N chemical shifts were referenced indirectly to liq-NH_3 (25 °C) via an external solid-state sample of $^{15}NH_4Cl$, in which the resonance frequency was set to 39.27 ppm.[37,39]

^{15}N CPMAS experiments on microcrystalline samples containing ^{15}N-BZI were performed at 18.8 T (800.12 MHz ^{1}H; 81.09 MHz ^{15}N) on a Bruker AVANCE 800 spectrometer equipped with an NHMFL low-E, double resonance 3.2 mm MAS probe[40] (sample volume ~ 40 µl) and spinning at a MAS rate of 11 kHz. The bearing gas was cooled to -15 °C, giving an effective sample temperature of -5 °C. Cross-polarization was accomplished at a ^{1}H spin-lock field of 45 kHz, ^{15}N spin-lock of 37 kHz (ramped +/- 2 kHz), and a 2 ms contact time; 100 kHz Spinal64 ^{1}H decoupling[36] was used throughout. The ^{15}N-BZI spectrum consists of the sum of 69,632 transients acquired with a relaxation

delay of 3 s, for a total acquisition time of 2 d 10 h. ^{15}N chemical shifts were referenced indirectly to liq-NH_3 (25 °C) via an external solid-state sample of $^{15}NH_4Cl$, in which the resonance frequency was set to 39.27 ppm.[37,39]

The acquisition of solid-state NMR spectra was interleaved with single pulse, low-power decoupling experiments (64 scans ^{13}C, 256 scans ^{15}N) reporting predominantly on free ligand and reaction products in solution (mother liquor). Acquisition of solid-state NMR spectra for the intermediate was halted before reactant concentrations in solution fell to zero.

^{31}P Solid-State NMR Spectroscopy: ^{31}P CPMAS experiments on the α-aminoacrylate species were performed at 14.1 T (600.01 MHz ^{1}H, 242.89 MHz ^{31}P) on a Bruker AVIII spectrometer equipped with an ^{1}H-X double resonance 4 mm MAS probe, spinning at a MAS rate of 10 kHz, while ^{31}P CPMAS experiments on the BZI-aminoacrylate species were performed at 9.4 T (400.37 MHz ^{1}H, 162.07 MHz ^{31}P) on a Bruker AVIII spectrometer equipped with a double resonance, 4 mm MAS probe, spinning at a MAS rate of 8 kHz. The bearing gas was cooled to -15 °C, giving an effective sample temperature of -5 °C in both cases. Cross-polarization was accomplished with a ^{1}H spin-lock field of 45 kHz and a ^{31}P spin-lock of 47 kHz (ramped +/- 5 kHz); 58 kHz Spinal64 ^{1}H decoupling[36] was used during detection. The ^{31}P spectra consist of the sum of 4,096 transients acquired with a relaxation delay of 3 s, for a total acquisition time of 3.4 h. ^{31}P chemical shifts were indirectly referenced to 85% H_3PO_4 (MAS). For comparison to measurements in solution, δ[85% H_3PO_4 (capillary)] = δ[85% H_3PO_4 (sphere/MAS)] + 0.36 ppm.[41]

^{15}N-observe, ^{31}P-dephased Rotational Echo Double Resonance (REDOR) Experiments: $^{15}N\{^{31}P\}$-REDOR[42] experiments were performed at 21.1 T (898.66 MHz

^{1}H; 91.06 MHz ^{15}N; 363.78 MHz ^{31}P) on a Bruker AVANCE 900 spectrometer equipped with an NHMFL low-E, triple resonance 3.2 mm MAS probe[40] (sample volume ~ 40 µl) and spinning at a MAS rate of 8 kHz. The bearing gas was cooled to -15 °C, giving an effective sample temperature of -5 °C. Cross-polarization was accomplished at a ^{1}H spin-lock field of 45 kHz, ^{15}N spin-lock of 37 kHz (ramped +/- 2 kHz), and a 2 ms contact time; 100 kHz Spinal64 ^{1}H decoupling[36] was used throughout. A single 10 µs π pulse was applied to ^{15}N at the center of the 25 ms echo period (S_o), while a series of 12 µs π pulses at half rotor intervals were applied to ^{31}P during the dephasing (S) experiments. The REDOR S and S_o spectra were acquired in an interleaved fashion, and each spectrum consists of the sum of 32,768 transients acquired with a relaxation delay of 2 s, for a total acquisition time of 18.2 h each.

X-Ray Crystallography

The X-ray crystal structure of the tryptophan synthase α-aminoacrylate intermediate with Cs^{+} bound to the monovalent cation site and N-(4'-trifluoromethoxybenzenesulfonyl)-2-aminoethyl phosphate (F9) bound to the α-site was solved at 1.65 Å resolution and previously reported.[19] The PDB accession code is 4HN4. The X-ray crystal structure of the tryptophan synthase BZI-aminoacrylate intermediate with Cs^{+} bound to the monovalent cation site and F9 bound to the α-site was also solved at 1.65 Å resolution and previously reported.[19] The PDB accession code is 4HPX.

4.3 Results and Discussion

^{15}N Chemical Shift Measurements

Figure 4.2 shows ^{15}N solid-state NMR spectra of the tryptophan synthase α-aminoacrylate intermediate prepared under the following four isotopic-labeling

conditions: (4.2a) natural abundance isotopomer concentration; (4.2b) selectively ^{13}C,^{15}N enriched on the PLP cofactor (2,2',3-$^{13}C_3$,^{15}N-PLP; TS); (4.2c) ^{15}N-enriched on the L-Ser substrate; (4.2d) selectively ^{15}N-enriched at all protein lysine ε-nitrogen side chain sites (ε-^{15}N-Lys TS). At natural abundance, figure 4.2a, the spectrum displays signals from the large number of protein backbone nitrogen atoms centered around 122 ppm. Incorporation of the isotopically enriched PLP cofactor generates a new peak in the spectrum at 297.6 ppm that can be assigned to the pyridine ring N1 atom, figure 4.2b. This chemical shift points to a predominately deprotonated pyridine nitrogen, as found for the internal aldimine form.[6,43,44] The chemical shift of the Schiff base linkage formed with ^{15}N-serine falls at 286.7 ppm, figure 4.2c, suggesting a deprotonated imine nitrogen. This chemical shift, however, is far below the limiting value for a fully deprotonated Schiff base, suggesting tautomeric exchange may be a feature of this intermediate.[8,45,46]

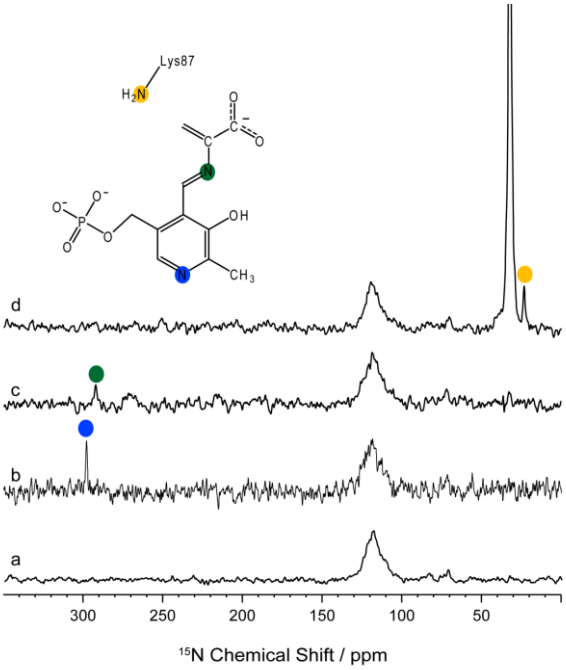

Figure 4.2 ^{15}N ssNMR CPMAS spectra of the microcrystalline TS α-aminoacrylate intermediate prepared with the following isotopic labeling: (a) natural abundance isotopomer concentration; (b) selectively ^{13}C,^{15}N enriched on the PLP cofactor; (c) ^{15}N-enriched on the substrate L-Ser; (d) selectively ^{15}N-enriched at lysine ε-nitrogen side chain sites. Spectra acquired at 9.4 T and 8 kHz MAS.

The charge state of the catalytic active-site βLys87 side chain was determined using a protein sample in which all lysine residues were ^{15}N-enriched at the ε-nitrogen sites (ε-^{15}N-Lys TS). This sample, figure 4.2d, shows a large number of mostly

overlapped resonances centered at 33 ppm. These correspond to charged ε-amino groups on the solvent-exposed, labeled lysine residues. Also evident in figure 4.2d is a peak at 24.2 ppm, indicative of a neutral amine. This signal does not appear until addition of serine to the microcrystalline sample of TS in the internal aldimine state, figure 4.3. These changes indicate that the Schiff base linkage to βLys87 in the enzyme active site has been broken at the same time that a neutral amine has been formed. Based on this correlation, we assign this new resonance to the neutral ε-NH_2 of βLys87.[7]

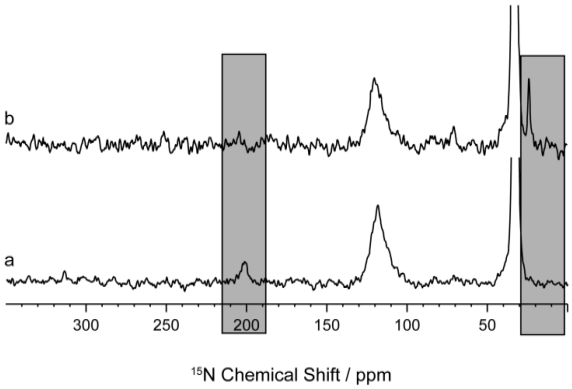

Figure 4.3 ^{15}N ssNMR CPMAS spectra of the microcrystalline TS (a) internal aldimine resting form and (b) α-aminoacrylate intermediate prepared selectively ^{15}N-enriched at lysine ε-nitrogen side chain sites. Upon addition of serine to (a), the aminoacrylate is formed, corresponding to the loss of the peak at 202.3 ppm in (a) and the appearance of the peak at 24.2 ppm in (b). Spectra acquired at 9.4 T and 8 kHz MAS.

Figure 4.4 shows ^{15}N solid-state NMR spectra of the tryptophan synthase BZI-aminoacrylate (BZI-AA) intermediate prepared under the following five isotopic-labeling conditions: (4.4a) natural abundance isotopomer concentration; (4.4b) selectively ^{13}C,^{15}N enriched on the PLP cofactor (2,2',3-$^{13}C_3$,^{15}N-PLP; TS); (4.4c) ^{15}N-enriched on the L-Ser substrate; (4.4d) selectively ^{15}N-enriched on the BZI inhibitor; and (4.4e/4.4f) selectively ^{15}N-enriched at all protein lysine ε-nitrogen side chain sites (ε-^{15}N-Lys TS). Again, the natural abundance spectrum, figure 4.4a, shows primarily signals from the large number of protein backbone nitrogens, while the incorporation of the isotopically enriched cofactor produces a new spectral feature at 302.4 ppm, assigned to the pyridine ring N1 atom, figure 4.4b. This chemical shift points to a predominately deprotonated pyridine

nitrogen, as found for the uninhibited α-aminoacrylate, figure 4.2b. The chemical shift of the Schiff base linkage formed with ^{15}N-serine falls at 292.3 ppm, figure 4.4c, suggesting a deprotonated Schiff base nitrogen. The spectrum containing ^{15}N-BZI shows two new signals at 165.5 and 227.8 ppm, the expected resonances of a protonated and deprotonated ring nitrogen, respectively.

The chemical shifts of the α-aminoacrylate and BZI-aminoacrylate so far have shown remarkable similarities, yet determination of the charge state of the active-site catalytic βLys87 side chain begins to show a divergence in electrostatic environment.

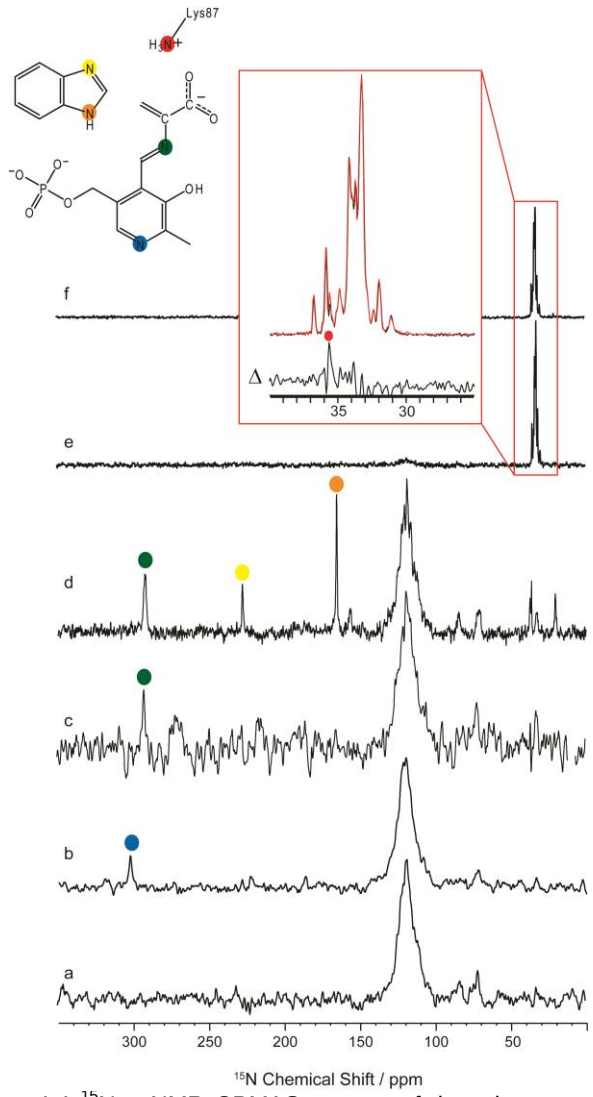

Figure 4.4 ^{15}N ssNMR CPMAS spectra of the microcrystalline TS BZI-aminoacrylate intermediate prepared with the following isotopic labeling: (a) natural abundance isotopomer concentration; (b) selectively ^{13}C,^{15}N enriched on the PLP cofactor; (c) ^{15}N-enriched on the substrate L-Ser; (d) selectively ^{15}N-enriched on the BZI inhibitor; and (e,f) selectively ^{15}N-enriched at lysine ε-nitrogen side chain sites. Spectra (e) and (f) form an ^{15}N{^{31}P}-REDOR pair; both have a 25 ms echo period on ^{15}N before detection, but (f) includes the application of dipolar dephasing to ^{31}P. Their difference spectrum (Δ) allows for the selective observation of N^{ε} for the active site lysine side chain. Spectra acquired at 9.4 T (a-d), 21.1 T (e,f), and 8 kHz MAS.

To determine this shift, a protein sample was prepared in which all lysine residues were

^{15}N-enriched at the ε-nitrogen sites (ε-^{15}N-Lys TS). The spectrum of this sample, figure 4.4e, shows only the large natural abundance ^{15}N-backbone signal and a large number of overlapped resonances centered at 33 ppm. These correspond to the 27 charged ε-amino groups on the labeled lysine residues, and presumably βLys87 is buried among them. To directly observe the βLys87 resonance, we turn to ^{15}N-observe,^{31}P-dephased rotational-echo double-resonance (^{15}N{^{31}P} –REDOR) experiments. REDOR exploits the dipolar coupling between two atoms; because the dipolar coupling interaction can only occur between atoms near in space, we take advantage of the 100% naturally abundant NMR active phosphorus atom on the PLP cofactor located 3.7 Å from the ε-nitrogen of βLys87 to selectively dephase the nitrogen magnetization (PDB ID: 4HPX).[42] No other lysine residue is located closer than 11.1 Å to the PLP phosphorus or 9.5 Å to the F9 phosphorus, the only other phosphorus atom to be found in the enzyme complex. This assures us that any dephasing observed in the REDOR nitrogen spectrum is due to the interaction between the PLP phosphorus and the ε-nitrogen of βLys87. The spectra in figure 4.4e and 4.4f form a REDOR pair; each has a 25 ms echo period on ^{15}N before detection, but 4.4f includes the application of dipolar dephasing to ^{31}P. There is a single resonance at 35.6 ppm that shows clear dephasing; this resonance is assigned to the ε-amino group of βLys87, confirming its charged state, a major contrast to the α-aminoacrylate.

^{13}C Chemical Shift Measurements

Figure 4.5 shows ^{13}C solid-state NMR spectra of the tryptophan synthase α-aminoacrylate intermediate prepared under the following three isotopic labeling conditions: (4.5a) natural abundance isotopomer concentration; (4.5b) selectively ^{13}C,^{15}N enriched on the PLP cofactor (2,2',3-$^{13}C_3$,^{15}N-PLP TS); and (4.5c) U-$^{13}C_3$,^{15}N-enriched

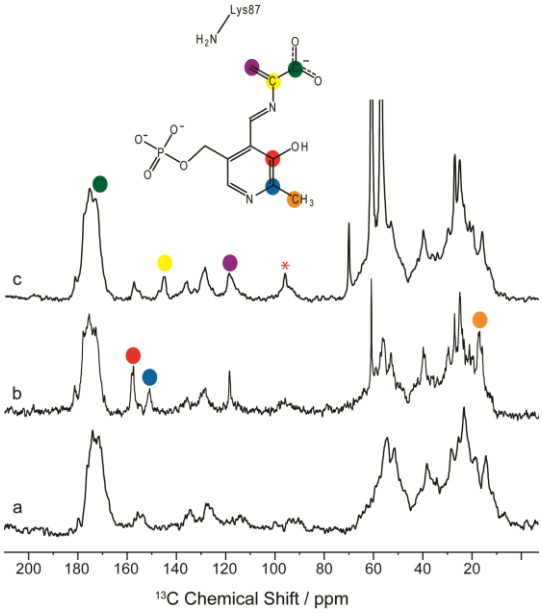

Figure 4.5 ^{13}C ssNMR CPMAS spectra of the microcrystalline TS α-aminoacrylate intermediate prepared under (a) natural abundance isotopomer concentration; (b) selectively ^{13}C,^{15}N-enriched on the PLP cofactor; and (c) U-^{13}C3,^{15}N-enriched on the substrate L-Ser. Spinning side bands are designated with an asterisk. Spectra acquired at 9.4 T and 8 kHz MAS.

on L-Ser. Considerably more background signals are observed at ^{13}C natural abundance (1.1%) compared to ^{15}N (0.36%), figure 4.2a. In figure 4.5b, the incorporation of isotopically ^{13}C-enriched PLP leads to three new resonances at 17.5, 151.2, and 158.1 ppm; based on their chemical shifts, these are assigned to C2′, C2, and C3 of PLP, respectively. The C2 and C3 shifts are important for establishing the charge state of the PLP phenolic oxygen, and model compound studies by Harruff and Jenkins[47] and O'Leary and Payne[48] indicate a protonated phenolic oxygen on PLP for this intermediate. These shifts can be contrasted with those for the TS internal aldimine, which fall at 158.4 ppm and 168.6 ppm for C2 and C3, respectively – values consistent with the zwitterionic form in which the phenolic oxygen is deprotonated.[6] The spectrum in figure 4.5c, measured for the intermediate formed with U-$^{13}C_3$,^{15}N-L-Ser, shows three new resonances at 170.9 ppm, 145.6 ppm, and 118.8 ppm that can be assigned to carbons that derive from the serine C', C^{α}, and C^{β}, respectively. The high chemical shift of C^{β} is due to its involvement in a double bond with C^{α}, and also indicates the more electrophilic nature of the site for the lifetime of this intermediate.

Figure 4.6 shows ^{13}C solid-state NMR spectra of the tryptophan synthase BZI-aminoacrylate intermediate prepared under the following three isotopic labeling conditions: (4.6a) natural abundance isotopomer concentration; (4.6b) selectively $^{13}C,^{15}N$ enriched on the PLP cofactor (2,2',3-$^{13}C_3$,^{15}N-PLP TS); and (4.6c) U-$^{13}C_3$,^{15}N-enriched on L-Ser. The measured ^{13}C chemical shifts for the BZI-aminoacrylate do not differ much from those measured for the uninhibited α-aminoacrylate intermediate. The signals from the ^{13}C-enriched PLP appear at 18.2, 153.1, and 158.0 ppm for C2′, C2, and C3 of PLP, respectively, figure 4.6b, while the spectrum in figure 4.6c shows three resonances at 169.8 ppm, 146.0 ppm, and 118.7 ppm that can be assigned to carbons that derive from the serine C', C^{α}, and C^{β}, respectively.

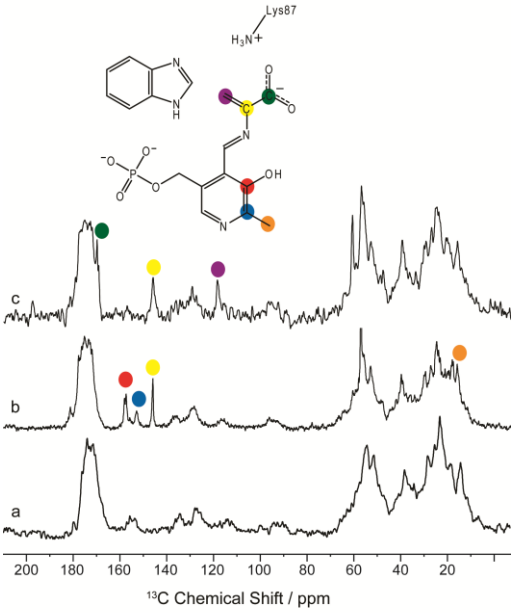

Figure 4.6 ^{13}C ssNMR CPMAS spectra of the microcrystalline TS BZI-aminoacrylate intermediate prepared under (a) natural abundance isotopomer concentration; (b) selectively $^{13}C,^{15}N$-enriched on the PLP cofactor; and (c) U-$^{13}C3,^{15}N$-enriched on the substrate L-Ser. Spectra acquired at 9.4 T and 8 kHz MAS.

<u>^{31}P Chemical Shift Measurements</u>

The ^{31}P solid-state NMR spectra of the tryptophan synthase α-aminoacrylate and BZI-aminoacrylate intermediates are shown in figure 4.7a and b, respectively. The isotropic shift of the PLP cofactor shows a characteristic response in solution as the

phosphoryl moves from the mono- to the dianionic form.[49] The isotropic shift in both intermediates at 5.0 ppm places them firmly in the dianionic regime.

Protonation States of the α-Aminoacrylate and BZI-Aminoacrylate Intermediates

These measured chemical shifts for the α-aminoacrylate and BZI-aminoacrylate intermediates, summarized in table 4.1, allow a preliminary model to be proposed for the protonation states on and near the cofactor-substrate complex in the active site of tryptophan synthase. With good confidence it can be concluded that the phosphoryl group is dianionic and the pyridine nitrogen is neutral. At the same time, the ^{15}N chemical shift of the Schiff base nitrogen, coupled with the PLP C2 and C3 shifts, point to an intermediate in its phenolic form, with a neutral Schiff base linkage to the substrate. However, the shift of the Schiff base nitrogen is lower than that of deprotonated imine model compounds, suggesting tautomeric exchange may occur in the aminoacrylate species.[45,46] The transient nature of this intermediate has precluded temperature dependence studies, as the longevity of the species is only preserved at the lowest accessible temperature (-5 °C) before freezing of the crystals and shutdown of catalytic activity, though evidence of tautomerism in other intermediates supports this idea.[6,8]

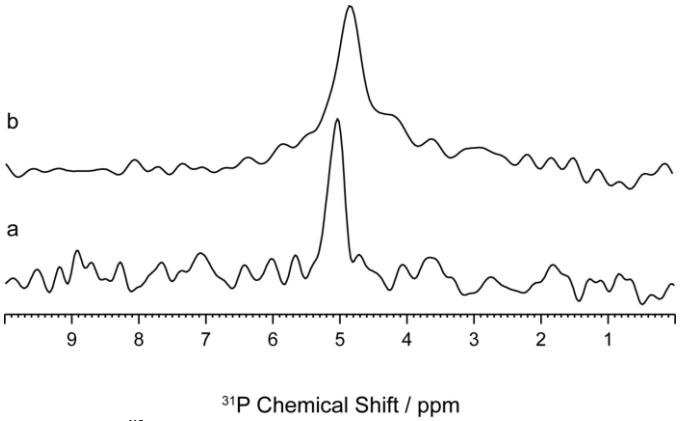

Figure 4.7 ^{31}P spectra of the (a) α-aminoacrylate and (b) BZI-aminoacrylate intermediate. The istotropic chemical shift confirms a dianionic state for the phosphoryl group in both intermediates. Spectra acquired at 14.1 T and 10 kHz MAS (a), and 9.4 T and 8 kHz MAS (b).

The main difference between the two aminoacrylate complexes is the change in

AA Chemical Shift (ppm)	Site	BZI-AA Chemical Shift (ppm)
24.2	ε-N-Lys87	35.6
151.2	PLP C2	153.1
17.5	PLP C2'	18.2
158.1	PLP C3	158.0
297.6	PLP N1	302.4
5.0	PLP Phosphorus	4.8
170.9	Serine CO	169.8
145.6	Serine C^{α}	146.0
118.8	Serine C^{β}	118.7
286.7	Serine N	292.3
292, 258	Serine Carboxylate Oxygens	287, 258
---	BZI-Nitrogens	165.5, 227.8

Table 4.1 Measured chemical shifts for the α-aminoacrylate and BZI-aminoacrylate intermediates.

ionization state of the βLys87 side chain. In the α-aminoacrylate complex, the side chain is neutral, figure 4.8a. This is consistent with βLys87 playing the role of acid in the previous catalytic step; formation of the first carbanionic species triggers the elimination of the serine-derived β-hydroxyl, generating a water molecule with the proton donated from the βLys87 side chain nitrogen.[7] A rearrangement of electron density forms a C^{α}-C^{β} double bond, defining the α-aminoacrylate structure. In the BZI-aminoacrylate structure, the βLys87 side chain is charged, figure 4.8b. Once the β-hydroxyl of the substrate has

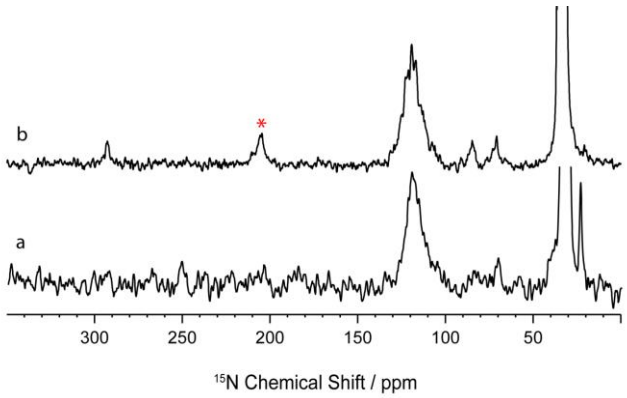

Figure 4.8 ε-^{15}N-Lys spectra for the (a) α-aminoacrylate and (b) BZI-aminoacrylate intermediates. The protonation state of this ionizable site is the only measured difference between the uninhibited (a) and inhibited (b) complexes. Spectra acquired at 9.1 T (a) and 21.1 T (b) and 8 kHz MAS. Spinning side bands are marked with an asterisk.

been cleaved and BZI enters the active site, a proton is abstracted from the inhibitor by βLys87, as with the natural substrate indole. However, though BZI is a nitrogen isostere of indole, catalysis is inhibited by the presence of BZI. The spectrum of ^{15}N-enriched BZI, figure 4.2d, shows two distinct nitrogen signals, not one as would be expected if both BZI nitrogens were equivalent, so it is not the resonance-derived stability of the BZI molecule itself that prevents it from reacting further. Rather, poor overlap of the lone pair electrons on the neutral nitrogen atom closest to the active site with the π-system keeps the system from making a nucleophilic attack on the electrophilic C^{β}. Instead, the inhibitor remains stably complexed in the active site, aided by the overall electrostatic environment.

X-Ray Crystal Structures

The differing protonation states of the two aminoacrylate complexes adds

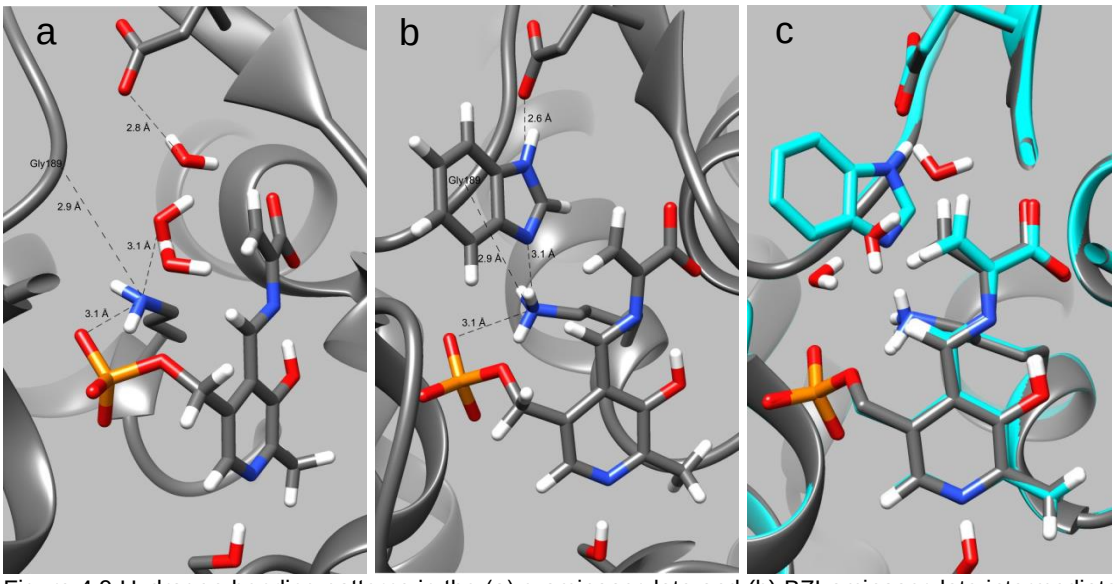

Figure 4.9 Hydrogen-bonding patterns in the (a) α-aminoacrylate and (b) BZI-aminoacrylate intermediates. Changes in the number of H-bonding partners is evidenced in the crystal structures for each intermediate, 4HN4 and 4HPX, respectively. (c) Overlay of the active sites for the α-aminoacrylate (gray) and BZI-aminoacrylate (cyan). Figures rendered with UCSF Chimera.[10]

motivation to the examination of their published crystal structures for evidence of this change in charge at βLys87. Indeed, the crystal structure for the α-aminoacrylate with both the α- and β-subunits in their stable, closed conformations (PDB ID: 4HN4) shows the ε-nitrogen of βLys87 acting as the donor in two different hydrogen bonds: one to an oxygen atom of the phosphoryl group, and one to the carbonyl oxygen of the backbone residue βGly189, figure 4.9a. The ionization state of the phosphoryl group has been established as dianionic, making it clear that the ε-nitrogen is the proton donor in this interaction. The backbone oxygen of βGly189 is also charged, so the ε-nitrogen again must be the proton donor. This nitrogen atom is also the acceptor in a hydrogen bond with a crystallographic water (water 914) molecule located in the active site.

In contrast, the crystal structure for the BZI-aminoacrylate shows the ε-nitrogen of βLys87 playing the role of donor in three hydrogen bonds: one to the phosphoryl group, one to Gly189, and one to N1 of the BZI molecule that is now in the active site, figure 4.9b. As seen in figure 4.9c, the positioning of BZI in the active site displaces three water molecules, and the charged βGlu109 side chain now forms an H-bond with N3 of BZI in place of the H-bond formed with water 583 in the uninhibited structure, suggesting the nitrogen is protonated. Furthermore, N1 on the BZI ring has taken the position of water 914. Our ssNMR results show two distinct nitrogen peaks from the BZI, indicating that the N1 must be deprotonated and now forms a hydrogen-bond with one of the protons on the charged ε-nitrogen, further validation of our protonation state assignments.

Stereoelectronic Control of Nucleophilic Attack

The reactions of indole with electrophilic centers invariably occur at the indole ring C3 carbon. The pronounced nucleophilic properties of the C3 carbon arise as a

consequence of the enamine-like character of the five-membered ring, which conveys high electron density to C3, figure 4.10. Studies on indole and BZI indicate they use fundamentally different mechanisms for reaction.[50-52] The addition of indole to the α-aminoacrylate complex requires formation of a carbon-carbon bond. The nucleophile must make an out-of-plane approach approximately orthogonal to the plane of the π-system for this to occur.[50-52] It is clear from figure 4.9b that indole would be in the correct position to make this approach. BZI was initially proposed to be an analogue of indole, but because BZI mimics the expected binding of indole in the E(A-A)(Indole) complex, BZI is incorrectly aligned for reaction with the electrophilic C^{β} of the α-aminoacrylate group.[51] Reaction of BZI with carbon electrophiles must occur via an in-plane approach at the unprotonated nitrogen.[50-52] Thus, in the BZI-aminoacrylate complex, the reactive BZI orbital lies in the plane of the π-system and is not aligned for nucleophilic attack on the electrophilic C^{β} of the structure, figure 4.9 a and b. Furthermore, owing to the relatively high resonance stabilization of BZI in comparison with indole, BZI is unable to complete the enamine rearrangement by which indole undergoes electrophilic attack, figure 4.10, preventing formation of the nitrogen-carbon bond.[50,53] These results provide direct evidence of the role played by stereoelectronics in directing reaction specificity and highlight the complementary information provided by x-ray crystallography and ssNMR.

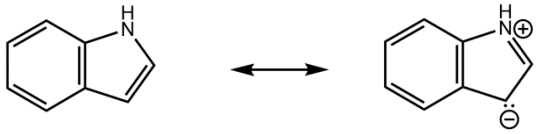

Indole

Figure 4.10 Enamine resonance structure displayed by indole.

Activation of C^{β} for Nucleophilic Attack

The formation of the α-aminoacrylate intermediate activates the α-site reaction and mobilizes the substrate indole to begin its movement through the tunnel to the β-

site. Once there, it makes a nucleophilic attack at C^{β} to give a new carbon-carbon bond and form the next intermediates in the pathway, the second and third carbanionic species. This requires indole to participate in the enamine mechanism, figure 4.10, to create a nucleophilic center at C3, and it also requires that C^{β} be slightly positive to make an attractive nucleophilic target.[3] Figure 4.11 depicts a resonance structure of the α-aminoacrylate intermediate that builds up positive charge at C^{β} and negative charge at C^{α}, creating an electrophilic center at C^{β}. Not only does this create the proper charge environment to ensure reaction with the incoming indole, it also allows a glimpse of the carbanionic intermediate that comes next, figure 4.11. Charge calculations are currently being run by other group members to confirm these mechanistic ideas, but a positively charged C^{β} at this stage of catalysis is consistent with long-standing ideas on PLP catalysis.[3]

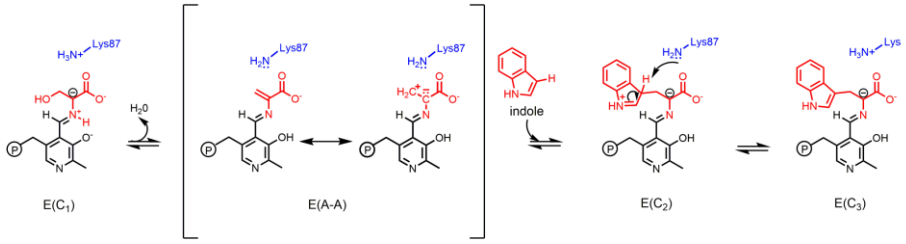

Figure 4.11 The resonance structure of the α-aminoacrylate intermediate allows a preview of the next carbanionic intermediate.

Reaction Specificity

Formation of the α-aminoacrylate intermediate represents a major divergent path in PLP catalysis, as this species is only associated with PLP enzymes that catalyze β-elimination reactions.[22-26] Indeed, in the canonical mechanism used to describe the transamination reaction catalyzed by PLP-dependent enzymes, reprotonation at C4' of the cofactor following the first quinonoid species precludes the establishment of the α-aminoacrylate form, instead forming a ketimine intermediate, figure 4.12.[2,5,54] These

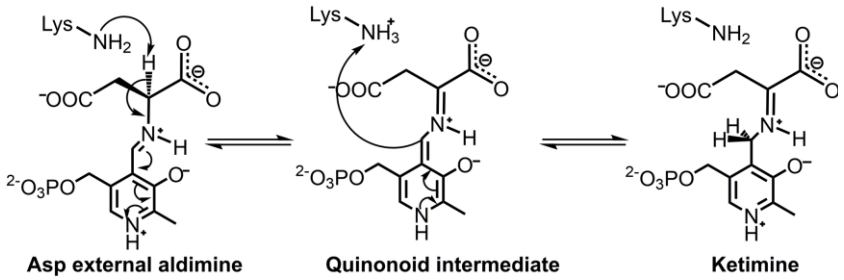

Figure 4.12 Enzymes that do not form an aminoacrylate intermediate instead form a ketimine intermediate.[5]

reactions require a protonated pyridine nitrogen for formation of a true quinonoid intermediate at this stage. For TS, a deprotonated pyridine nitrogen coupled with a protonated phenolic oxygen on the PLP cofactor creates the proper microenvironment for the α-aminoacrylate intermediate to form and the β-elimination and replacement reaction to occur. Furthermore, investigation of the catalytically essential βLys87 shows it poised to act as both acid and base throughout the reaction.[7] A neutral βLys87 in the α-aminoacrylate intermediate suggests that the residue donates a proton to facilitate production of a water molecule, which positions this residue to play the role of base in the next stage of catalysis, consisting of proton abstraction from the attacking nucleophile to give the next stable intermediate, the carbanionic species. Thus, the essential function of ionization states is highlighted in the different roles played by the βLys87 side chain, while stereoelectronic control of reaction of reaction specificity, as proposed by Dunathan,[55] is seen in the inhibited complex with BZI. Improper overlap of orbitals on BZI and the aminoacrylate complex prevents formation of the carbanionic species and shuts down catalysis, stabilizing this intermediate.

4.4 Conclusion

The α-aminoacrylate intermediate formed during TS catalysis ensures a positive charge at C^{β} of the serine substrate to facilitate nucleophilic attack by the incoming indole substrate. Reaction specificity is therefore accomplished through a combination of correct electrostatic environment (*i.e.* protonation states) and stereoelectronic control. The inhibited BZI-aminoacrylate complex allows a rare glimpse of the reaction that occurs with indole, as BZI is presumably positioned where indole would be in the natural reaction, but due to differences in their electronic structures cannot react further. The aminoacrylate structure, on the other hand, suggests the fate of the substrate's β-hydroxyl group and the role of βLys87 as the general acid-base catalyst in the active site. Together, the X-ray crystal structures and protonation states from ssNMR give a generous picture of the reaction and transition states both into and out of the α-aminoacrylate species that would be otherwise unattainable using only ssNMR or X-ray crystallography in isolation.

4.5 References

(1) Metzler, D. E.; Ikawa, M.; Snell, E. E. *J Am Chem Soc* **1954**, *76*, 648.

(2) Kallen, R. G.; Korpela, T.; Martell, A. E.; Matsushima, Y.; Metzler, C. M.; Metzler, D. E.; Morozov, Y. V.; Ralston, I. M.; Savin, F. A.; Torchinsky, Y. M.; Ueno, H. In *Transaminases*; Christen, P., Metzler, D. E., Eds.; John Wiley & Sons, Inc.: New York, 1985, p 37.

(3) Walsh, C. *Enzymatic Reaction Mechanisms*; W. H. Freeman: San Francisco, 1979.

(4) Hayashi, H. *J Biochem* **1995**, *118*, 463.

(5) Toney, M. D. *BBA - Protein Proteom* **2011**, *1814*, 1407.

(6) Caulkins, B. G.; Bastin, B.; Yang, C.; Neubauer, T. J.; Young, R. P.; Hilario, E.; Huang, Y. M.; Chang, C. E.; Fan, L.; Dunn, M. F.; Marsella, M. J.; Mueller, L. J. *J Am Chem Soc* **2014**, *136*, 12824.

(7) Caulkins, B. G.; Yang, C.; Hilario, E.; Fan, L.; Dunn, M. F.; Mueller, L. J. *BBA - Protein Proteom* **2015**, *1854*, 1194.

(8) Caulkins, B. G.; Young, R. P.; Kudla, R. A.; Yang, C.; Bittbauer, T. J.; Bastin, B.; Hilario, E.; Fan, L.; Marsella, M. J.; Dunn, M. F.; Mueller, L. J. *J Am Chem Soc* **2016**, *138*, 15214.

(9) Young, R. P.; Caulkins, B. G.; Borchardt, D.; Bulloch, D. N.; Larive, C. K.; Dunn, M. F.; Mueller, L. J. *Angew Chem Int Ed Engl* **2016**, *55*, 1350.

(10) Pettersen, E. F.; Goddard, T. D.; Huang, C. C.; Couch, G. S.; Greenblatt, D. M.; Meng, E. C.; Ferrin, T. E. *J Comput Chem* **2004**, *25*, 1605.

(11) Fischer, E. H.; Kent, A. B.; Snyder, E. R.; Krebs, E. G. *J Am Chem Soc* **1958**, *80*, 2906.

(12) Hughes, R. C.; Jenkins, W. T.; Fischer, E. H. *Proc Natl Acad Sci USA* **1962**, *48*, 1615.

(13) Hyde, C. C.; Ahmed, S. A.; Padlan, E. A.; Miles, E. W.; Davies, D. R. *J Biol Chem* **1988**, *263*, 17857.

(14) Dunn, M. F.; Niks, D.; Ngo, H.; Barends, T. R.; Schlichting, I. *Trends Biochem Sci* **2008**, *33*, 254.

(15) Lane, A. N.; Kirschner, K. *Eur J Biochem* **1983**, *129*, 571.

(16) Miles, E. W. *Adv Enzymol Relat Areas Mol Biol* **1979**, *49*, 127.

(17) Yanofsky, C.; Crawford, I. P. In *The Enzymes Third Edition*; Boyer, P. D., Ed.; Academic Press, Inc.: New York, NY, 1972; Vol. 7, p 1.

(18) Dunn, M. F. *Arch Biochem Biophys* **2012**, *519*, 154.

(19) Hilario, E.; Caulkins, B. G.; Huang, Y. M.; You, W.; Chang, C. E.; Mueller, L. J.; Dunn, M. F.; Fan, L. *BBA - Protein Proteom* **2016**, *1864*, 268.

(20) Dunn, M. F.; Aguilar, V.; Brzovic, P.; Drewe, W. F., Jr.; Houben, K. F.; Leja, C. A.; Roy, M. *Biochemistry* **1990**, *29*, 8598.

(21) Miles, E. W. *Chemical Record* **2001**, *1*, 140.

(22) Phillips, R. S.; Chen, H. Y.; Faleev, N. G. *Biochemistry* **2006**, *45*, 9575.

(23) Schnell, R.; Oehlmann, W.; Singh, M.; Schneider, G. *J Biol Chem* **2007**, *282*, 23473.

(24) Shimon, L. J.; Rabinkov, A.; Shin, I.; Miron, T.; Mirelman, D.; Wilchek, M.; Frolow, F. *J Mol Biol* **2007**, *366*, 611.

(25) Woehl, E. U.; Tai, C. H.; Dunn, M. F.; Cook, P. F. *Biochemistry* **1996**, *35*, 4776.

(26) Yadav, P. K.; Banerjee, R. *J Biol Chem* **2012**, *287*, 43464.

(27) Ngo, H.; Kimmich, N.; Harris, R.; Niks, D.; Blumenstein, L.; Kulik, V.; Barends, T. R.; Schlichting, I.; Dunn, M. F. *Biochemistry* **2007**, *46*, 7740.

(28) Niks, D.; Hilario, E.; Dierkers, A.; Ngo, H.; Borchardt, D.; Neubauer, T. J.; Fan, L.; Mueller, L. J.; Dunn, M. F. *Biochemistry* **2013**, *52*, 6396.

(29) Schneider, T. R.; Gerhardt, E.; Lee, M.; Liang, P. H.; Anderson, K. S.; Schlichting, I. *Biochemistry* **1998**, *37*, 5394.

(30) Brzovic, P. S.; Hyde, C. C.; Miles, E. W.; Dunn, M. F. *Biochemistry* **1993**, *32*, 10404.

(31) Ferrari, D.; Niks, D.; Yang, L. H.; Miles, E. W.; Dunn, M. F. *Biochemistry* **2003**, *42*, 7807.

(32) Ngo, H.; Harris, R.; Kimmich, N.; Casino, P.; Niks, D.; Blumenstein, L.; Barends, T. R.; Kulik, V.; Weyand, M.; Schlichting, I.; Dunn, M. F. *Biochemistry* **2007**, *46*, 7713.

(33) Kirschner, K.; Lane, A. N.; Strasser, A. W. M. *Biochemistry* **1991**, *30*, 472.

(34) Goriya, Y.; Ramana, C. V. *Tetrahedron* **2010**, *66*, 7642.

(35) Hornberger, K. R.; Adjabeng, G. M.; Dickson, H. D.; Davis-Ward, R. G. *Tetrahedron Lett* **2006**, *47*, 5359.

(36) Fung, B. M.; Khitrin, A. K.; Ermolaev, K. *J Magn Reson* **2000**, *142*, 97.

(37) Harris, R. K.; Becker, E. D.; Cabral de Menezes, S. M.; Granger, P.; Hoffman, R. E.; Zilm, K. W. *Pure Appl Chem* **2008**, *80*, 59.

(38) Morcombe, C. R.; Zilm, K. W. *J Magn Reson* **2003**, *162*, 479.

(39) Hayashi, S.; Hayamizu, K. *Bull Chem Soc Jpn* **1991**, *64*, 688.

(40) McNeill, S. A.; Gor'kov, P. L.; Shetty, K.; Brey, W. W.; Long, J. R. *J Magn Reson* **2009**, *197*, 135.

(41) Maurer, T.; Kalbitzer, H. R. *J Magn Reson, Ser B* **1996**, *113*, 177.
(42) Gullion, T.; Schaefer, J. *J Magn Reson* **1989**, *81*, 196.

(43) Limbach, H. H.; Chan-Huot, M.; Sharif, S.; Tolstoy, P. M.; Shenderovich, I. G.; Denisov, G. S.; Toney, M. D. *BBA - Protein Proteom* **2011**, *1814*, 1426.

(44) Sharif, S.; Fogle, E.; Toney, M. D.; Denisov, G. S.; Shenderovich, I. G.; Buntkowsky, G.; Tolstoy, P. M.; Huot, M. C.; Limbach, H. H. *J Am Chem Soc* **2007**, *129*, 9558.

(45) Chan-Huot, M.; Dos, A.; Zander, R.; Sharif, S.; Tolstoy, P. M.; Compton, S.; Fogle, E.; Toney, M. D.; Shenderovich, I.; Denisov, G. S.; Limbach, H. H. *J Am Chem Soc* **2013**, *135*, 18160.

(46) Harbison, G. S.; Herzfeld, J.; Griffin, R. G. *Biochemistry* **1983**, *22*, 1.

(47) Harruff, R. C.; Jenkins, W. T. *Org Magn Reson* **1976**, *8*, 548.

(48) O'Leary, M. H.; Payne, J. R. *J Biol Chem* **1976**, *251*, 2248.

(49) Schnackerz, K. D.; Andi, B.; Cook, P. F. *BBA - Protein Proteom* **2011**, *1814*, 1447.

(50) Hofmann, K. *Imidazole and Its Derivatives*; Wiley-Interscience, 1953; Vol. 6.

(51) Roy, M.; Keblawi, S.; Dunn, M. F. *Biochemistry* **1988**, *27*, 6698.

(52) Sundberg, R. J. *The Chemistry of Indoles*; Academic Press, Inc.: New York, NY, 1970; Vol. 18.

(53) Faour, M.; Akasheh, T. S. *J Chem Soc, Perkin Trans 2* **1985**, 811.

(54) Arnone, A.; Christen, P.; Jansonius, J. N.; Metzler, D. E. In *Transaminases*; Christen, P., Metzler, D. E., Eds.; John Wiley & Sons, Inc.: New York, 1985, p 326.

(55) Dunathan, H. C. *Proc Natl Acad Sci USA* **1966**, *55*, 712.

Chapter 5 – The Carbanion

5.1 Introduction

Pyridoxal-5'-phosphate (PLP), figure 5.1, acts as a cofactor in a large family of enzymes involved in the metabolism of amino acids and other amine-containing biomolecules.[1-4] This single cofactor can participate in a diverse array of chemical transformations, including racemization, transamination, α/β-decarboxylation, and α/β/γ- elimination and substitution, yet the factors that fine-tune PLP for a specific reaction have yet to be fully delineated.[5-8] While stereoelectronic considerations play a clear role in directing the first step of catalysis,[12] the majority of PLP-dependent transformations are initiated by the same α-deprotonation step, so additional specificity must be conferred during subsequent stages.[5-7] Studies of model PLP compounds show the important function of both protonation states and tautomerization in modulating chemical reactivity.[8,14-17] In enzymes, it has been proposed that the active-site residues interacting with the cofactor establish the appropriate chemical and electrostatic environment to favor a particular protonation state and a corresponding reaction pathway.[5,7,8] Here, we critically test this hypothesis by determining the protonation states of a carbanionic/quinonoid intermediate in the β-subunit active site of the PLP-requiring enzyme tryptophan synthase (TS, EC 4.2.1.20).

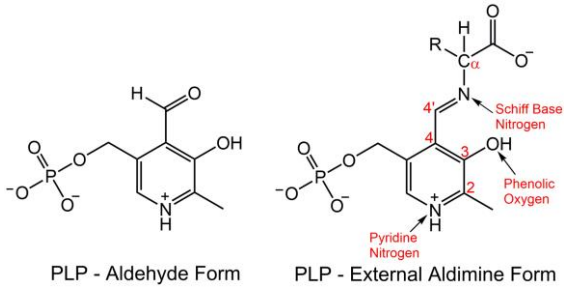

Figure 5.1 Pyridoxal-5′-phosphate (PLP) in both its aldehyde and external aldimine forms.

The canonical mechanism for PLP-dependent enzyme catalysis, first proposed to explain the reaction that occurs in aminotransferase enzymes, relies on the intrinsic

property of quinonoid species to function as electron sinks to effect bond cleavage and formation in the reacting amino acid moieties.[1,18] Scheme 5.1 highlights the initial mechanistic steps common to all PLP-dependent enzymes that undergo α-

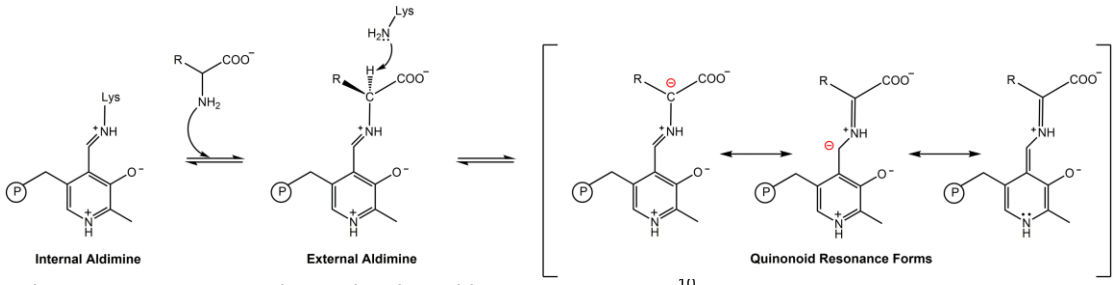

Scheme 5.1 α-Deprotonation and Quinonoid Resonance Forms[10]

deprotonation.[7,19] In the resting holoenzyme form, the cofactor is bound via a Schiff base linkage to the ε-nitrogen of a lysine side chain (the internal aldimine state). In the first step of the catalytic cycle, an incoming amino acid substrate makes a nucleophilic attack at C4' of the internal aldimine Schiff base, displacing the covalent bond between the enzyme and the cofactor and replacing it with a Schiff base linkage between the substrate and PLP (the external aldimine species). Next, a base abstracts the proton from the substrate C^{α}, forming a carbanionic intermediate that is resonance-stabilized through charge delocalization.[7,18] This intermediate is generally referred to as the quinonoid intermediate due to its quinone-like resonance structure. In practice, the quinone resonance form can only contribute significantly to the ground-state electronic structure when the pyridine ring nitrogen is protonated (the canonical/true quinonoid form). Experimental support for the formation of a true quinonoid intermediate comes from UV/Vis spectroscopy, which shows a characteristic absorption in the 460 to 550 nm range,[18,20,21] and X-ray crystallography, which identifies acidic residues hydrogen bonded

to the pyridine nitrogen in several large classes of PLP-dependent enzymes; these residues are expected to form ion pairs with a protonated pyridine ring nitrogen.[22-26]

Recently, the requirement to move through a canonical quinonoid intermediate in all PLP-dependent enzymes has been called into question.[7,27-29] Several groups have put forward the hypothesis that in certain cases the intermediate that forms is not a true quinonoid, but rather a carbanionic species – the chief distinction again being whether the pyridine ring nitrogen is protonated and can thus support significant quinone character.[7,30-32] This hypothesis is supported by structural studies of several PLP-dependent enzymes that find hydrogen bonding interactions between the pyridine ring nitrogen and side chains of polar, non-acidic residues, such as serine, and positively charged residues, such as arginine.[33-36] These side chains are not logical proton donors for conversion to the canonical quinonoid structure. But due in part to the paucity of atomic-resolution structural data (neither X-ray crystallography nor UV/Vis spectroscopy can directly identify proton locations), the obligatory formation of canonical quinonoid intermediates has remained the dominant view of PLP catalysis.[37,38]

A growing number of solid-state nuclear magnetic resonance (ssNMR) studies have shown the essential role that NMR can play in the atomic-resolution characterization of chemical structure for intermediates and intermediate analogues in PLP-dependent enzymes.[8,39-45] In particular, ^{15}N ssNMR chemical shift measurements of the pyridine ring nitrogen in the internal aldimine form of aspartate aminotransferase confirm that at the start of catalysis the pyridine nitrogen is protonated and ready to assist in the formation of a canonical quinonoid intermediate.[8] This is in contrast to the neutral pyridine nitrogen found by ssNMR in the resting internal aldimine forms of tryptophan synthase and alanine racemase.[8,40] However, in the case of TS, the pyridine

nitrogen interacts with the hydroxyl group of a serine residue.[33] The serine hydroxyl can act as both a hydrogen bond donor and acceptor, and it is unclear whether the pyridine ring nitrogen becomes protonated as the reaction unfolds, thus assuming the canonical quinonoid form, or if a carbanion is formed that is stabilized by a combination of charge delocalization and electrostatic interactions involving other atoms in the site. To date there have been no reports of ^{15}N NMR chemical shift measurements for the PLP nitrogen of any quinonoid/carbanionic intermediate.

Here we report ssNMR chemical shifts for a carbanionic/quinonoid intermediate in the β-subunit active site of *S. typhimurium* tryptophan synthase, including the first such measurement for the cofactor pyridine ring nitrogen in a quinonoid species. There are several intermediates formed during the β-reaction that can be rendered quasi-stable through the choice of monovalent cation[46] and α-active site ligand,[47] control of pH,[48] and introduction of indole analogues, scheme 5.2.[39,49] In this work, we interrogate the

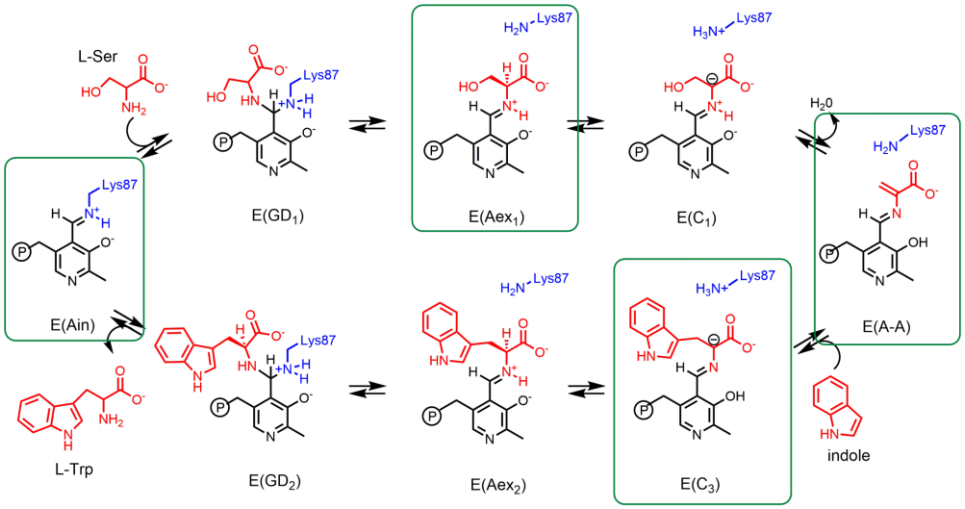

Scheme 5.2 The β-subunit reaction in TS. Stable intermediates are boxed in green.

substrate-cofactor active-site complex formed by the reaction of L-Ser and 2-aminophenol (2AP) with the PLP-cofactor in TS.[40,50] This intermediate, termed the 2AP-

quinonoid ($E(C_3)_{2AP}$), scheme 5.3, is a long-lived analogue of the transient $E(C_3)$, scheme 5.2, allowing for measurement of the ^{15}N chemical shift of the PLP pyridine ring nitrogen and ^{13}C, ^{15}N, ^{17}O, and ^{31}P isotropic and anisotropic chemical shifts on the coenzyme, substrates and active-site side chains.[51] Several of the key chemical shifts, including that for the PLP pyridine nitrogen, are found to fall outside the ranges anticipated based on model compound studies. To interpret these shifts in terms of the protonation states of the intermediate, we turn to "NMR Crystallography" – the combination of X-ray diffraction and solid-state NMR spectroscopy coupled with computational chemistry.[52-56] For the 2AP quinonoid analogue in TS, NMR crystallography provides direct, atomic-resolution support for the carbanionic form of the intermediate, ruling out a true quinonoid species and suggesting an equilibrium between the phenolic and protonated Schiff base tautomers that favors the phenolic form. Natural bond orbital (NBO) calculations[11] show the buildup of negative charge at the substrate C^{α} for the protonated Schiff base form, implicating it as the catalytically significant tautomer. This is consistent with the proposed role of protonation states in directing reaction specificity in tryptophan synthase and points to the vital contribution that NMR crystallography can make to linking both atomic-resolution structure and chemical dynamics to enzyme mechanism.

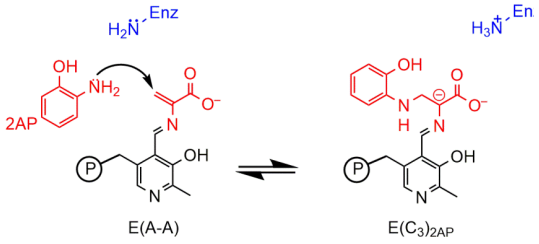

Scheme 5.3 Formation of the 2AP Quinonoid Intermediate

5.2 Experimental Details

Protein Preparation

Tryptophan synthase was prepared by overexpression of *S. typhimurium* TS in *E. coli* as previously described.[40,41] Samples were prepared with the following isotopic labeling schemes for the cofactor and protein components: (1) Protein and cofactor unlabeled/natural abundance isotopomer concentration; (2) Protein ^{15}N-labeled at lysine ε-nitrogen sites; PLP unlabeled (ε-^{15}N-Lys TS); (3) PLP cofactor selectively ^{13}C enriched at carbon sites C2, C2', and C3 and ^{15}N enriched at the pyridine ring nitrogen; protein unlabeled (2,2',3-$^{13}C_3$,^{15}N-PLP; TS); and (4) PLP cofactor selectively ^{13}C,^{15}N enriched; protein uniformly ^{15}N-labeled (2,2',3-$^{13}C_3$,^{15}N-PLP; U-^{15}N TS).

Microcrystalline Protein Samples for Solid-State NMR

Microcrystalline samples of TS were prepared by diluting enzyme solution 1:1 with 50 mM Cs-bicine buffer, pH 7.8, containing 14% PEG-8000 and 3.0 mM spermine as previously described.[40] Microcrystals were collected and washed with 50 mM Cs-bicine, pH 7.8, containing 8% PEG-8000, 1.8 mM spermine, and 3 mM N-(4'-trifluoromethoxybenzenesulfonyl)-2-aminoethyl phosphate (F9; a high affinity alpha site ligand and analogue of the natural α-site substrate 3-idole-D-glycerol-3'-phosphate (IGP)). The crystals were packed at 10,000 rpm into a Bruker 4 mm magic-angle spinning (MAS) rotor with an approximate volume of 80 µL; each rotor contained 25-30 mg of protein. To form the 2AP quinonoid intermediate, serine was introduced by direct addition of 5 µL of 1.2 M L-Ser to the packed MAS rotor, while 2AP was introduced by addition of 8 µL of a concentrated stock solution of 2AP in acetonitrile. Stabilization of the 2AP quinonoid species is enhanced by low temperature (-5 °C), the use of the tight

binding α-subunit ligand F9, and the presence of Cs^+,[47] which binds to the monovalent cation site in the β-subunit.

NMR Spectroscopy

^{13}C and ^{15}N Solid-State NMR Spectroscopy: ^{13}C and ^{15}N cross-polarization (CP) magic-angle-spinning (MAS) experiments were performed at 9.4 T (400.37 MHz ^{1}H, 100.69 MHz ^{13}C, 40.57 MHz ^{15}N) on a Bruker AVIII spectrometer equipped with a double resonance, 4 mm MAS probe, spinning at MAS rates of 8 kHz; the bearing gas was cooled to -15 °C, giving an effective sample temperature of -5 °C in both cases. Cross-polarization was accomplished at a ^{1}H spin-lock field of 45 kHz and a ^{13}C/^{15}N spin-lock of 54 kHz (^{13}C) and 37 kHz (^{15}N) (ramped +/- 2 kHz); 85 kHz Spinal64 ^{1}H decoupling[57] was used throughout. Standard ^{13}C spectra consist of the sum of 16,384 transients acquired with a relaxation delay of 4 s, for a total acquisition time of 18.3 h; slow MAS spectra consist of the sum of 122,880 transients acquired with a relaxation delay of 4 s, for a total acquisition time of 5 d 16 h. ^{13}C chemical shifts were referenced indirectly to neat TMS via an external solid-state sample of adamantane with the downfield-shifted peak set to 38.48 ppm.[58,59] Standard ^{15}N spectra consist of the sum of 81,920 transients acquired with a relaxation delay of 4 s, for a total acquisition time of 3 d 19 h. ^{15}N chemical shifts were referenced indirectly to liq-NH_3 (25 °C) via an external solid-state sample of $^{15}NH_4Cl$, in which the resonance frequency was set to 39.27 ppm.[58,60]

The acquisition of solid-state NMR spectra was interleaved with single pulse, low-power decoupling experiments (64 scans ^{13}C, 256 scans ^{15}N) reporting predominantly on free ligand and reaction products in solution (mother liquor). Acquisition of solid-state NMR spectra for the intermediate was halted before reactant concentrations in solution fell to zero.

^{31}P Solid-State NMR Spectroscopy: ^{31}P CPMAS experiments were performed at 14.1 T (600.01 MHz ^{1}H, 242.89 MHz ^{31}P) on a Bruker AVIII spectrometer equipped with a ^{1}H-X double resonance 4 mm MAS probe, spinning at a MAS rate of 10 kHz. The bearing gas was cooled to -15 °C, giving an effective sample temperature of -5 °C. Cross-polarization was accomplished with a ^{1}H spin-lock field of 45 kHz and a ^{31}P spin-lock of 47 kHz (ramped +/- 5 kHz); 58 kHz Spinal64 ^{1}H decoupling[57] was used during detection. The ^{31}P spectrum consists of the sum of 4,096 transients acquired with a relaxation delay of 3 s, for a total acquisition time of 3.4 h. ^{31}P chemical shifts were indirectly referenced to 85% H_3PO_4 (MAS). For comparison to measurements in solution, δ[85% H_3PO_4 (capillary)] = δ[85% H_3PO_4 (sphere/MAS)] + 0.36 ppm.[61]

^{13}C-observe, ^{15}N-dephased Rotational Echo Double Resonance (REDOR) Experiments: ^{13}C{^{15}N}-REDOR[9] experiments were performed at 9.4 T (400.37 MHz ^{1}H, 100.69 MHz ^{13}C, 40.57 MHz ^{15}N) on a Bruker AVIII spectrometer equipped with a triple resonance 4 mm MAS probe (sample volume ~80 µl) and spinning at a MAS rate of 5 kHz. The bearing gas was cooled to -15 °C, giving an effective sample temperature of -5 °C. Cross-polarization was accomplished at a ^{1}H spin-lock field of 45 kHz, ^{13}C spin-lock of 54 kHz (ramped +/- 2 kHz), and a 2 ms contact time; 85 kHz Spinal64 ^{1}H decoupling[57] was used throughout. A single 10 µs π pulse was applied to ^{13}C at the center of the 10 ms echo period (S_o), while a series of 14 µs π pulses at half rotor intervals were applied to ^{15}N during the dephasing (S) experiments. The REDOR S and S_o spectra were acquired in an interleaved fashion, and each spectrum consists of the sum of 2,048 transients acquired with a relaxation delay of 4 s, for a total acquisition time of 2.3 h.

^{15}N-observe, ^{31}P-dephased Rotational Echo Double Resonance (REDOR) Experiments: ^{15}N{^{31}P}-REDOR[9] experiments were performed at 14.1 T (600.11 MHz ^{1}H;

60.81 MHz ^{15}N; 242.93 MHz ^{31}P) on a Bruker AVANCE 600 spectrometer equipped with an NHMFL low-E, triple resonance 3.2 mm MAS probe[62] (sample volume ~ 40 µl) and spinning at a MAS rate of 8 kHz. The bearing gas was cooled to -15 °C, giving an effective sample temperature of -5 °C. Cross-polarization was accomplished at a ^{1}H spin-lock field of 45 kHz, ^{15}N spin-lock of 37 kHz (ramped +/- 2 kHz), and a 2 ms contact time; 100 kHz Spinal64 ^{1}H decoupling[57] was used throughout. A single 10 µs π pulse was applied to ^{15}N at the center of the 25 ms echo period, while a series of 10 µs π pulses at half rotor intervals were applied to ^{31}P during the dephasing (*S*) experiments. The REDOR *S* and S_o spectra were acquired in an interleaved fashion, and each spectrum consists of the sum of 12,288 transients acquired with a relaxation delay of 3 s, for a total acquisition time of 10.4 h.

X-Ray Crystallography

The X-ray crystal structure of the tryptophan synthase 2AP quinonoid intermediate analogue with Cs^+ bound to the monovalent cation site and N-(4'-trifluoromethoxybenzenesulfonyl)-2-aminoethyl phosphate (F9) bound to the α-site was solved at 1.45 Å resolution and previously reported.[50] The PDB accession code is 4HPJ.[11]

First Principles Calculations

Natural bond orbital (NBO) partial atomic charges were calculated for the geometry-optimized models using natural population analysis[63] within the NBO 6.0 program.[64] These calculations were performed on the same structures and at the same level of theory used for the NMR calculations by Robert Young.[11]

5.3 Results and Discussion

^{15}N Chemical Shift Measurements

Figure 5.2 shows ^{15}N solid-state NMR spectra of the tryptophan synthase 2AP quinonoid intermediate prepared under the following five isotopic-labeling conditions: (5.2a) natural abundance isotopomer concentration; (5.2b) selectively ^{13}C,^{15}N enriched on the PLP cofactor (2,2',3-$^{13}C_3$,^{15}N-PLP; TS); (5.2c) ^{15}N-enriched on the L-Ser substrate; (5.2d) ^{15}N-labeled on the 2AP substrate; and (5.2e/5.2f) selectively ^{15}N-enriched at all protein lysine ε-nitrogen side chain sites (ε-^{15}N-Lys TS). The spectrum acquired at natural abundance, figure 5.2a, shows primarily signals from the large

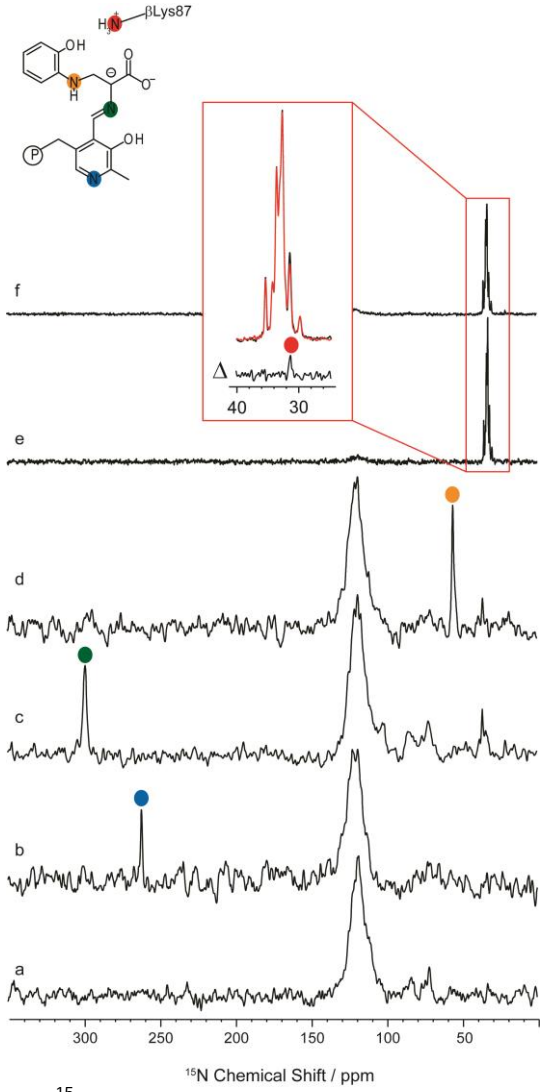

Figure 5.2 ^{15}N ssNMR CPMAS spectra of the microcrystalline TS 2AP quinonoid intermediate prepared with the following isotopic labeling: (a) natural abundance isotopomer concentration; (b) selectively ^{13}C,^{15}N enriched on the PLP cofactor; (c) ^{15}N-enriched on the substrate L-Ser; (d) ^{15}N-labeled on the substrate 2AP; and (e,f) selectively ^{15}N-enriched at lysine ε-nitrogen side chain sites. Spectra (e) and (f) form an ^{15}N{^{31}P}-REDOR pair; both have a 25 ms echo period on ^{15}N before detection, but (f) includes the application of dipolar dephasing to ^{31}P. Their difference spectrum (Δ) allows for the selective observation of N^{ε} for the active site lysine side chain. Spectra acquired at 9.4 T (a-d),14.1 T (e,f), and 8 kHz MAS.

number of protein backbone nitrogen atoms; these are centered near 122 ppm. With the incorporation of the isotopically enriched PLP cofactor, a new spectral feature at 262.0 ppm is observed that can be assigned to the pyridine ring N1 atom, figure 5.2b. This chemical shift immediately presents a puzzle – a protonated pyridine nitrogen would be expected to fall below 200 ppm, while the signal for a deprotonated pyridine nitrogen should be greater than 300 ppm.[14,17,45] Negligible temperature dependence is found for the PLP nitrogen chemical shift, figure 5.3a, which together with the narrow line width

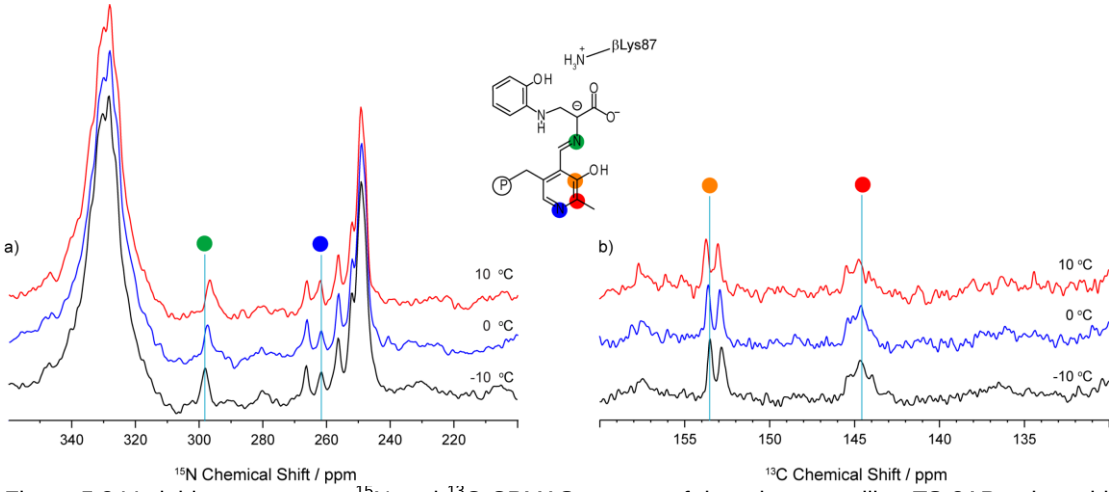

Figure 5.3 Variable-temperature ^{15}N and ^{13}C CPMAS spectra of the microcrystalline TS 2AP quinonoid intermediate prepared with 2,2',3-$^{13}C_3$,^{15}N-PLP, ^{15}N-Ser, and U-^{15}N-TS. Substantial temperature dependence is observed for the Schiff base nitrogen (green dot) and PLP carbon-3 sites (orange dot). In (b), the scalar coupling between C3 and C2 is resolved. The large spectral feature at 330 ppm in (a) is a spinning sideband of the uniformly-^{15}N labeled amide backbone. Spectra acquired at 9.4 T and 8 kHz MAS.

argues against proton exchange as the source of the intermediate shift value. Pyridine ring nitrogen chemical shifts in this range have been observed for model PLP-aldimine complexes that participate in strong hydrogen bonds with carboxylic acids.[8] But an upfield shift of this magnitude would require a significant displacement of the proton towards the pyridine nitrogen, and it is unclear whether it would form such a strong hydrogen bond with its partner, the side-chain hydroxyl of βSer377.

Figure 5.2c shows the spectrum of the 2AP quinonoid prepared using ^{15}N-enriched L-Ser, which introduces a ^{15}N isotopic label at the Schiff base position. At 298.6 ppm, the chemical shift of this site is indicative of a (mostly) neutral imine. Variable temperature experiments show a more substantial chemical shift temperature dependence for the Schiff-base nitrogen (-0.07 ppm/K), figure 5.3a, suggesting that this site may be participating in chemical exchange. Figure 5.2d shows the spectrum of the intermediate prepared using ^{15}N-labeled 2AP. The chemical shift of 56.0 ppm for the amine linkage helps establish that the connection from serine to 2AP is through the amino rather than the 2AP phenolic group, a fact that cannot be determined directly from crystallography. This bond is confirmed by ^{13}C-observe, ^{15}N-dephased rotational echo double resonance (REDOR) experiments performed on the microcrystalline TS 2AP quinonoid intermediate prepared with ^{15}N-2AP, 3-^{13}C-Ser, and NA-TS, figure 5.4 a and b. Both have a 10 ms echo period on ^{13}C after cross-polarization, but differ in the application of π pulses to ^{15}N (at the quarter and three-quarter mark of each rotor period) in b. Strong dipolar coupling of the 2AP nitrogen to its directly bonded neighbor, the C^{β} of serine, leads to efficient REDOR dephasing, substantiating the connectivity between the substrates is through the amino group of 2AP.

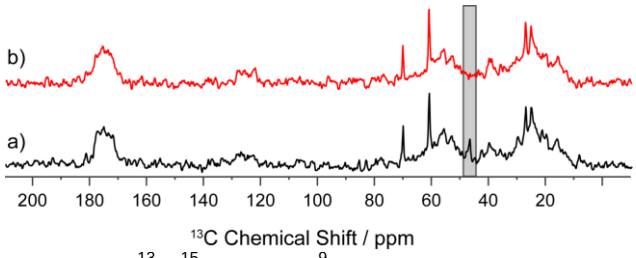

Figure 5.4 ^{13}C{^{15}N}-REDOR[9] S_o *and* S spectra of the microcrystalline TS 2AP quinonoid intermediate prepared with ^{15}N-2AP, 3-^{13}C-Ser, and NA-TS. Both have a 10 ms echo period after cross-polarization, but differ in the application of π pulses to ^{15}N (at the quarter and three-quarter mark of each rotor period) in b. Spectra acquired at 9.4 T and 8 kHz MAS.

To determine the charge state of the active-site, catalytic βLys87 side chain, a protein sample was prepared in which all lysine residues were ^{15}N-enriched at the ε-

nitrogen sites (ε-^{15}N-Lys TS). The spectrum of this sample, figure 5.2e, shows a large number of mostly overlapped resonances centered at 33 ppm. These correspond to charged ε-amino groups on the labeled lysine residues, and presumably βLys87 is among them. We previously reported that the amino group of βLys87 is neutral and resonates at 24.2 ppm in the TS aminoacrylate intermediate, and that the addition of 2AP to form the quinonoid correlates with the loss of this resonance.[41] These data suggest that upon moving from the aminoacrylate to the 2AP quinonoid form, the βLys87 side chain switches from neutral to positively charged, consistent with the proposed mechanism in which βLys87 plays an alternating acid and base role.[41] To directly observe the βLys87 resonance, we take advantage of the fact that it is the only lysine residue within the active site and the only lysine with close spatial proximity to the phosphoryl group of PLP; the crystal structure shows that βLys87 and the cofactor phosphoryl are hydrogen bonded with a distance of 3.7 Å between the PLP phosphorus atom and the side chain ε-nitrogen (PDB ID: 4HPJ). The other 26 lysines in the TS αβ-dimer are located on the exterior of the protein, and none is closer than 11.1 Å to the PLP phosphorus or 9.5 Å to the F9 phosphorus (the only other phosphorus atom present in the complex). This allows for observation of βLys87 using ^{15}N-observe,^{31}P-dephased rotational-echo double-resonance[9] (^{15}N{^{31}P} -REDOR) difference experiments, figure 5.2e/5.2f. These experiments selectively edit out ^{15}N resonances that are strongly dipolar coupled, and therefore close in space, to a phosphorus atom. The spectra in figure 5.2e and 5.2f form a REDOR pair; each has a 25 ms echo period on ^{15}N before detection, but 5.2f includes the application of dipolar dephasing to ^{31}P. There is a single resonance at 31.5 ppm that is selectively attenuated. Based on proximity to the

phosphoryl group, this resonance is assigned to the ε-amino group of βLys87, confirming its charged state.

^{13}C Chemical Shift Measurements

Figure 5.5 shows ^{13}C solid-state NMR spectra of the tryptophan synthase 2AP quinonoid intermediate prepared under the following three isotopic labeling conditions: (5.5a) natural abundance isotopomer concentration; (5.5b) selectively ^{13}C,^{15}N enriched on the PLP cofactor (2,2',3-$^{13}C_3$,^{15}N-PLP TS); and (5.5c) U-$^{13}C_3$,^{15}N-enriched on L-Ser. Considerably more background signals are observed at ^{13}C natural abundance (1.1%) compared to ^{15}N (0.36%), figure 5.2a. In figure 5.5b, the incorporation of isotopically ^{13}C-enriched PLP leads to three new resonances at 17.0, 144.6, and 153.1 ppm; based on their chemical shifts and *J*-coupling patterns, figure 5.3b, these are assigned to C2′, C2, and C3 of PLP, respectively. The C2 and C3 shifts are important for establishing the charge state of the PLP phenolic oxygen, and comparison to model compound studies by Harruff and Jenkins[65] and O'Leary and Payne[66] indicates a protonated phenolic oxygen on PLP for this intermediate. These shifts can be contrasted with those for the TS internal aldimine, which fall at 158.4 ppm and 168.6 ppm for C2 and C3, respectively[40] – values consistent

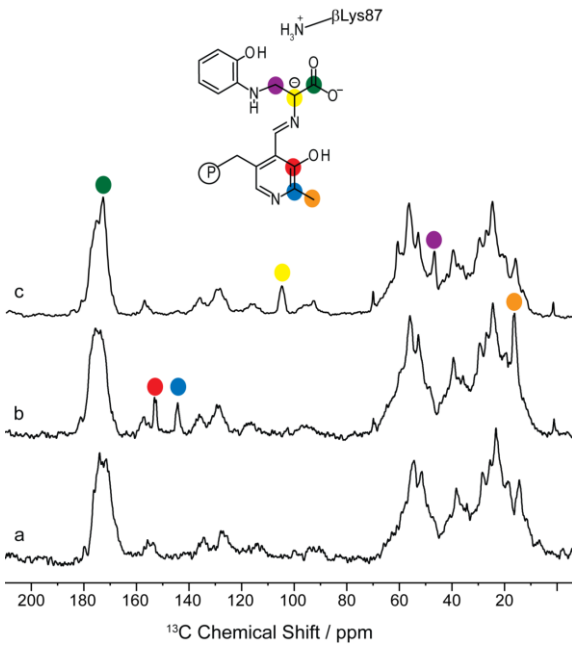

Figure 5.5 ^{13}C ssNMR CPMAS spectra of the microcrystalline TS 2AP quinonoid intermediate prepared under (a) natural abundance isotopomer concentration; (b) selectively ^{13}C,^{15}N-enriched on the PLP cofactor; and (c) U-$^{13}C_3$,^{15}N-enriched on the substrate L-Ser. Spectra acquired at 9.4 T and 8 kHz MAS.

with the zwitterionic form in which the phenolic oxygen is deprotonated. Figure 5.3b shows that C3 has a slight temperature dependence of +0.012 ppm/K for the 2AP quinonoid intermediate, moving downfield away from the protonated, phenolic form and toward the deprotonated, phenolate form. The spectrum in Figure 5.5c, measured for the intermediate formed with U-$^{13}C_3$,^{15}N-L-Ser, shows three new resonances at 173.1 ppm, 105.1 ppm, and 47.0 ppm that can be assigned to carbons that derive from the serine C', C^{α}, and C^{β}, respectively. These shifts are similar to those reported for the TS quinonoid formed with indoline.[39]

^{31}P Chemical Shift Measurements

The ^{31}P solid-state NMR spectrum of the tryptophan synthase 2AP quinonoid intermediate is shown in figure 5.6. The isotropic shift of the PLP cofactor shows a characteristic response in solution as the phosphoryl moves from the mono- to the dianionic form.[67] The isotropic shift in the 2AP quinonoid at 4.9 ppm places it firmly in the dianionic regime.

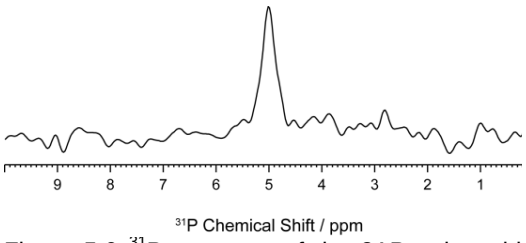

Figure 5.6 ^{31}P spectrum of the 2AP quinonoid intermediate formed with NA-TS, 2AP, and serine. The istotropic chemical shift confirms a dianionic state for this functional group. Spectrum acquired at 14.1 T and 10 kHz MAS.

Protonation States of the 2AP Quinonoid Intermediate from NMR Crystallography

Taken together, the chemical shifts for the 2AP quinonoid intermediate, summarized in table 5.1, allow a preliminary model to be proposed for the protonation states on and near the cofactor-substrate complex in the active site of tryptophan synthase. With good confidence it can be concluded that the phosphoryl group is dianionic and the ε-amino group of βLys87 is positively charged. At the same time, the ^{15}N chemical shift of the Schiff base nitrogen, coupled with the PLP C2 and C3 shifts,

Atom	Chemical Shift (ppm)	
C^{α} (Ser)	105.1	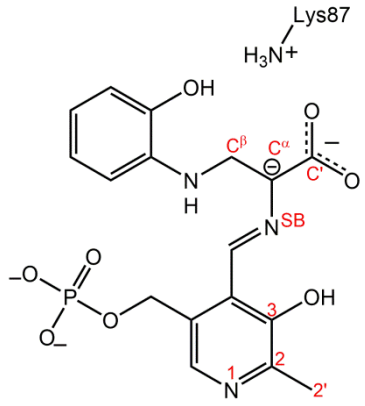
C^{β} (Ser)	47.0	
C′ (Ser)	173.1	
N (Schiff Base)	298.6	
N (2AP)	55.9	
C2 (PLP)	144.6	
C2′ (PLP)	17.0	
C3 (PLP)	153.1	
N1 (Pyridine)	262.0	
P (Phosphoryl)	5.0	
N (Lys87)	31.5	

Table 5.1 Experimentally determined chemical shifts for the 2AP quinonoid intermediate. Oxygen chemical shifts taken from Young *et al.*[51]

point to an intermediate in its phenolic form, with a neutral Schiff base linkage to substrate. However, the shift of the Schiff base nitrogen is somewhat lower than that of deprotonated imine model compounds.[8,68] The temperature dependence of the chemical shifts for both the Schiff base nitrogen and PLP C3 are away from the phenolic form and toward the protonated Schiff base form, suggesting a fast tautomeric exchange between these two species. The intramolecular hydrogen bond in model PLP-Schiff base complexes is known to exhibit proton exchange, and a two-site model has been proposed by Chan-Hout et al. to interpret the nitrogen chemical shift in terms of the corresponding equilibrium constant.[8]

The chemical shift of the pyridine ring nitrogen at 262.0 ppm, however, remains enigmatic; based on model aldimine complexes, a deprotonated PLP nitrogen would be expected to fall above 300 ppm, and a protonated pyridine nitrogen below 200 ppm.[17,45] As noted above, the narrow resonance and lack of significant temperature dependence suggest that this shift is not the result of chemical exchange. Strong hydrogen bonding to the pyridine nitrogen could elicit such a shift, but would require a stronger hydrogen

bond than seems reasonable for the interaction between the pyridine ring nitrogen and the side-chain hydroxyl of βSer377. The carboxylate oxygen chemical shifts measured by Young *et al.*[51] similarly present a puzzle, as they too fall outside the range expected based on model compound studies. The unexpected chemical shift results obtained at these sites triggered the application of computational chemistry to the 2AP quinonoid intermediate for aid in unraveling the enigma of the chemical shifts.

The application of NMR crystallography – the synergistic combination of X-ray crystallography, solid-state NMR spectroscopy, and computational chemistry – to the 2AP quinonoid intermediate in tryptophan synthase required that three-dimensional models of the active site first be constructed. 30 candidate structures with varying protonation states were systematically generated by Robert Young.[51] These models were based on the framework of the pre-determined X-ray crystal structures, geometry optimized, and their NMR parameters predicted. These candidate structural models were then ranked based on the agreement between their predicted and experimental isotropic chemical shifts using the reduced-χ^2 statistic.[69] None of the candidate structures shows the expected agreement with the experimental chemical shifts. This is not entirely unexpected, as the temperature dependence of the Schiff base nitrogen resonance suggests tautomeric exchange. This possibility was considered by modeling possible fast-exchange equilibria, in which tautomers that differed by the position of a single proton were paired and their populations optimized for best agreement with the

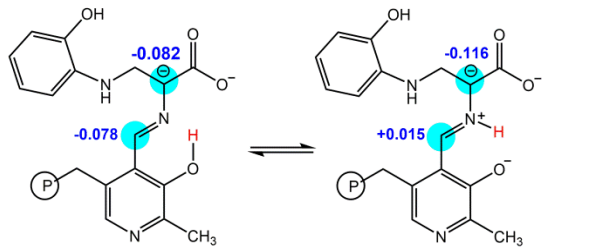

Phenolic Carbanion (C-Phen) Protonated Schiff Base Carbanion (C-PSB)

Scheme 5.4 Carbanionic Phenolic and Protonated Schiff Base Tautomers with NBO Partial Charges Indicated at C^{α} and C4′.

experimental chemical shifts. These models were again ranked, and the best-fit, with a reduced-χ^2 of 0.52, is for the exchange between the carbanionic phenolic (81%) and protonated Schiff-base (19%) forms, scheme 5.4, with no three-site exchange model performing better. In this equilibrium, both exchange partners have a charged βLys87 side chain. The next best exchange model is between the same major species, the carbanionic phenolic form, and the acid form of the substrate, in which the proton has transferred to the nearer carboxylate oxygen. But with a reduced-χ^2 of 3.12, this model can be ruled out with greater than 95% confidence, yet it should be noted that this equilibrium had previously been postulated by Lai *et al*.[39] Importantly, all models with a protonated pyridine nitrogen can also be confidently excluded, allowing us to conclude that the 2AP quinonoid intermediate in tryptophan synthase is in fact a carbanionic species. Although we will still loosely refer to the intermediate as the "2AP quinonoid," it should more accurately be referred to as the "2AP carbanionic intermediate."[11]

For the 2AP carbanionic intermediate, the best-fit equilibrium model is consistent with the chemical shift temperature dependence observed for the Schiff base nitrogen and PLP C3 resonances. The 81:19 population ratio corresponds to a free energy difference of +0.78 kcal/mol, and a two-site exchange model would predict chemical shift temperature coefficients of -0.099 and +0.012 ppm/K for the nitrogen and carbon sites, compared to the

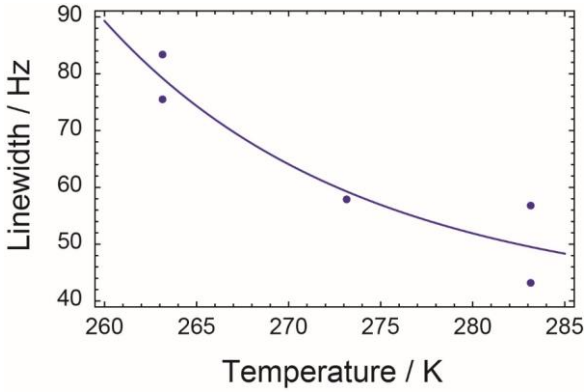

Figure 5.7 The experimental Schiff-base nitrogen linewidth vs. temperature for the 2AP quinonoid. A fit of this data to the two-site fast-exchange model described below allows a barrier to proton exchange of +8.9 kcal/mol to be estimated.[11]

experimental values of -0.07 and +0.012 ppm/K. The Schiff base nitrogen line shape also shows narrowing with increased temperature as expected for a system in fast exchange. A detailed analysis of the temperature-dependent line shape allowed the barrier to proton exchange to be estimated at 8.9 kcal/mol, figure 5.7.[11]

Protonation States and Reaction Specificity in Tryptophan Synthase

The application of NMR crystallography to the 2AP quinonoid intermediate in tryptophan synthase allows an atomic-resolution structural model of the active site to be established that not only reveals the chemical structure and protonation states of the cofactor and substrates, but also reports on charge states and intermolecular hydrogen bonding interactions with active site residues. Several of the structural conclusions are highlighted in figure 5.8. Most significantly, the 2AP quinonoid intermediate is found to be a carbanionic species in which the PLP pyridine ring nitrogen is deprotonated and participates in a (standard) hydrogen bond with βSer377. At the same time, the catalytic

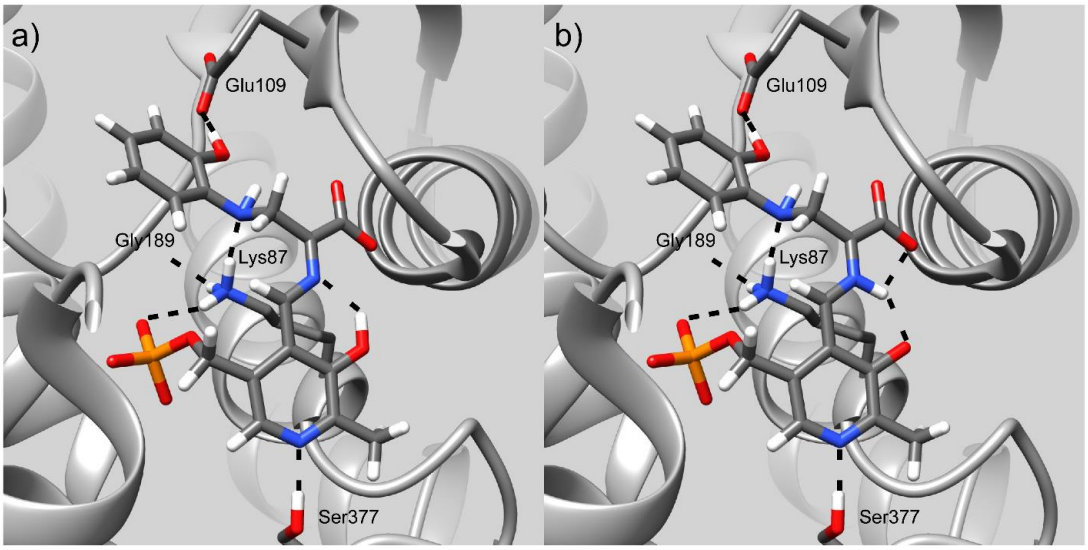

Figure 5.8 Protonation states and hydrogen bonding interactions revealed by NMR crystallography in the tryptophan synthase β-subunit active site. The 2AP quinonoid intermediate is found to be a carbanionic species undergoing fast proton exchange between its (a) phenolic (81% occupancy) and (b) protonated Schiff base (19% occupancy) tautomeric forms. The PLP pyridine ring nitrogen is deprotonated and participates in a (standard) hydrogen bond with βSer377. Images rendered in UCSF Chimera.[13]

βLys87 side chain is positively charged and hydrogen bonded to the dianionic PLP phosphoryl group. Two additional hydrogen bonds are formed from βLys87 to the backbone carbonyl of βGly189 and the 2AP nitrogen, and another from the 2AP phenolic group to βGlu109. Importantly, this carbanionic intermediate is found to be undergoing fast proton exchange between its phenolic and protonated Schiff base tautomers.

These structures and this equilibrium have fundamental implications for the mechanism in tryptophan synthase. While traditional views of PLP catalysis maintain the need for a protonated pyridine nitrogen to stabilize the build-up of negative charge generated during the reaction, more recent experimental[37,70-72] and theoretical[29,31,73,74] considerations point to a trade-off between the maximum electrophilic strength offered by a true quinonoid intermediate and reaction specificity that may be conferred by alternative protonation states.[30] In the case of the TS quinonoid intermediate, E(Q_3), the next step in catalysis requires protonation at the substrate C^{α}, scheme 5.2. This proton is presumably supplied by the positively charged ε-amino group of βLys87, which is positioned nearly equidistant between C4' of the cofactor and C^{α}. In order to maintain reaction specificity, protonation must be directed away from C4', the site of protonation for the competing transamination pathway. Factors that lead to the buildup of negative charge at C^{α} and a large charge differential with C4' are therefore expected to help direct and maintain reaction specificity. To delineate the role of protonation states in this process, atomic partial charges were calculated for the active site computational clusters using natural population analysis[63] in NBO 6.0.[64] Four tautomers were considered: the exchanging carbanionic phenolic and protonated Schiff base, C-Phen and C-PSB, forms found by NMR crystallography, scheme 5.4, and their canonical quinonoid counterparts, Q-Phen and Q-PSB, scheme 5.5. The resulting NBO charges at C^{α} and C4' are shown in

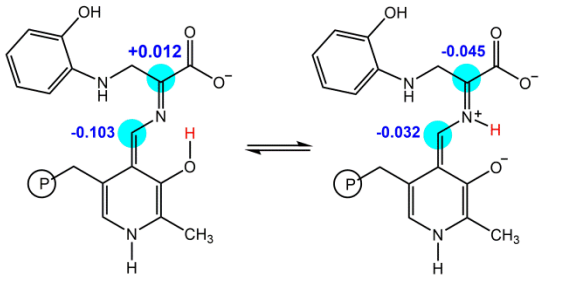

Phenolic Quinonoid (Q-Phen) Protonated Schiff Base Quinonoid (Q-PSB)

Scheme 5.5 Quinonoid Phenolic and Protonated Schiff Base Tautomers with NBO Partial Charges Indicated at C^{α} and C4′.

the respective schemes. For C-Phen, the C4' and C^{α} partial charges are both negative and similar in magnitude: -0.078 au and -0.082 au, respectively. Upon transfer of the proton to the Schiff base nitrogen to give C-PSB, the charges diverge with C^{α} becoming more negative, -0.116 au, and C4' slightly positive, +0.015 au; this is consistent with the proposed ylide stabilization of negative charge at C^{α} for the PSB form.[6] Protonation of the pyridine nitrogen to give the canonical quinonoid Q-Phen shows a reversal of these trends: now the phenolic form has C4' at its most negative value, -0.103 au, and C^{α} positive at +0.012 au. The protonated Schiff base tautomer Q-PSB sees the charges at both C^{α} and C4' converge to nearly equal values, -0.045 au and -0.032 au, respectively. These results mirror the trends found by Casasnovas et al.[32] in smaller quinonoid intermediate model systems in implicit solvent. The larger clusters used here (over 600 atoms), however, maintain important intermolecular interactions between the cofactor and enzyme residues that appear capable of influencing the overall charge on the cofactor/substrate complex.[11]

Most critical for understanding mechanism and reaction specificity in tryptophan synthase, it is the carbanionic protonated Schiff-base tautomer, C-PSB, that builds up the largest negative charge at C^{α} and the greatest charge differential with C4'. This charge distribution favors protonation at C^{α}, as required for the TS β-elimination and replacement reaction, and disfavors protonation at C4'. The carbanionic phenolic tautomer, C-Phen, shows minimal charge differential between C^{α} and C4' and provides a

less attractive target for protonation. We therefore propose that C-PSB is the more catalytically active and important tautomer, despite the fact that it is only transiently populated by fluctuations (proton exchange) from the more stable phenolic form. Protonating the pyridine nitrogen to form the canonical quinonoid intermediate reverses the relative charges at C4' and C^{α}, giving tautomers more likely to be found on the transamination pathway. These partial charge calculations help to place the TS 2AP protonation states in context: although the carbanionic species are expected to be less electrophilic than their corresponding canonical quinonoid forms, it appears that tryptophan synthase sacrifices this electrophilicity in order to maintain reaction specificity.

5.4 Conclusion

The application of NMR crystallography – the highly-integrated combination of solid-state NMR spectroscopy, X-ray crystallography, and computational chemistry – to the 2AP quinonoid intermediate in tryptophan synthase provides an atomic-resolution description of structure, protonation states, and chemical dynamics that would be impossible to achieve by the individual application of these techniques. Indeed several of the key active-site chemical shifts fall outside of the range established in model compound studies, and it is only through first principles calculation of NMR parameters that a model can be confidently established. This model reveals that the 2AP quinonoid is in fact a carbanionic species with a deprotonated pyridine ring nitrogen, and that this intermediate is undergoing fast proton exchange between its phenolic and protonated Schiff base tautomeric forms. These results provide direct experimental support that true quinonoid formation is not a prerequisite for carbanion stabilization in PLP-dependent

enzymes. Natural bond orbital analysis confirms the catalytic significance of these protonation states in tryptophan synthase: the buildup of negative charge for the protonated Schiff base in particular helps to direct the proton from N^{ε} of βLys87 to the C^{α} site, and the concomitant buildup of positive charge at C4' helps maintain reaction specificity by disfavoring the competing transamination pathway. These findings support the hypothesis that reaction specificity in PLP-dependent enzymes is conferred in part by the protonation states of ionizable groups on PLP and the reacting substrates and that some PLP-dependent enzymes eschew the stabilization of a canonical quinonoid form in order to maintain this specificity. These results also underscore the powerful role that NMR crystallography can play in characterizing chemical structure within enzyme active sites, and its ability – demonstrated here for the 2AP carbanionic intermediate – to quantify fluctuations away from stable structures to transient and more reactive species.

5.5 References

(1) Metzler, D. E.; Ikawa, M.; Snell, E. E. *J Am Chem Soc* **1954**, *76*, 648.

(2) Walsh, C. *Enzymatic Reaction Mechanisms*; W. H. Freeman: San Francisco, 1979.

(3) Jencks, W. P. *Catalysis in Chemistry and Enzymology*; McGraw-Hill: New York, 1969.

(4) Percudani, R.; Peracchi, A. *EMBO Rep* **2003**, *4*, 850.

(5) Hayashi, H. *J Biochem* **1995**, *118*, 463.

(6) Toney, M. D. *Arch Biochem Biophys* **2005**, *433*, 279.

(7) Toney, M. D. *Biochim Biophys Acta* **2011**, *1814*, 1407.

(8) Chan-Huot, M.; Dos, A.; Zander, R.; Sharif, S.; Tolstoy, P. M.; Compton, S.; Fogle, E.; Toney, M. D.; Shenderovich, I.; Denisov, G. S.; Limbach, H. H. *J Am Chem Soc* **2013**, *135*, 18160.

(9) Gullion, T.; Schaefer, J. *J Magn Reson* **1989**, *81*, 196.

(10) Toney, M. D. *BBA - Protein Proteom* **2011**, *1814*, 1407.

(11) Caulkins, B. G.; Young, R. P.; Kudla, R. A.; Yang, C.; Bittbauer, T. J.; Bastin, B.; Hilario, E.; Fan, L.; Marsella, M. J.; Dunn, M. F.; Mueller, L. J. *J Am Chem Soc* **2016**, *138*, 15214.

(12) Dunathan, H. C. *Proc Natl Acad Sci U S A* **1966**, *55*, 712.

(13) Pettersen, E. F.; Goddard, T. D.; Huang, C. C.; Couch, G. S.; Greenblatt, D. M.; Meng, E. C.; Ferrin, T. E. *J Comput Chem* **2004**, *25*, 1605.

(14) Sharif, S.; Denisov, G. S.; Toney, M. D.; Limbach, H. H. *J Am Chem Soc* **2007**, *129*, 6313.

(15) Chan-Huot, M.; Sharif, S.; Tolstoy, P. M.; Toney, M. D.; Limbach, H. H. *Biochemistry* **2010**, *49*, 10818.

(16) Chan-Huot, M.; Sharif, S.; Tolstoy, P. M.; Toney, M. D.; Limbach, H. H. *Biochemistry* **2010**, *49*, 10818.

(17) Limbach, H. H.; Chan-Huot, M.; Sharif, S.; Tolstoy, P. M.; Shenderovich, I. G.; Denisov, G. S.; Toney, M. D. *Biochim Biophys Acta* **2011**, *1814*, 1426.

(18) Kallen, R. G.; Korpela, T.; Martell, A. E.; Matsushima, Y.; Metzler, C. M.; Metzler, D. E.; Morozov, Y. V.; Ralston, I. M.; Savin, F. A.; Torchinsky, Y. M.; Ueno, H. In *Transaminases*; Christen, P., Metzler, D. E., Eds.; John Wiley & Sons, Inc.: New York, 1985, p 37.

(19) Mozzarelli, A.; Bettati, S. *Chem Rec* **2006**, *6*, 275.

(20) Metzler, D. E. *J Am Chem Soc* **1957**, *79*, 485.

(21) Metzler, C. M.; Harris, A. G.; Metzler, D. E. *Biochemistry* **1988**, *27*, 4923.

(22) Katsura, Y.; Shirouzu, M.; Yamaguchi, H.; Ishitani, R.; Nureki, O.; Kuramitsu, S.; Hayashi, H.; Yokoyama, S. *Proteins: Struct, Funct, Bioinf* **2004**, *55*, 487.

(23) Astner, I.; Schulze, J. O.; van den Heuvel, J.; Jahn, D.; Schubert, W. D.; Heinz, D. W. *EMBO J* **2005**, *24*, 3166.

(24) McPhalen, C. A.; Vincent, M. G.; Jansonius, J. N. *J Mol Biol* **1992**, *225*, 495.

(25) Ikushiro, H.; Islam, M. M.; Okamoto, A.; Hoseki, J.; Murakawa, T.; Fujii, S.; Miyahara, I.; Hayashi, H. *J Biochem* **2009**, *146*, 549.

(26) Yard, B. A.; Carter, L. G.; Johnson, K. A.; Overton, I. M.; Dorward, M.; Liu, H.; McMahon, S. A.; Oke, M.; Puech, D.; Barton, G. J.; Naismith, J. H.; Campopiano, D. J. *J Mol Biol* **2007**, *370*, 870.

(27) Lin, Y. L.; Gao, J.; Rubinstein, A.; Major, D. T. *BBA - Proteins Proteom* **2011**, *1814*, 1438.

(28) Rubinstein, A.; Major, D. T. *Biochemistry* **2010**, *49*, 3957.

(29) Bach, R. D.; Canepa, C.; Glukhovtsev, M. N. *J Am Chem Soc* **1999**, *121*, 6542.

(30) Richard, J. P.; Amyes, T. L.; Crugeiras, J.; Rios, A. *Curr Opin Chem Biol* **2009**, *13*, 475.

(31) Casasnovas, R.; Salva, A.; Frau, J.; Donoso, J.; Munoz, F. *Chem Phys* **2009**, *355*, 149.

(32) Casasnovas, R.; Adrover, M.; Ortega-Castro, J.; Frau, J.; Donoso, J.; Munoz, F. *J Phys Chem B* **2012**, *116*, 10665.

(33) Hyde, C. C.; Ahmed, S. A.; Padlan, E. A.; Miles, E. W.; Davies, D. R. *J Biol Chem* **1988**, *263*, 17857.

(34) Shaw, J. P.; Petsko, G. A.; Ringe, D. *Biochemistry* **1997**, *36*, 1329.

(35) Burkhard, P.; Rao, G. S.; Hohenester, E.; Schnackerz, K. D.; Cook, P. F.; Jansonius, J. N. *J Mol Biol* **1998**, *283*, 121.

(36) Omi, R.; Goto, M.; Miyahara, I.; Mizuguchi, H.; Hayashi, H.; Kagamiyama, H.; Hirotsu, K. *J Biol Chem* **2003**, *278*, 46035.

(37) Griswold, W. R.; Toney, M. D. *J Am Chem Soc* **2011**, *133*, 14823.

(38) Osborne, A.; Teng, Q.; Miles, E. W.; Phillips, R. S. *J Biol Chem* **2003**, *278*, 44083.

(39) Lai, J.; Niks, D.; Wang, Y.; Domratcheva, T.; Barends, T. R.; Schwarz, F.; Olsen, R. A.; Elliott, D. W.; Fatmi, M. Q.; Chang, C. E.; Schlichting, I.; Dunn, M. F.; Mueller, L. J. *J Am Chem Soc* **2011**, *133*, 4.

(40) Caulkins, B. G.; Bastin, B.; Yang, C.; Neubauer, T. J.; Young, R. P.; Hilario, E.; Huang, Y. M.; Chang, C. E.; Fan, L.; Dunn, M. F.; Marsella, M. J.; Mueller, L. J. *J Am Chem Soc* **2014**, *136*, 12824.

(41) Caulkins, B. G.; Yang, C.; Hilario, E.; Fan, L.; Dunn, M. F.; Mueller, L. J. *Biochim Biophys Acta* **2015**, *1854*, 1194.

(42) Copie, V.; Faraci, W. S.; Walsh, C. T.; Griffin, R. G. *Biochemistry* **1988**, *27*, 4966.

(43) Mcdowell, L. M.; Lee, M. S.; Schaefer, J.; Anderson, K. S. *J Am Chem Soc* **1995**, *117*, 12352.

(44) McDowell, L. M.; Schmidt, A.; Cohen, E. R.; Studelska, D. R.; Schaefer, J. *J Mol Biol* **1996**, *256*, 160.

(45) Sharif, S.; Fogle, E.; Toney, M. D.; Denisov, G. S.; Shenderovich, I. G.; Buntkowsky, G.; Tolstoy, P. M.; Huot, M. C.; Limbach, H. H. *J Am Chem Soc* **2007**, *129*, 9558.

(46) Woehl, E.; Dunn, M. F. *Biochemistry* **1999**, *38*, 7131.

(47) Ngo, H.; Harris, R.; Kimmich, N.; Casino, P.; Niks, D.; Blumenstein, L.; Barends, T. R.; Kulik, V.; Weyand, M.; Schlichting, I.; Dunn, M. F. *Biochemistry* **2007**, *46*, 7713.

(48) Schiaretti, F.; Bettati, S.; Viappiani, C.; Mozzarelli, A. *J Biol Chem* **2004**, *279*, 29572.

(49) Harris, R. M.; Dunn, M. F. *Biochemistry* **2002**, *41*, 9982.

(50) Niks, D.; Hilario, E.; Dierkers, A.; Ngo, H.; Borchardt, D.; Neubauer, T. J.; Fan, L.; Mueller, L. J.; Dunn, M. F. *Biochemistry* **2013**, *52*, 6396.

(51) Young, R. P.; Caulkins, B. G.; Borchardt, D.; Bulloch, D. N.; Larive, C. K.; Dunn, M. F.; Mueller, L. J. *Angew Chem Int Ed Engl* **2016**, *55*, 1350.

(52) Elena, B.; Pintacuda, G.; Mifsud, N.; Emsley, L. *J Am Chem Soc* **2006**, *128*, 9555.

(53) Harris, R. K.; Hodgkinson, P.; Pickard, C. J.; Yates, J. R.; Zorin, V. *Magn Reson Chem* **2007**, *45 Suppl 1*, S174.

(54) Harris, R. K.; Wasylishen, R. E.; Duer, M. J. *NMR Crystallography*; Wiley: Chichester, U.K., 2009.

(55) Bonhomme, C.; Gervais, C.; Babonneau, F.; Coelho, C.; Pourpoint, F.; Azais, T.; Ashbrook, S. E.; Griffin, J. M.; Yates, J. R.; Mauri, F.; Pickard, C. J. *Chem Rev* **2012**, *112*, 5733.

(56) Baias, M.; Dumez, J. N.; Svensson, P. H.; Schantz, S.; Day, G. M.; Emsley, L. *J Am Chem Soc* **2013**, *135*, 17501.

(57) Fung, B. M.; Khitrin, A. K.; Ermolaev, K. *J Magn Reson* **2000**, *142*, 97.

(58) Harris, R. K.; Becker, E. D.; Cabral de Menezes, S. M.; Granger, P.; Hoffman, R. E.; Zilm, K. W. *Pure Appl Chem* **2008**, *80*, 59.

(59) Morcombe, C. R.; Zilm, K. W. *J Magn Reson* **2003**, *162*, 479.

(60) Hayashi, S.; Hayamizu, K. *Bull Chem Soc Jpn* **1991**, *64*, 688.

(61) Maurer, T.; Kalbitzer, H. R. *J Magn Reson, Ser B* **1996**, *113*, 177.

(62) McNeill, S. A.; Gor'kov, P. L.; Shetty, K.; Brey, W. W.; Long, J. R. *J Magn Reson* **2009**, *197*, 135.

(63) Reed, A. E.; Weinstock, R. B.; Weinhold, F. *J Chem Phys* **1985**, *83*, 735.

(64) Glendening, E. D.; Landis, C. R.; Weinhold, F. *J Comput Chem* **2013**, *34*, 1429.

(65) Harruff, R. C.; Jenkins, W. T. *Org Magn Reson* **1976**, *8*, 548.

(66) O'Leary, M. H.; Payne, J. R. *J Biol Chem* **1976**, *251*, 2248.

(67) Schnackerz, K. D.; Andi, B.; Cook, P. F. *BBA - Proteins Proteom* **2011**, *1814*, 1447.

(68) Harbison, G. S.; Herzfeld, J.; Griffin, R. G. *Biochemistry* **1983**, *22*, 1.

(69) Garland, C. W.; Nibler, J. W.; Shoemaker, D. P. *Experiments in Physical Chemistry*; 8th ed.; McGraw-Hill Higher Education: Boston, 2009.

(70) Cook, P. F. *BBA - Protein Proteom* **2003**, *1647*, 66.

(71) Daum, S.; Tai, C. H.; Cook, P. F. *Biochemistry* **2003**, *42*, 106.

(72) Jhee, K. H.; McPhie, P.; Ro, H. S.; Miles, E. W. *Biochemistry* **1998**, *37*, 14591.

(73) Liao, R. Z.; Ding, W. J.; Yu, J. G.; Fang, W. H.; Liu, R. Z. *J Phys Chem A* **2007**, *111*, 3184.

(74) Toney, M. D. *Biochemistry* **2001**, *40*, 1378.

Chapter 6 – Future Work

6.1 Introduction

While great progress has been made in the understanding of the tryptophan synthase catalytic cycle, there are still many atomic-level details to be teased out to confirm and refine our hypothesis. We believe that for a given stereoelectronic environment, reaction specificity in PLP-dependent enzymes is determined by the specific protonation states on the cofactor and substrate and these, in turn, are dictated by the surrounding active site side chain residues. Our initial work on the internal aldimine, aminoacrylate, and 2AP carbanionic intermediates, scheme 6.1, orange boxes, points to the critical role of protonation states in TS catalysis.[1-3] For the internal aldimine state, a protonated Schiff base activates catalysis; this state is effected by a transfer of the phenolic oxygen proton to the Schiff base nitrogen, which is stabilized (despite the

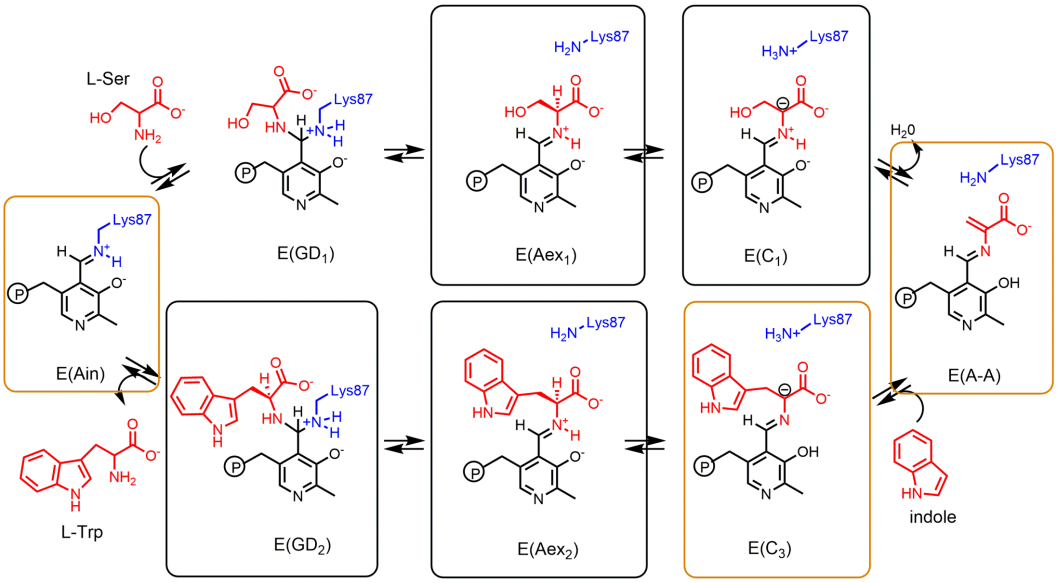

Scheme 6.1 The β-reaction of TS. Orange boxes represent complete structures, black solid boxes represent future structural targets for characterization.

deprotonated pyridine ring nitrogen atom) by hydrogen bonding of water molecules to the phenolic oxygen.[1] Formation of the aminoacrylate intermediates is encouraged by a deprotonated pyridine nitrogen, which allows this species to build up positive charge at C^{β} to create an electrophilic center suitable for reaction with the incoming indole, but not the inhibitor benzimidazole (BZI). For the carbanionic intermediate, the deprotonated pyridine nitrogen leads to a carbanionic species with greater electron density at the substrate C^{α}. This negative charge is further enhanced by a tautomer in which the phenolic proton transfers to the Schiff base nitrogen. Both help to direct the proton transfer to C^{α} which ultimately directs the reaction down the β-elimination/replacement pathway.[3] For both aminoacrylate intermediates and the carbanionic intermediate, it is βLys87 that acts as the primary acid-base catalyst, abstracting and returning protons to the substrate as necessary.[2] These ideas can be tested and refined in three different ways: elucidation of the structures of more transient intermediates on the catalytic cycle using techniques like dynamic nuclear polarization (DNP), the use of TS mutants designed to specifically scramble the protonation states of the active site, and the study of PLP-dependent enzymes from different fold types.

6.2 Elucidation of Transient Intermediates

The intermediates in black boxes in scheme 6.1 are targets for future stabilization and characterization. The first external aldimine intermediate ($E(Aex_1)$) forms upon introduction of serine to the system, but the equilibrium between the $E(Aex_1)$, first carbanion ($E(C_1)$), and α-aminoacrylate (E(A-A)) intermediates lies well to the right, favoring E(A-A). These complexes derived from reactions involving serine are potentially compromised by a deleterious side reaction in which serine, via the α-aminoacrylate

intermediate, reacts with water to give pyruvate and an ammonium ion, a reaction enhanced by the open conformation of the subunit.[4] Complications due to the pyruvate side reaction can be minimized by judicious choice of experimental conditions (low temperature, allosteric ligands, monovalent cation, and pH).[5-11] The choice of effector ligands also determines whether or not the subunits assume open or closed conformations. For example, the binding of Cs^+ and F9 biases complexes toward closed conformations of the α- and β-subunits. The substitution of Na^+ for Cs^+ and the absence of an α-site ligand favors the open α- and β-subunit conformations.[5,11-13] Experiments on external aldimine species in open and closed conformations enable interrogation of the hypothesis that catalysis occurs via the closed β-subunit conformation. Several X-ray crystal structures have been published for E(Aex_1) complexes in which the β-subunit exhibits an open conformation,[12,14] and two wild type structures have been published with the β-subunit in the closed conformation.[15] Detailed chemical shift analysis for these structures would allow a complete comparison of chemical structure in open and closed conformations for closely analogous intermediates.

Addition of L-tryptophan to catalytically active microcrystals in the resting internal aldimine form causes the reaction to run in reverse, giving an equilibrating mixture of the second gem-diamine (E(GD_2)), external aldimine (E(Aex_2)), and carbanionic species (E(C_3)). The quinonoid species undergoes a very slow cleavage to give indole and E(A-A).[16] At cryo temperatures (100 K), this cleavage occurs at a negligible rate. However, at room temperature, the presence of the gem-diamine and external aldimine species is significant. The presence of all three species makes the L-Trp system more complicated for ssNMR and X-ray structural studies. Conditions that selectively stabilize each of these individual intermediates need to be optimized for a full picture of catalysis to be

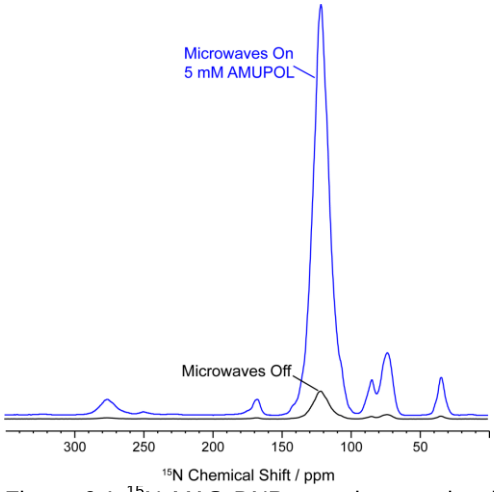

Figure 6.1 ^{15}N MAS DNP experiments showing an enhancement of ~15 compared to standard ^{15}N CPMAS detection for U-^{13}C,^{15}N TS. Experiments were performed at 100 K at 8 kHz MAS and were carried out at NHMFL.

achieved, an effort that will involve variation of pH, temperature in solution and in crystals, α-site ligand, and cation to determine the effects of these parameters on the distribution of intermediates.

These intermediates may prove too transient to acquire NMR data at or near room temperature. The use of cryo-temperature NMR experiments to trap intermediates, coupled with dynamic nuclear polarization (DNP),[17,18] will allow for long-term stabilization of trapped intermediates.

Figure 6.1 shows the first DNP experiments on TS, which were performed at the National High Magnetic Field Laboratory (NHMFL) DNP User Facility. Although the sensitivity increase

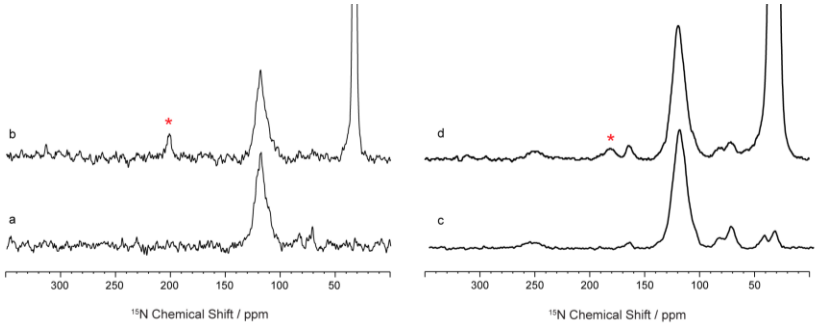

Figure 6.2 The spectra obtained from ε-^{15}N-lysine TS using (a,b) ssNMR and (c,d) DNP. (b) shows the Schiff base nitrogen resonance at 202.3 ppm, while (d) shows this signal at 180 ppm. The upfield movement toward a chemical shift more indicative of a fully protonated Schiff base is attributed to the trapping of the protonated Schiff base tautomer, resulting in a lower population of the protonated phenolic oxygen tautomer. Figures a and c are both spectra collected on unlabeled TS for comparison. Magic-angle-spinning (MAS) NMR spectra of the enzyme complex were acquired on a Bruker DSX 400 Spectrometer (400.42 MHz ^{1}H; 100.70 MHz ^{13}C) using a double resonance 4 mm MAS probe (sample volume ~ 80 µl) and a MAS rate of 8 kHz. Spectra shown consist of 32k scans collected at 265 K. DNP experiments were acquired on a Bruker AV III 600 Spectrometer (600 MHz ^{1}H; 150 MHz ^{13}C) using a triple resonance 3.2 mm MAS probe (sample volume ~ 30 µl) and a MAS rate of 8 kHz. The sample was irradiated with continuous ~15 W of microwaves at 395 GHz generated from a Bruker/CPI gyrotron. The power was measured via a pyrometer integrated into a custom built quasi-optics microwave transmission system. Spectra shown consist of 1k scans collected at 105 K.

is modest (~15) compared to the best enhancements reported,[19,20] many experimental factors can still be optimized, including crystallization conditions, radical added, and cryoprotectant used. Ultimately, the improved signal-to-noise ratio and low temperature (100 K) will permit the efficient measurement of transient intermediates. Already, the use of DNP has implicated a tautomeric exchange in the internal aldimine resting form of TS. Figure 6.2b shows the ssNMR spectrum recorded using ε-^{15}N-Lys TS at 268 K and 8 kHz magic angle spinning (MAS). The spectrum recorded on the same sample using DNP at 100 K shows the Schiff base peak at 180 ppm, figure 6.2d. The upfield movement of this resonance toward a chemical shift more indicative of a fully protonated Schiff base is attributed to the trapping of the protonated Schiff base tautomer, resulting in a lower population of the protonated phenolic oxygen tautomer. The insight to be gained by intermediate trapping and the use of DNP will allow for a fuller understanding of how protonation states in the active site of TS uniquely tune this enzyme to follow the β-elimination/replacement pathway.

6.3 Tryptophan Synthase Mutants

The role that ionization states play in directing reaction specificity can be tested by site-directed mutagenesis of active site residues that scramble the protonation states of the cofactor and substrate that will alter reaction specificity in a predictable way. We have seen that for the 2AP intermediate, chapter 5, subsequent protonation of the carbanion at C^{α} or C4′ determines whether the reaction is ultimately on the elimination/replacement or transamination pathway, respectively.[3] The natural bond order (NBO) calculations of partial charges for the 2AP carbanion intermediate in TS performed by Robert Young help rationalize the importance of protonation states to this

process: the carbanionic/protonated Schiff base (PSB) form of the intermediate shows maximum negative charge at C^{α} and maximum positive charge for C4', while the quinonoid/phenolic form of the intermediate shows maximum negative charge at C4' and maximum positive charge at C^{α}; the former favors protonation at C^{α} and the latter the competing transamination pathway, figure 6.3.[3] We have found that the 2AP intermediate is best described as a carbanionic intermediate in which there is a fast exchange equilibrium between the phenolic (~80%) and PSB (~20%) tautomers. Because the minor tautomer builds up negative charge at the C^{α} site, we believe it is the catalytically active tautomer.

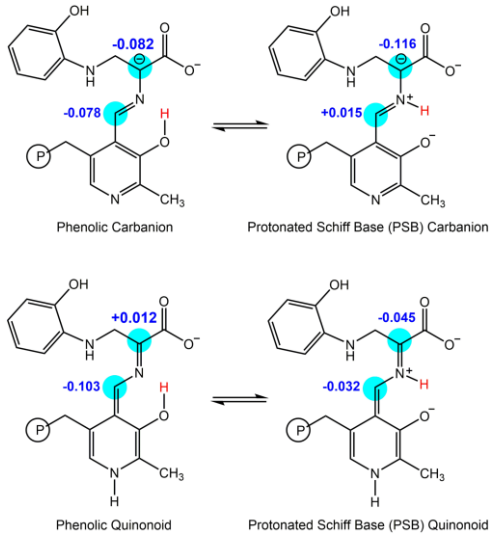

Figure 6.3 Charge calculations of the 2AP complex indicate that the carbanionic form builds up more negative charge at C^{α}, ensuring protonation at that site over C4′ and completion of the β-elimination/replacement reaction.

Toney and Limbach[21-24] have found that the acid base properties of the pyridine nitrogen and phenolic oxygen sites are coupled: a deprotonated pyridine nitrogen favors a protonated phenolic oxygen, while a protonated pyridine nitrogen favors a deprotonated phenolic oxygen. They also note that an alternative way to deprotonate the phenolic oxygen is to directly hydrogen bond to that site[21] (as we found in the internal aldimine intermediate, which shows crystallographic water hydrogen bonding to the phenolic oxygen[1]). Given the deprotonated pyridine nitrogen for the TS tautomers, how is it possible to deprotonate the phenolic oxygen in the carbanion intermediates without the benefit of crystallographic water? One possibility is that strong hydrogen bonding of βS377 to the PLP pyridine nitrogen is sufficient; another is that βQ114 rotates into the

active site and hydrogen bonds to phenolic oxygen, helping to stabilize the PSB form. The possibility that βQ114 plays a stabilizing role is suggested by our MD simulations[25] and by an earlier published crystal structure of the Q114N mutant (PDBID: 2J9Y),[26] which shows this alternate side-chain conformation. Mutation of this residue to alanine, Q114A, should render the enzyme unable to help stabilize the PSB form, which will manifest as a downfield shift in the Schiff base resonance (lower population of PSB tautomer) and a lower overall conversion rate.

Another residue crucial to directing reaction specificity is βSer377. This residue sits directly below the PLP pyridine nitrogen and prevents protonation of the pyridine nitrogen, precluding formation of a true quinonoid intermediate. In PLP fold type I enzymes, an acidic residue interacts with the pyridine nitrogen, which in turn must be protonated.[27-29] Mutation of βSer377 in the fold type II TS to one of these acidic residues is expected to push a proton onto the pyridine ring and allow the formation of a true quinonoid intermediate. Based on our NBO calculations, figure 6.3, it would follow that this will decrease negative charge at C^{α} and lead to intermediates far more stable than the native protein and therefore unlikely to react further (or give altered reaction specificity). Indeed, Miles reports that the mutation of βSer377 to Asp (as found in *E. coli* aspartate aminotransferase) converts TS to a protein with transaminase-like spectroscopic properties (longer wavelength λ_{max}, pH dependent absorption spectra), suggesting this quinonoid species is on a transamination-like path rather than on the β-addition/elimination path.[30,31] More interestingly, the S377D mutant promoted dissociation of the α- and β-subunits and was inactivated L-Ser, the substrate in the natural reaction.[30] The large impact this one perturbation in electrostatic environment has on catalysis in TS underscores the critical importance of protonation states on

directing reaction outcome in PLP-dependent enzymes, and the wealth of information provided by ssNMR chemical shifts would lend great insight to the mechanism of inactivation in this mutant.

6.4 PLP-Dependent Enzymes of Different Fold Types

A final approach to understanding how reaction specificity in PLP-enzymes is conveyed by protonation states on the cofactor and substrates is to compare TS to enzymes from different fold types. Two fold type I enzymes present a good starting point for this endeavor: serine palmitoyltransferase (SPT) and aspartate aminotransferase (AAT). Both have an aspartate residue hydrogen bonded to the PLP pyridine nitrogen, which is therefore expected to be protonated.[32,33] SPT and AAT catalyze distinct reactions – SPT an α-decarboxylation and replacement[32,34] and AAT the canonical transamination reaction.[35] The interplay of stereoelectronic factors and protonation states that allows this distinct reaction specificity within the same fold type family makes these particularly interesting case studies.

Serine palmitoyltransferase (SPT) catalyzes the first step of sphingolipid synthesis in all organisms. Defects in sphingolipid metabolism in humans have been linked to lipid storage disorders such as Tay-Sachs disease and metachromatic leukodystrophy.[32,36] Consequently, understanding the catalytic mechanism could provide insights for developing SPT as a target for drug design. SPT from *Sphingomonas paucimobilis* is a 90 kDa PLP-dependent homodimeric enzyme.[37] The proposed mechanism, scheme 6.2, begins with L-Ser external aldimine formation, followed by binding of palmitoyl-CoA, and α-proton abstraction by Lys265 to form the (first) quinonoid species. Subsequent acyl group transfer to C^{α} and loss of CoA gives

palmitoylation of the L-Ser moiety. Finally, irreversible loss of carbon dioxide produces the carbanionic intermediate, followed by protonation at C^{α} and release of 3-ketodihydrosphingosine (KDS).[32] The success of this reaction relies on strong hydrogen

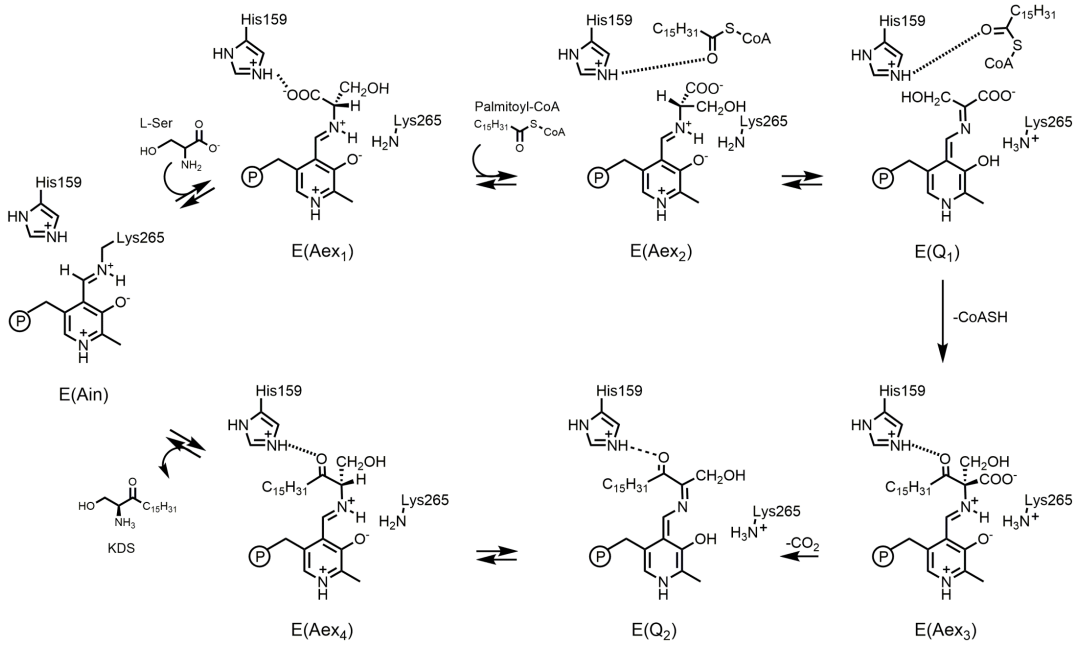

Scheme 6.2 Mechanism of serine palmitoyltransferase (SPT).

bonds between the substrate-cofactor complex and surrounding active site residues. His159 is stacked directly above the PLP ring and provides a hydrogen bonding/acidic catalytic partner for activation of the palmitoyl-CoA carbonyl.[32,37,38] This arrangement is proposed to convey proper stereochemical arrangement of the substrate-cofactor complexes and effect the desired reaction. The acidic D231 side chain hydrogen bonds to the pyridine ring nitrogen and ensures the nitrogen remains protonated for the course of the reaction.[32,37] The Lys265 side chain is expected to play alternating acid and base roles in the mechanism, as observed in TS.[2] Finally, an exchange of the proton between the hydrogen-bonded phenolic oxygen and the imine nitrogen is postulated to affect the stability of specific intermediates necessary for the intended outcome of the reaction.

We have performed initial work on SPT using ^{15}N-serine and catalytically active

microcrystals. Figure 6.4 shows the ^{13}C spectrum taken at 268 K and 8 kHz MAS for the external aldimine intermediate formed during catalysis. All three carbons in the substrate are clearly visible in the spectrum. Figure 6.5 shows the ^{15}N spectrum acquired at 268 K and 8 kHz MAS for the same intermediate. A large peak is visible at 190 ppm, the resonance of a protonated Schiff base nitrogen, consistent with the proposed reaction mechanism. These initial results highlight the power of ssNMR and its ability to directly probe the active sites of catalytically active, microcrystalline enzymes. More work can be done in SPT with site-specific labeling and the use of PLP analogues[28] to ascertain the crucial electrostatic aspects of this enzyme for catalysis.

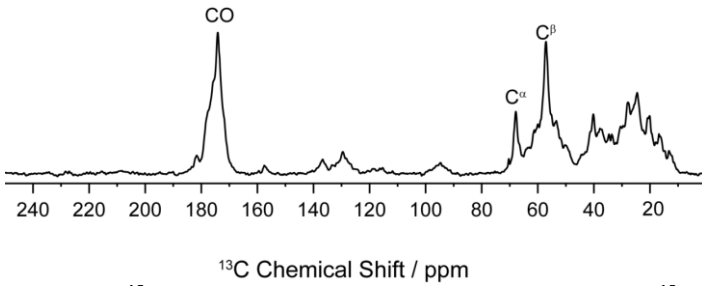

Figure 6.4 ^{13}C spectrum of SPT microcrystals reacted with ^{13}C-serine to form the external aldimine complex. Experiments were performed at 263 K and 8 kHz MAS.

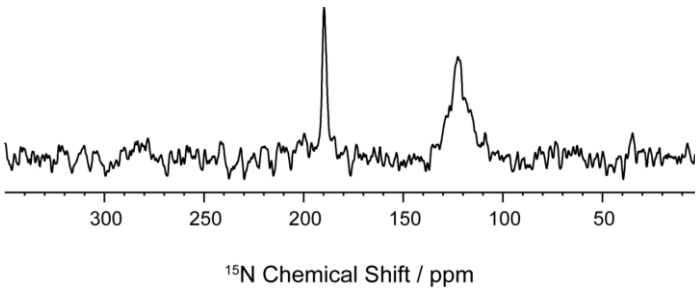

Figure 6.5 ^{15}N spectrum of SPT microcrystals reacted with ^{15}N-serine to form the external aldimine complex. Experiments were performed at 263 K and 8 kHz MAS.

In contrast to SPT, AAT, an enzyme found in every living thing,[29] undergoes the canonical aminotransferase reaction, scheme 6.3, transforming L-aspartate to L-glutamate. This provides an opportunity to explore contrasting reaction specificity within the same PLP fold type. NMR studies by Toney and Limbach[21,22,33,39] demonstrated that the pyridine nitrogen is indeed protonated in the internal aldimine state, but no other chemical shifts were reported, leaving an incomplete picture of the reaction. Current

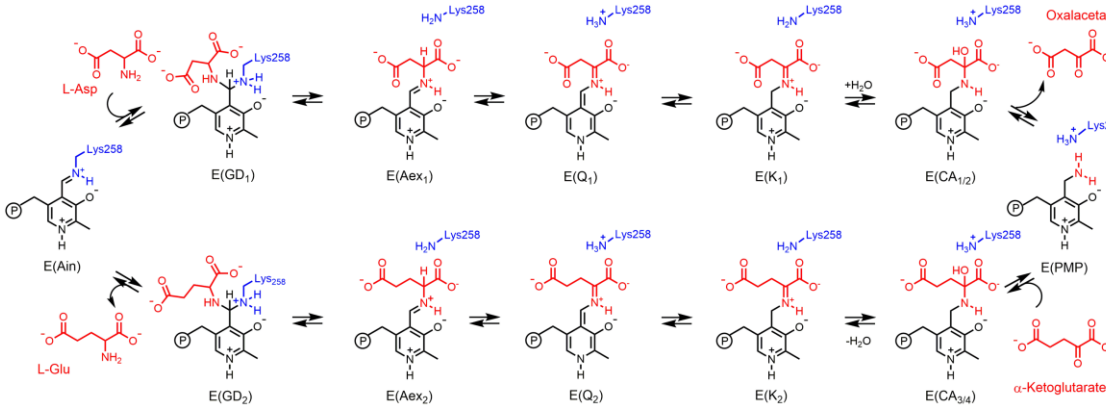

Scheme 6.3 Mechanism of aspartate aminotransferase (AAT).

mechanisms drawn for AAT depict a protonated pyridine nitrogen with a consistently deprotonated phenolic oxygen and protonated Schiff base. However, our NBO calculations indicate that transfer of the proton from Schiff base to the phenolic oxygen allows a greater build-up of negative charge at C4′, a necessity for protonation at C4′ in the next step.[3] The use of ^{13}C and ^{15}N enriched PLP would be an effective probe into the protonation states on the cofactor-substrate complex for both of these enzymes, while use of ε-^{15}N-lysine would help tease out the cooperation of the protonation states of the Schiff base and pyridine nitrogens. Studies on enzymes of different fold types will allow for the determination of the interplay between protonation states and reaction specificity in PLP enzymes and the importance that stereoelectronic constraints can play within the same fold type family.

6.5 Conclusion

The overall goal of this project is to understand the factors that control the transformation of substrate to product in tryptophan synthase at the atomic level. The use of solid-state NMR in this endeavor led to structural and mechanistic insights that

could not have been otherwise achieved. While there are still questions to be answered, many subtleties of the TS reaction have been teased out. The results offer chemically-detailed molecular views into functioning enzyme catalysis and are already rewriting the story on PLP-enzyme mechanism.

6.6 References

(1) Caulkins, B. G.; Bastin, B.; Yang, C.; Neubauer, T. J.; Young, R. P.; Hilario, E.; Huang, Y. M.; Chang, C. E.; Fan, L.; Dunn, M. F.; Marsella, M. J.; Mueller, L. J. *J Am Chem Soc* **2014**, *136*, 12824.

(2) Caulkins, B. G.; Yang, C.; Hilario, E.; Fan, L.; Dunn, M. F.; Mueller, L. J. *BBA - Protein Proteom* **2015**, *1854*, 1194.

(3) Caulkins, B. G.; Young, R. P.; Kudla, R. A.; Yang, C.; Bittbauer, T. J.; Bastin, B.; Hilario, E.; Fan, L.; Marsella, M. J.; Dunn, M. F.; Mueller, L. J. *J Am Chem Soc* **2016**, *138*, 15214.

(4) Ferrari, D.; Niks, D.; Yang, L. H.; Miles, E. W.; Dunn, M. F. *Biochemistry* **2003**, *42*, 7807.

(5) Ngo, H.; Kimmich, N.; Harris, R.; Niks, D.; Blumenstein, L.; Kulik, V.; Barends, T. R.; Schlichting, I.; Dunn, M. F. *Biochemistry* **2007**, *46*, 7740.

(6) Woehl, E.; Dunn, M. F. *Biochemistry* **1999**, *38*, 7131.

(7) Woehl, E.; Dunn, M. F. *Biochemistry* **1999**, *38*, 7118.

(8) Woehl, E. U.; Dunn, M. F. *Biochemistry* **1995**, *34*, 9466.

(9) Peracchi, A.; Bettati, S.; Mozzarelli, A.; Rossi, G. L.; Miles, E. W.; Dunn, M. F. *Biochemistry* **1996**, *35*, 1872.

(10) Peracchi, A.; Mozzarelli, A.; Rossi, G. L. *Biochemistry* **1995**, *34*, 9459.

(11) Barends, T. R. M.; Dunn, M. F.; Schlichting, I. *Curr Opin Chem Biol* **2008**, *12*, 593.

(12) Ngo, H.; Harris, R.; Kimmich, N.; Casino, P.; Niks, D.; Blumenstein, L.; Barends, T. R.; Kulik, V.; Weyand, M.; Schlichting, I.; Dunn, M. F. *Biochemistry* **2007**, *46*, 7713.

(13) Dierkers, A. T.; Niks, D.; Schlichting, I.; Dunn, M. F. *Biochemistry* **2009**, *48*, 10997.

(14) Kulik, V.; Weyand, M.; Seidel, R.; Niks, D.; Arac, D.; Dunn, M. F.; Schlichting, I. *J Mol Biol* **2002**, *324*, 677.

(15) Rhee, S.; Parris, K. D.; Hyde, C. C.; Ahmed, S. A.; Miles, E. W.; Davies, D. R. *Biochemistry* **1997**, *36*, 7664.

(16) Ahmed, S. A.; Martin, B.; Miles, E. W. *Biochemistry* **1986**, *25*, 4233.

(17) Akbey, U.; Franks, W. T.; Linden, A.; Orwick-Rydmark, M.; Lange, S.; Oschkinat, H. *Hyperpolarization Methods in NMR Spectroscopy* **2013**, *338*, 181.

(18) Hall, D. A.; Maus, D. C.; Gerfen, G. J.; Inati, S. J.; Becerra, L. R.; Dahlquist, F. W.; Griffin, R. G. *Science* **1997**, *276*, 930.

(19) Smith, A. N.; Long, J. R. *Anal Chem* **2016**, *88*, 122.

(20) Akbey, U.; Oschkinat, H. *J Magn Reson* **2016**, *269*, 213.

(21) Chan-Huot, M.; Dos, A.; Zander, R.; Sharif, S.; Tolstoy, P. M.; Compton, S.; Fogle, E.; Toney, M. D.; Shenderovich, I.; Denisov, G. S.; Limbach, H. H. *J Am Chem Soc* **2013**, *135*, 18160.

(22) Limbach, H. H.; Chan-Huot, M.; Sharif, S.; Tolstoy, P. M.; Shenderovich, I. G.; Denisov, G. S.; Toney, M. D. *BBA - Protein Proteom* **2011**, *1814*, 1426.

(23) Sharif, S.; Denisov, G. S.; Toney, M. D.; Limbach, H. H. *J Am Chem Soc* **2007**, *129*, 6313.

(24) Toney, M. D. *Biochim Biophys Acta* **2011**, *1814*, 1407.

(25) Huang, Y. M.; You, W.; Caulkins, B. G.; Dunn, M. F.; Mueller, L. J.; Chang, C. E. *Protein Sci* **2016**, *25*, 166.

(26) Blumenstein, L.; Domratcheva, T.; Niks, D.; Ngo, H.; Seidel, R.; Dunn, M. F.; Schlichting, I. *Biochemistry* **2007**, *46*, 14100.

(27) Grishin, N. V.; Phillips, M. A.; Goldsmith, E. J. *Protein Sci* **1995**, *4*, 1291.

(28) Griswold, W. R.; Fisher, A. J.; Toney, M. D. *Biochemistry* **2011**, *50*, 5918.

(29) Percudani, R.; Peracchi, A. *EMBO Rep* **2003**, *4*, 850.

(30) Jhee, K. H.; McPhie, P.; Ro, H. S.; Miles, E. W. *Biochemistry* **1998**, *37*, 14591.

(31) Jhee, K. H.; Yang, L. H.; Ahmed, S. A.; McPhie, P.; Rowlett, R.; Miles, E. W. *J Biol Chem* **1998**, *273*, 11417.

(32) Ikushiro, H.; Hayashi, H. *Biochim Biophys Acta* **2011**, *1814*, 1474.

(33) Toney, M. D. *Arch Biochem Biophys* **2014**, *544*, 119.

(34) Hanada, K. *Biochim Biophys Acta* **2003**, *1632*, 16.

(35) Christen, P.; Metzler, D. E. *Transaminases*; Wiley: New York, 1985.

(36) Kolter, T.; Sandhoff, K. *Biochimica Et Biophysica Acta-Biomembranes* **2006**, *1758*, 2057.

(37) Ikushiro, H.; Islam, M. M.; Okamoto, A.; Hoseki, J.; Murakawa, T.; Fujii, S.; Miyahara, I.; Hayashi, H. *J Biochem* **2009**, *146*, 549.

(38) Yard, B. A.; Carter, L. G.; Johnson, K. A.; Overton, I. M.; Dorward, M.; Liu, H. T.; McMahon, S. A.; Oke, M.; Puech, D.; Barton, G. J.; Naismith, J. H.; Campopiano, D. J. *J Mol Biol* **2007**, *370*, 870.

(39) Sharif, S.; Fogle, E.; Toney, M. D.; Denisov, G. S.; Shenderovich, I. G.; Buntkowsky, G.; Tolstoy, P. M.; Huot, M. C.; Limbach, H. H. *J Am Chem Soc* **2007**, *129*, 9558.